PELAGIC PLANKTON NET COMMUNITY PRODUCTION AND RESPIRATION IN THE SEA OF MARMARA

A THESIS SUBMITTED TO
THE GRADUATE SCHOOL OF MARINE SCIENCES
OF
MIDDLE EAST TECHNICAL UNIVERSITY

BY

MELİKE KAZAK

IN PARTIAL FULFILLMENT OF THE REQUIREMENTS
FOR
THE DEGREE OF MASTER OF SCIENCE
IN
MARINE BIOLOGY AND FISHERIES

AUGUST 2023

Approval of the thesis:

PELAGIC PLANKTON NET COMMUNITY PRODUCTION AND RESPIRATION IN THE SEA OF MARMARA

submitted by **MELİKE KAZAK** in partial fulfillment of the requirements for the degree of **Master of Science** i**n Marine Biology and Fisheries, Middle East Technical University** by,

Prof. Dr. Barış Salihoğlu
Director, **Institute of Marine Sciences, METU** _____

Prof. Dr. Zahit Uysal
Head of the Department, **Marine Biology and Fisheries** _____

Prof. Dr. Mustafa Yücel
Supervisor, **Oceanography, METU** _____

Dr. Asım Mustafa Mantıkçı
Co-Supervisor, **Oceanography, METU** _____

Examining Committee Members:

Prof. Dr. Zahit Uysal
Marine Biology and Fisheries, METU _____

Prof. Dr. Mustafa Yücel
Oceanography, METU _____

Prof. Dr. Dilek Ediger
Marine Sciences and Management, İstanbul University _____

Date: 28.08.2023

I hereby declare that all information in this document has been obtained and presented in accordance with academic rules and ethical conduct. I also declare that, as required by these rules and conduct, I have fully cited and referenced all material and results that are not original to this work.

Name Last name : Melike Kazak

Signature :

ABSTRACT

PELAGIC PLANKTON NET COMMUNITY PRODUCTION AND RESPIRATION IN THE SEA OF MARMARA

Kazak, Melike
Master of Science, Marine Biology and Fisheries
Supervisor: Prof. Dr. Mustafa Yücel
Co-Supervisor: Dr. Asım Mustafa Mantıkçı

August 2023, 92 pages

Respiration is a critical process in biological pump with primary production. This study quantified net community production (NCP) and community respiration (CR) for stations selected from various locations in the Sea of Marmara for the March 2022 and June 2022 seasons. NCP and CR experiments were conducted as in-vitro bottle incubations at in-situ temperature using a relatively new tool in aquatic science: OPTODES (fiber optical oxygen sensors). One of the essential aspects of this study is that community respiration samples were taken from different depths in both the euphotic zone and the sub-halocline to represent community respiration in the water column. In general, CR had a decreasing pattern with depth and it was positively correlated with dissolved oxygen and particulate organic carbon. For the euphotic zone, in March 2022, the hourly CR rate was in the range of 0.01-2.05 μmol O_2 L^{-1} h^{-1}, and in June 2022, it was in the range of 0.01-1.63 μmol O_2 L^{-1} h^{-1}. Sub-halocline community respiration rates were calculated as 89 ± 111mg C m^{-3} day^{-1} for March, 2022 and 75 ± 35 mg C m^{-3} day^{-1} for June, 2022. Spatial differences in hourly NCP rates were found to be positively correlated with dissolved oxygen and Chl-*a*. When the daily NCP for the Sea of Marmara is roughly calculated, the system was found to be heterotrophic, especially in less productive seasons.

Keywords: Respiration, Net Community Production, the Sea of Marmara, OPTODEs

ÖZ

MARMARA DENİZİ'NDE PELAJİK PLANKTON NET KOMUNİTE ÜRETİMİ VE SOLUNUMU

Kazak, Melike
Yüksek Lisans, Deniz Biyolojisi ve Balıkçılık
Tez Yöneticisi: Prof. Dr. Mustafa Yücel
Ortak Tez Yöneticisi: Dr. Asım Mustafa Mantıkcı

Ağustos 2023, 92 sayfa

Solunum, birincil üretim ile birlikte biyolojik pompayı oluşturan kritik bir süreçtir. Bu çalışmada, Mart 2022 ve Haziran 2022 sezonlarında Marmara Denizi'ndeki farklı konumlardan seçilen istasyonlarda net komünite üretim ve komünite solunumu hızları ölçülmüştür. Net komünite üretimi ve komünite solunumu deneyleri, deniz bilimlerinde görece yeni bir cihaz ve teknik olan fiber optik oksijen sensörleri (OPTODE) kullanılarak in-situ sıcaklıkta in vitro şişe inkübasyonları olarak gerçekleştirilmiştir. Bu çalışmanın önemli yönlerinden biri, komünite solunumu ölçümlerinin su kolonu boyunca hem fotik katmanı hem de haloklin altı katmanı kapsayacak şekilde farklı derinliklerden alınan örneklerle yapılmış olmasıdır. Genel olarak, komunite solunumunun derinlikle birlikte azalan bir eğilimi vardır ve ayrıca komunite solunumu çözünmüş oksijen ve partikül organik karbon ile pozitif yönde ilişkili bulunmuştur. Fotik katmanda ve Mart, 2022'de komünite solunum hızları 0.01-2.05 μmol O_2 L^{-1} sa^{-1} aralığında ölçülürken, Haziran, 2022'de 0.01-1.63 μmol O_2 L^{-1} sa^{-1} aralığında ölçülmüştür. Haloklin altı komunite solunum hızları Mart, 2022 için 89 ± 111mg C m^{-3} $gün^{-1}$ ve Haziran, 2022 için 75 ± 35 mg C m^{-3} $gün^{-1}$ olarak hesaplanmıştır. Net komunite üretim hızındaki istasyonlar arası değişimler

çözünmüş oksijen ve Chl-a ile pozitif yönde ilişkili olarak bulunmuştur. Marmara Denizi için günlük net komunite üretimi kabaca hesaplandığında, sistem özellikle daha az üretken dönemlerde heterotrofik olarak gözlenmiştir.

Anahtar Kelimeler: Solunum, Net Komunite Üretimi, Marmara Denizi, OPTODE

In memory of my uncle,

To every other soul coping with mental illnesses everyday

ACKNOWLEDGMENTS

I am deeply thankful to my PI and co-supervisor, Dr. Mustafa Mantıkcı for giving me the opportunity to conduct this study, and for his guidance, support, criticism and valuable time.

I am deeply grateful to my supervisor, Prof. Dr. Mustafa Yücel for his encouragement and criticism.

I would like to thank my thesis committee members, Prof. Dr. Zahit Uysal and Prof. Dr. Dilek Ediger for their time and evaluation.

I am thankful to Dr. Hasan Örek, the crew of R/V Bilim-2 and cruise participants for their crucial assistance during scientific expeditions.

I am grateful to Dr. Yeşim Ak Örek, Şehmus Başduvar, and all chemistry laboratory members for their technical assistance.

I would like to thank Buse Uysaler, Emel Kocaman and Deniz Eşkinat for their emotional support and friendship. I would like to thank my cousin Hakan Şimşek and his wife, Oya Şimşek for their emotional support during my master's studies.

I am grateful to my parents for their unconditional love, lifelong encouragement and support. Especially, I would like to thank my brother, Barış Kazak, for being my favorite human since his birth. I am also thankful to my cat, Romi, for choosing me as his human.

This work is partially funded by the Scientific and Technological Research Council of Turkey under grant number 121G001 ("Plankton Metabolism and Effects of Mucilage on Oxygen Consumption in the Sea of Marmara", TUBITAK-1001). This study has been supported by DEKOSIM (Center for Marine Ecosystem and Climate Research) and the MARMOD project (Republic of Türkiye Ministry of Environment, Urbanization and Climate Change).

TABLE OF CONTENTS

ABSTRACT v

ÖZ vii

ACKNOWLEDGMENTS x

LIST OF TABLES xiv

LIST OF FIGURES xv

LIST OF ABBREVIATIONS xix

CHAPTER 1

1 INTRODUCTION 1

1.1 General Properties of the Sea of Marmara 1

1.2 Plankton Metabolism 4

1.3 Measurement of Primary Production and Respiration 10

1.4 Aim of the Study 13

CHAPTER 2

2 MATERIAL AND METHODS 15

2.1 Sample Collection 15

2.2 Biochemical Analysis 19

2.2.1 Dissolved Nutrients 19

2.2.2 Chlorophyll-*a* 20

2.2.3 Dissolved Oxygen 20

2.2.4 Particulate Organic Matter 20

2.3 Oxygen Measurements with Fiber Optic Oxygen Sensors (OPTODEs) . 21

2.3.1 Calibration and Performance of OPTODEs 22
2.3.2 Community Respiration Measurements 24
2.3.3 Sub-Halocline Community Respiration Measurements 25
2.3.4 Net Community Production Measurements 26
2.4 Calculation of Rates 29
2.4.1 Calculation of Rates for Community Respiration 29
2.4.2 Calculation of Rates for Sub-halocline measurements 33
2.4.3 Calculation of Rates for Net Community Production 34
CHAPTER 3
3 RESULTS 37
3.1 Physical and Biochemical Properties of the Sea of Marmara during the Sample Collection 37
3.1.1 Surface Nutrients and Dissolved Oxygen Distributions 42
3.1.2 Nutrients and Chlorophyll-*a* Distributions 45
3.1.3 Particulate Organic Carbon 55
3.2 Community Respiration Rates 56
3.3 Sub-Halocline Community Respiration Rates 60
3.4 Net Community Production Rates 67
3.5 Statistics 70
CHAPTER 4
4 DISCUSSION 73
4.1 Parameters towards Eutrophication 73
4.2 Pelagic Plankton Metabolism 74
4.3 Comparison of the Sea of Marmara with other similar systems 77

4.4 Regulation of Plankton Metabolism..... 79

CHAPTER 5

5 CONCLUSION.....83

REFERENCES 85

LIST OF TABLES

TABLES

Table 2.1 Geographical locations of sampling station on Spring 2022 Cruise 16
Table 2.2 Sampling Details (Depth, Experiment type) of Stations of Spring,2022 Cruise.....17
Table 2.3 Geographical location of stations sampled at Summer,2022 Cruise.....18
Table 2.4 Sampling Details (Depth, Sampling Date and Experiment type) of Stations of Summer, 2022 Cruise.....19
Table 2.5 Mean and standard deviation of % air saturation of 30 min of measurement taken after 0% calibration done.....23
Table 2.6 Mean and standard deviation of % air saturation of half an hour of measurement taken after 100% calibration done.....24
Table 2.7 PAR values of each bottle and percentages.....28
Table 3.1 Model results on respiration rate, α (specific turnover rate) value and estimated organic carbon (OC) concentration of corresponding stations and depths for Sub-halocline samples of both of the cruises.....63
Table 3.2 Average temperature and salinity values of samples belongs to different layers as layer 1 (0-10 m), layer 2 (11-20), layer 3 (21-32 m), layer 4 (33-50 m) and layer 5 (100 m). 67
Table 3.3 Maximum NCP, Chl-*a* and NCP_{chl} values for corresponding Stations and Depths for both Spring and Summer Cruises. 68

LIST OF FIGURES

FIGURES

Figure 1.1 Photosynthesis versus irradiance (P-I) curve (Lalli & Parsons, 1993).... 6
Figure 1.2 Number of observations versus Depth range as meters for studies from 1980 to 2002 (Robinson&Williams,2005)..... 9
Figure 2.1 Map of Sea of Marmara showing 11 sampling stations on Spring 2022 Cruise 16
Figure 2.2 Map of the stations that are sampled on Summer,2022 Cruise 18
Figure 2.3 (left) Placement of an oxygen sensor spot into a custom bottle, (right) 4-channel FireSting®-O2 (FSO2-C4) optical oxygen–temperature meters connected with fiber optic cables and Pt100 temperature sensor TSUB21. 22
Figure 2.4 OPTODEs and dark incubator system..... 25
Figure 2.5 Dark Incubator system for Sub halocline samples. 26
Figure 2.6 OPTODEs and temperature controlled linear light on and dark incubator system 27
Figure 2.7 PAR values of each BOD bottles 28
Figure 2.8 Oxygen and temperature measurement example raw data 30
Figure 2.9 Oxygen and temperature measurement example data, first hour of the experiment removed from data due to temperature instability that interrupts quality of measurement to obtain a fine linear section 31
Figure 2.10 Diagnostic plots of linear regression applied to surface of station K39J24 to calculate CR 33
Figure 2.11 Box plot of 8 different channels for measurements and respiration rates taken from that channel..... 35
Figure 3.1 Spring 2022 (28.03 – 01.04) from Dardanelles to İzmit Bay west to east section distributions of Temperature (°C), Salinity (psu), Dissolved oxygen measured by probes in situ (mg/L), Fluorescence (mg/m^3) and Turbidity (NTU). 39

Figure 3.2 Spring 2022 (28.03 – 01.04) north to south section profiles of Temperature (°C), Salinity (psu), Dissolved oxygen measured by probes in situ (mg/L), Fluorescence (mg/m^3) and Turbidity (NTU).....40
Figure 3.3 Summer 2022 (31.05 – 05.06) from Dardanelles to İzmit Bay west to east section distributions of Temperature (°C), Salinity (psu), Dissolved oxygen measured by probes in situ (mg/L), Fluorescence (mg/m^3) and Turbidity (NTU)..41
Figure 3.4 Summer 2022 (31.05 – 05.06) north to south section distributions of Temperature (°C), Salinity (psu), Dissolved oxygen measured by probes in situ (mg/L), Fluorescence (mg/m^3) and Turbidity (NTU).....42
Figure 3.5 Surface distribution maps for Spring,2022 (28.03 – 01.04) for the properties as DO as measured by Winkler's method (µM), PO_4^{3-} (µM), NO_X-N (µM), NH_4^+ (µM), TP (µM), Si, Secchi disk depth (m) and Fluorescence (mg/m^3) 43
Figure 3.6 Surface distribution maps for Summer,2022 (31.05 – 05.06) for the properties as DO measure by Winkler's method (µM), PO_4^{3-} (µM), NO_X-N (µM), NH_4^+ (µM), TP (µM), Si, Secchi disk depth (m) and Fluorescence (mg/m^3) 45
Figure 3.7 Spring 2022 (28.03.2022 – 01.04.2022) from Dardanelles to İzmit Bay west to east section distributions of Chlorophyll-*a* 46
Figure 3.8 Summer 2022 (31.05 – 05.06) from Dardanelles to İzmit Bay west to east section distributions of Chlorophyll-*a*.....47
Figure 3.9 Spring 2022 (28.03.2022 – 01.04.2022) from Dardanelles to İzmit Bay west to east section distributions of NO_X-N (µM), PO_4^{3-} (µM), NH_4^+ (µM), TP (µM), and Si (µM).....48
Figure 3.10 Spring 2022 (28.03 – 01.04) north to south section distributions of NO_X-N (µM), PO_4^{3-} (µM), NH_4^+ (µM), TP (µM), and Si (µM).....49
Figure 3.11 Summer 2022 (31.05 – 05.06) from Dardanelles to İzmit Bay west to east section distributions of NO_X-N (µM), PO_4^{3-} (µM), NH_4^+ (µM), TP (µM), and Si (µM). 50
Figure 3.12 Summer 2022 (31.05 – 05.06) north to south section distributions of NO_X-N (µM), PO_4^{3-} (µM), NH_4^+ (µM), TP (µM), and Si (µM). 51

Figure 3.13 Spring 2022 (28.03 – 01.04) Southern Shelf section distributions of NO_X-N (µM), PO_4^{3-} (µM), NH_4^+ (µM), TP (µM), and Si (µM). 52
Figure 3.14 Summer 2022 (31.05 – 05.06) Southern Shelf section distributions of NO_X-N (µM), PO_4^{3-} (µM), NH_4^+ (µM), TP (µM), and Si (µM). 53
Figure 3.15 Spring 2022 (28.03 – 01.04) İzmit Bay section distributions of NO_X-N (µM), PO_4^{3-} (µM), NH_4^+ (µM), TP (µM), and Si (µM). 54
Figure 3.16 Summer 2022 (31.05 – 05.06) İzmit Bay section distributions of NO_X-N (µM), PO_4^{3-} (µM), NH_4^+ (µM), TP (µM), and Si (µM). 55
Figure 3.17 POC concentrations of corresponding stations and depths on March,2022 and June, 2022. 56
Figure 3.18 Spring, 2022 Cruise CR (µmol O_2 $L^{-1}h^{-1}$) versus Depth (m) plots for all corresponding stations. Bottom depths are given for all stations as BD in short as m. 57
Figure 3.19 Distribution maps for CR rates of corresponding stations shown for 3 separate layers as layer 1 (0-10 m), layer 2 (11-20), and layer 3 (21-32 m) for the spring,2022 cruise. 58
Figure 3.20 Summer, 2022 Cruise CR Rates (µmol O_2 $L^{-1}h^{-1}$) versus Depth (m) plots for all corresponding stations. Bottom depths are given for all stations as BD in short as m. 59
Figure 3.21 Distribution maps for CR rates of corresponding stations shown for 2 separate layers as layer 1 (0-10 m), layer 2 (11-20) for the summer 2022 cruise... 60
Figure 3.22 Spring, 2022 cruise, model fitted plots to show daily change of oxygen (µM) of sub -halocline samples 61
Figure 3.23 Summer, 2022 cruise, model fitted plots to show daily change of oxygen (µM) of sub-halocline samples..... 62
Figure 3.24 Spring, 2022 layer 4 (33 – 48 m) sub-halocline samples respiration rates distribution map..... 64
Figure 3.25 Spring, 2022 layer 4 (35-40 m) and layer 5 (100 m) sub-halocline samples respiration rates distribution map..... 65

Figure 3.26 Bar plot of average CR and CR_{sub} values at layers in both sampling periods. Error bars represent standard deviation. Corresponding layers are as following: layer 1 (0-10 m), layer 2 (11-20), layer 3 (21-32 m), layer 4 (33-50 m) and layer 5 (100 m). Separate cruises shown in different colors.....66
Figure 3.27 Spring, 2022 Cruise PAR (µ einstein $s^{-1}m^{-1}$) versus NCP rate µmol O_2 L^{-1} h^{-1} PI curve fitted plots of corresponding stations and depths.....69
Figure 3.28 Summer, 2022 Cruise PAR (µ einstein $s^{-1}m^{-1}$) versus NCP rate µmol O_2 L^{-1} h^{-1} PI curve fitted plots of corresponding stations and depths.....70
Figure 3.29 CR rates correlation table with depth (m), DO (µM), Chl-*a* (mg/L) and POC (µmol C/L).....71

LIST OF ABBREVIATIONS

ABBREVIATIONS

NCP: Net Community Production

NCP_{chl}: Chlorophyll-*a* normalized Net Community Production

CR: Community Respiration

CR_{sub}: Sub-halocline Community Respiration

DO: Dissolved Oxygen

POC: Particulate Organic Carbon

PAR: Photosynthetically Active Radiation

DOC: Dissolved Organic Carbon

Chl-*a*: Chlorophyll-*a*

CHAPTER 1

INTRODUCTION

1.1 General Properties of the Sea of Marmara

The Sea of Marmara is a semi-enclosed basin with a two-layer counterflow regime and is part of the Turkish Straits System (TSS) with the narrow straits of the Bosporus and the Dardanelles. TSS is connecting the Black Sea and Mediterranean Sea. The Sea of Marmara is 210 km long and 75 km wide, with a total area of 11.500 km^2 and a total volume of 3378 km^3. The Sea of Marmara features three topographic depressions with a maximum depth of 1390 m. The Black Sea outflow dominates the upper layer, which is colder and has a salinity signature of roughly 18 ppt. Higher temperatures and salinity levels of around 38–39 ppt are characteristic of the Mediterranean outflow (Ünlülata et al., 1990; Beşiktepe et al., 1994).

Black Sea-originating, top flow water renews itself in 4-5 months, in contrast to the 6–7 years residence time of the Mediterranean-originating sub-halocline layer (Ünlülata et al., 1990; Beşiktepe et al., 1994). Limited ventilation due to the density gradient of two water masses creates a permanent halocline and stratification at around 25 m. This intermediate layer is where temperature and salinity rapidly change due to vertical mixing (Beşiktepe et al., 1994; Tugrul & Polat, 1995; Tugrul et al., 2002).

Winds, air pressure, water level, and, most significantly, the speed of the flow coming from the Black Sea, called the Bosporus jet, all contribute to the speed of the top flow of the Marmara Sea. The velocity of the jet is mainly affected by the topography of the Bosporus. The flow speed, which is around 50 cm/s at the north

of the Bosporus, reaches 100 cm/s when the width of the Bosporus narrows (Beşiktepe et al., 1994).

The biochemical properties of the Sea of Marmara are intensively affected by the Black Sea and the Mediterranean Sea through TSS. The two-layer flow regime strongly affects dissolved oxygen dynamics and distributions of nutrients (Tuğrul et al., 2002) due to counter-flow water circulation and the permanent halocline which prevents water mass mixing (Besiktepe et al., 1994). A low amount of nutrients characterizes the euphotic zone of the Sea of Marmara at the surface due to high photosynthetic activity that varies seasonally (Polat et al., 1998). Even though Mediterranean water is oligotrophic because of low nutrient input (Yılmaz & Tugrul, 1998; Tugrul et al., 2016; 2018), it is enriched 10–20 times by nutrients coming from the upper layer, and the final nutrient amount is even higher than Black Sea outflow (Tuğrul et al., 1995). The denser Mediterranean water sinks to the bottom and creates the sub-halocline water mass of the Sea of Marmara. Throughout its way to the Bosporus, Mediterranean-originated water loses almost all of its oxygen because of the respiration and decomposition of overproduced organic matter due to eutrophication (Polat et al., 1998; Ediger et al., 2016; Yalçın et al., 2017), and oxygen produced at the surface cannot reach the bottom water.

The Sea of Marmara is a eutrophic basin due to high anthropogenic pressures mainly caused by highly populated industrial areas such as İstanbul and Kocaeli and river discharges to the western Black Sea, particularly from the Danube, Dnieper, and Dniester. Since the Black Sea is nutrient-rich, Black Sea outflow likely contributes to the eutrophication phenomenon (Tuğrul et al., 2014). Fast industrialization and urbanization in the area cause pollution to increase with both industrial discharges and pollution caused by urban settlements (Morkoc & Tugrul, 1995).

The water quality and trophic status of the Sea of Marmara are impacted by the more than 15 wastewater treatment plants found in the Bosporus Strait and along the Sea of Marmara's coastline. The high levels of anthropogenic, industrial, and agricultural

activity and pollutants from the Black Sea that travel via the Bosporus affect the (Arslan-Alaton et al., 2009) pollution level.

The upper layer of the Sea of Marmara has excessive primary production, mainly because of nutrient input from the Black Sea and local anthropogenic sources (Polat & Tugrul, 1995). As a result, chl-*a* concentrations are higher than 1.0 $\mu g L^{-1}$ (Coban-Yildiz et al., 2000). Eventually, eutrophication and limited ventilation caused permanent hypoxia at the bottom layer of the Sea of Marmara (Akçay, 2022). Due to the mineralization of organic matter that has been integrated into the deep layer from the highly photosynthetic surface, the deep layer becomes depleted in dissolved oxygen (< 2 mg l^{-1}) and enriched in inorganic nutrients during the journey of the Mediterranean-originated water from the Dardanelles to the Bosporus in 6-7 years of residence time. That is because deep waters become richer in inorganic nutrients. In the Sea of Marmara, most of the primary production occurs in the upper layer and the halocline. The deep layer is permanently hypoxic, with oxygen concentrations of approximately 50 μM and nitrate concentrations of 9 mmol m^{-3} (Polat & Tuğrul, 1995), in contrast to the upper layer's limited nutrient availability, less than one mmol m^{-3}. In 2019, in Çınarcık Basin, dissolved oxygen concentrations had been found to be less than 7.8 μM. In addition to this, hydrogen sulfide had been detected in January 2019 in Çınarcık Basin and İzmit Bay, indicating a regime shift from oxidative respiration to denitrification and sulfate reduction. Rapid deoxygenation took place from 1995 to 2019 (Akçay, 2022).

As a eutrophication driven event, mucilage (sea snot) has been detected multiple times in the Sea of Marmara since the 1990s. Fishermen were the first to notice something strange happening, but these occurrences have never been systematically studied. In 1992, scuba divers with underwater cameras captured a massive mucilage occurrence in the western section of the Sea of Marmara, near Erdek Bay. For the mucilage incidents were recorded in October 2007 and January 2008; Tübitak-MAM analyzed the phytoplankton composition of the mucilage with environmental variables (Tufekçi et al., 2010). A larger region of the Marmara Sea was covered

with mucilage aggregates in June 2021 than it had been during the 2007 mucilage bloom. When the top 30 m of the water column was studied in addition to the surface waters in June 2021, mucilage was found to cover nearly the whole Sea of Marmara (Yücel et al., 2021).

1.2 Plankton Metabolism

Phytoplankton are unicellular algae capable of photosynthesis and are the dominant photosynthetic organisms in the ocean. Phytoplankton has a central role in marine ecosystems. Their contribution to primary production, carbon sequestration, and global nutrient cycling highlights their ecological importance. Phytoplankton are photoautotrophs, meaning they produce organic matter and oxygen as a side product of photosynthesis using the energy from the photons. This organic carbon and oxygen are consumed throughout the marine food web by heterotrophs, including bacteria, zooplankton, nekton, and benthos (Sigman & Hain, 2012). Nearly half of all global primary production of 36-65 Gt C y^{-1} is produced by phytoplankton (Falkowski et al., 2000; del Giorgio & Duarte, 2002).

Gross primary production (GPP), defined many times (Riley, 1940; Nielsen, 1963; Odum, 1971), is the input of bond energy into the ecosystem. It is also defined as the rate of photosynthesis: the rate of organic carbon or oxygen production (Bender et al., 1987). Net primary production is the substruction of phytoplankton respiration from GPP, and NPP indicates the growing phytoplankton biomass or standing stock. On the other hand, we can obtain net ecosystem production (NEP) or net community production (NCP) by subtracting all respiration performed by both photoautotrophs and heterotrophs, or total ecosystem respiration, from GPP. If we narrow down the boundaries of the ecosystem to the euphotic zone, NEP would be equal to sinking particulate organic carbon and dissolved organic carbon out to the deep ocean. Furthermore, the net quantity of carbon extracted from the atmosphere by the biological pump is the net community production (NCP) (Stanley et al., 2010).

The NCP difference between community respiration and GPP is used to estimate if the system exports or imports carbon. If production exceeds respiration (P>R), meaning positive NCP, the system is autotrophic or exporting carbon. When respiration exceeds production (R>P), a negative NCP indicates a heterotrophic system, thus importing carbon. A system is defined as autotrophic when GPP is larger than CR (i.e., NCP is positive) and as heterotrophic when CR is larger than GPP (i.e., NCP is negative) (Ducklow & Doney, 2013).

The marine food web is supported by organic matter as a product of photosynthesis. The remaining small proportion of organic matter is exported to the deep ocean and only the 1% buried into the sediment (Hedges & Keil, 1995). As a result, CO_2 is captured from the atmosphere and stored in the ocean basin for centuries, referred to as a "biological pump" (Quay et al., 2020).

The chemical reactions of photosynthesis and respiration can be summarized as follows (Lalli & Parsons, 1993):

Photosynthesis (requiring sunlight)

$$\mathbf{6CO_2 + 6H_2O \rightleftharpoons C_6H_{12}O_6 + 6O_2}$$

Respiration (requiring metabolic energy)

Photosynthesis is the conversion of inorganic carbon to organic carbon using solar energy to drive the process. Photosynthesis reduces carbon dioxide to create high-energy organic substances to feed the food web. This process results in the production of free oxygen derived from water molecules. On the other hand, respiration is an oxidative reaction to obtain energy from high-energy organic substances by breaking the high-energy bonds to sustain the metabolism. All kinds of organisms carry out respiration in both light and dark (Lalli & Parsons, 1993).

On the contrary, light and photosynthetic pigments to use solar energy are necessary for photosynthesis. The most abundant photosynthetic pigment is chl-*a*. The maximum absorption wavelength of chl-*a* is red (650-700 nm) and blue-violet (450 nm) (Lalli & Parsons, 1993).

Solar radiation affects the amount and rate of photosynthesis. Photosynthesis increases with photosynthetically available radiation (PAR, 400-700nm); however, photoinhibition occurs at high PAR (Lalli & Parsons, 1993).

Equations to describe the relationship between photosynthesis and PAR (Lalli & Parsons, 1993):

$$P_g = \frac{P_{max}\,[I]}{K_I + [I]} \qquad P_n = \frac{P_{max}[I - I_C]}{K_I + [I - I_C]}$$

P_g: GPP; P_n: NPP; P_{max}: maximal value; [I]: amount of PAR; K_I: half saturation constant; I_C: Compensation PAR

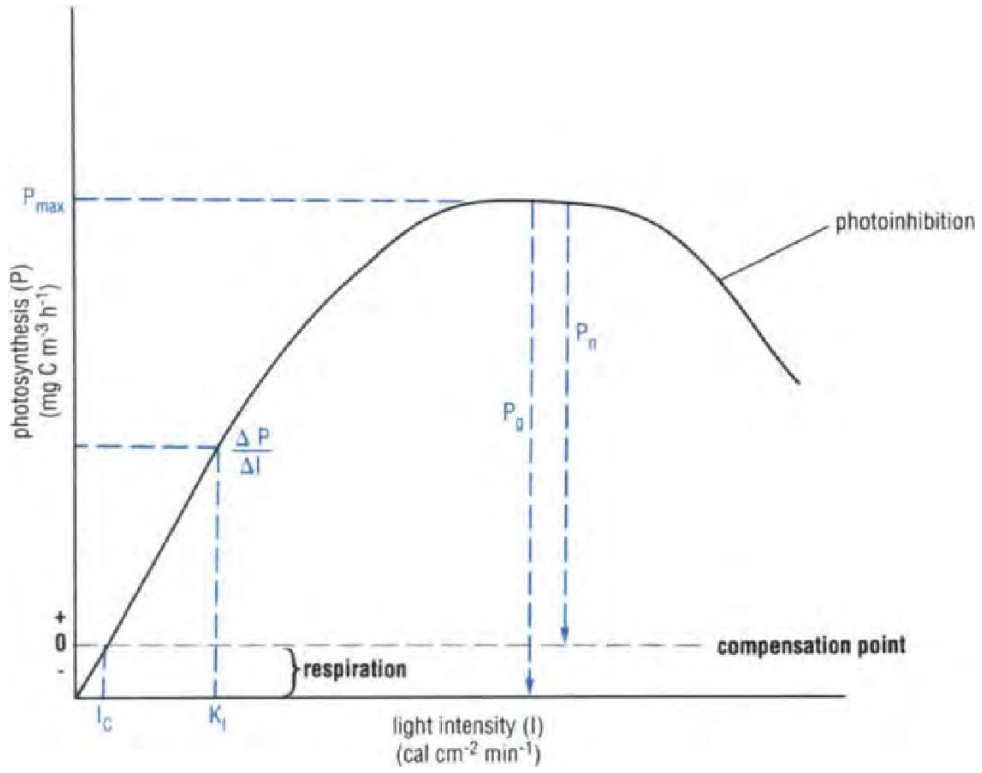

Figure 1.1 Photosynthesis versus irradiance (P-I) curve (Lalli & Parsons, 1993).

Photosynthesis's relationship with PAR depends on P_{max} and K_I values. These values are species-specific and also change with environmental conditions. Compensation

light is the amount of light required to balance the rate of photosynthesis with the rate of respiration in an individual cell. The depth that corresponds to compensation light is called compensation depth. These two are physiological concepts, meaning the rate of photosynthesis and respiration compensate for each other in a phytoplankton cell (Lalli & Parsons, 1993).

On the other hand, critical depth (Sverdrup, 1953) is an ecological concept related to the community of phytoplankton. The total amount of production the phytoplankton community performs adds up to its respiratory loss throughout the water column. The placement of critical depth and mixing depth in the water column designates if there is a net amount of production. Positive net primary production should be expected if the mixing depth is above the critical depth. However, negative net primary production should be expected if the mixing depth is below the critical depth (Lalli & Parsons, 1993).

Primary production is the main process that is closely related to eutrophication. Eutrophication is characterized by the high amount of nutrients coming into coastal marine environments from land-based or atmospheric sources (Nixon, 1995). Eutrophication may have many adverse effects on coastal marine ecosystems, such as hypoxia/anoxia, changes in the food web, and decreased underwater vegetation and water clarity (Conley et al., 2007).

The availability of dissolved oxygen (DO) is essential for the sustainability of marine ecosystems. It is mainly controlled by the biogeochemistry of the particular region of the ocean (Ulloa et al., 2012; Wright et al., 2012; Gilly et al., 2013). Physiochemical properties and, more importantly, plankton metabolism (photosynthesis and respiration) play a crucial role in controlling DO concentrations. DO and organic matter can be produced only in the sunlit surface ocean; however, respiration occurs throughout the water column (Wilson et al., 2017). DO may drop too low levels at deeper parts of the water column, called hypoxia ($DO < 2.0$ mg L^{-1}), due to eutrophication-driven high production and limited ventilation in areas such as the Sea of Marmara (Akçay, 2022).

The respiration rate corresponds to the overall oxidation and decomposition of organic matter and the overall flux of organic carbon in the biota (Williams & del Giorgio, 2005). Respiration can be classified as heterotrophic or autotrophic. Autotrophic respiration is a component of GPP and is only conducted by autotrophs. On the other hand, the distribution of respiration in heterotrophic communities may shed light on how ecosystems operate (Robinson & Williams, 2005). Depending on environmental factors such as nutrient availability, improvements in the rate of photosynthesis at the community level may be followed by increased algal respiration. Phytoplankton community composition can define the relationship between algal respiration and primary production. Thus, there is variability in respiration rates among major algal groups (Raven & Beardall, 2005). Heterotrophic respiration is supported primarily by organic matter from primary production and secondarily by other sources (river discharges, atmospheric inputs, etc.) (Williams & del Giorgio, 2005).

The fact that there are frequently significant migrations of organic matter between different marine ecosystems or within a single ecosystem complicates our understanding of the relationships between respiration and primary production in aquatic ecosystems. No ecosystem is closed; thus, all export and import material is too variable degrees (Williams & del Giorgio, 2005).

Since it incorporates all the numerous sources of organic carbon and the affecting temporal dynamics in its rate, respiration could be the most significant indicator of the flux of organic matter in aquatic ecosystems. As a result, respiration may be used to constrain biogeochemical models of organic matter flow in aquatic ecosystems since it is a reliable indicator of the movement of organic matter in the environment. However, in reality, respiration is derived from models instead of constrained by them. This may be because of the dearth of direct data on respiration or the conventional understanding of respiration as an entirely dependent reaction to production (Williams & del Giorgio, 2005).

From 1980 to 2002, various respiration studies were conducted (Robinson & Williams, 2005 and references therein), with simultaneous measurements of in-situ temperature, chl-*a* concentration, bacterial abundance, particulate organic carbon, light attenuation, and gross production used to support the respiration data if possible. The majority of the data was generated using Winkler's method. Many measurements were conducted at the euphotic zone, and there are a few studies conducted below 100 meters. The number of measurements tends to decrease with depth (Figure 1.2). Additionally, the respiration rate tends to slow down as depth increases (Robinson & Williams, 2005).

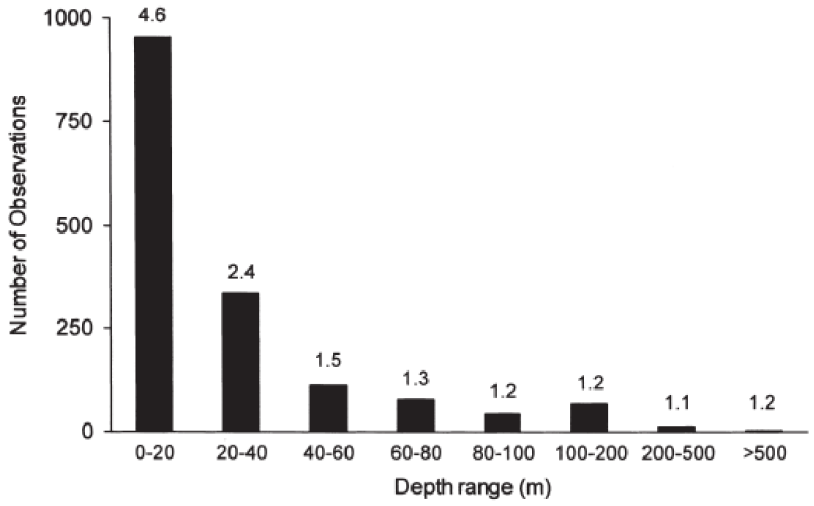

Figure 1.2 Number of observations versus Depth range as meters for studies from 1980 to 2002 (Robinson&Williams,2005)

These studies tried to correlate environmental and biological parameters (bacterial abundance, chl-*a*, beam attenuation, particulate organic carbon (POC), and bacterial and microzooplankton biomass) with respiration. These chemical parameters are less time-consuming to measure, and their measurements are taken more frequently. POC, chl-*a*, standing stock, could be predictors for respiration. However, they were

not enough to fully understand the respiration (Robinson & Williams, 2005 and references there in).

Furthermore, the relationship between photosynthesis and respiration was found to be poor. Even though they are strongly correlated, depth-integrated photosynthesis and respiration have a low correlation (Williams & Bowers, 1999; Serret et al., 2001; 2002; del Giorgio & Williams, 2005). This finding explains the importance of respiration studies because it is hard to estimate respiration by looking at other parameters.

1.3 Measurement of Primary Production and Respiration

Measurement of the rate of the flux of product and/or reactants is one of the several approaches to calculating planktonic respiration and primary production, together with the methods of enzymatic assays, derivation from biomass, and finally inverse modeling of community composition and activity. Oxygen is the reactant for respiration whereas carbon dioxide is the product. For photosynthesis, oxygen is the product whereas carbon dioxide is the reactant (Robinson & Williams, 2005).

The most widely used method is in vitro bottle incubation to investigate the flux of a reactant or product. Dark bottle incubation to measure respiration originated to take respiration into account when evaluating photosynthesis. The determination of photosynthesis requires light bottle incubation. The use of oxygen as a determinant is the most commonly used technique for respiration studies, it accounts for more than 90% of the studies (Robinson & Williams, 2005). However, carbon dioxide (pCO_2) and dissolved inorganic carbon (DIC) are also used to determine respiration rate (Johnson et al., 1983; 1987; Robinson et al., 1999; Robinson & Williams 1999).

Many of the early studies that investigated primary production and respiration in aquatic ecosystems used the Winkler technique, developed by Winkler in 1888, to measure oxygen concentration. This technique was used by Gaarder and Gran (1927) to measure biological oxygen fluxes in sea water to understand photosynthesis and

they used dark bottles (respiration) to correct the photosynthesis measurement. They placed dark and light bottles at different depths in the sea to obtain different irradiances for light bottles for 24 hours and measure initial and final oxygen concentrations. The need to investigate respiration first came with the idea that bacteria may play a major role in carbon cycling in oceans (Romenenko, 1964), contrary to popular belief. In addition, environmental problems such as marine pollution started to rise in the first half of the twentieth century in multiple parts of the world. In situ oxygen concentrations or in vitro bottle incubations are performed to investigate organic matter pollution for environmental reasons (Kolkwitz & Marsson, 1908; Sladécek, 1973).

The Carbon-14 technique was published by Nielsen in 1952 to measure primary production. This development has triggered many studies regarding primary production, on the other hand, respiration studies have been underestimated. Later, fast repetition rate fluorometers enable in situ measurement of primary production from chl-*a* also accelerates primary production studies. If the rate of primary production remained constant, the number of plankton might be used to compare the productivity of plankton. However, this is not the case; instead, environmental elements like temperature, light, nutrient availability, and species composition have a large impact on the rate of production (Nielsen, 1952).

The Carbon-14 technique is widely used in primary production studies. However, the Carbon-14 technique is not suitable to measure the rate of respiration (Nielsen, 1952). There is an unresolved debate on what the Carbon-14 technique measures; GPP, or NPP, or most probably something in between. It is possibly gets close to NPP when production rate is high and gets close to GPP when production rate is low (del Giorgio & Williams, 2005).

There are various methods to measure NCP. The most common one is the calculation of rates for GPP and respiration in pelagic communities. By subtracting respiration from GPP, NCP can be calculated (van Es, 1977; Garside & Malone, 1978; Jassby et al., 1993). Another method is to measure diel and seasonal changes of inorganic

carbon (DIC) or oxygen pools for the entire water column (Odum, 1956; Kenney et al., 1988; Howarth et al., 1996). Alternatively, biogeochemical models can be used to calculate NCP (Nixon & Pilson, 1984; Smith et al., 1991).

Additionally, there are few direct estimates of NCP for coastal ecosystems that suggest net annual heterotrophy for productive systems (Smith & Hollihaugh, 1993; Kemp et al., 1997). It is expected that organic matter will be transported from net autotrophic ecosystems to net heterotrophic ecosystems (Heath, 1995). In this study, direct measurements of NCP were taken to reveal net heterotrophy or net autotrophy of the Sea of Marmara.

Coated platinum cathodes that were developed for use in physiology were improved for use in marine sediment as Clark-type oxygen microelectrodes with enhanced measurement specifications. The main problem with Clark-type electrodes is their relatively long construction time and their usage demands a high amount of training. Although the construction of cathode-type sensors is less constraining, they are less preferable due to their fewer measuring properties. Commercially available oxygen microsensors had these limitations back in time, which created the need for alternative oxygen sensors that better suit aquatic environments. Optical sensors (OPTODES) that have undergone rapid development (Klimant et al., 1995). Optical fiber illuminates the sample, and OPTODES collects back transmitted light. From its parameters, such as intensity, polarization, and spectral distribution, analyte concentrations can be calculated. In contrast to oxygen electrodes, oxygen optodes don't use oxygen, and the signal is independent of flow rate. In addition, optode sensors are not affected by electromagnetic fields. High CO_2 and H_2S concentrations did not have an impact on the signal of oxygen optodes, contrary to Clark-type electrodes. Moreover, respiration and production measurements conducted by optodes have enhanced precision, though they are very sensitive to temperature. (Klimant et al., 1995 and references there in). Later on, optodes start to be used in aquatic science, including the measurement of photosynthesis and respiration rates (Mantikci et al. 2017; Vikström et al., 2020). However, it is still a relatively new and innovative method. Optodes allow us to take continues measurement without losing

sample for further chemical investigation as in the Winkler technique. Measurements with optodes can be conducted with less amount of sample. Discrete measurements, as used in this study for sub-halocline samples, can be conducted without removing sample for Winkler analysis. This is advantageous because it required less sample and may result in less bottle effect.

1.4 Aim of the Study

The Sea of Marmara is a eutrophic basin that has experienced hypoxia for decades. Studying pelagic metabolism is an excellent choice to reveal oxygen dynamics and the carbon cycle of the Sea of Marmara. Innovative methods used in this study are fiber optic oxygen sensors (optodes), which enable experimentation of photosynthesis and respiration to quantify NCP, CR and CR_{sub} in the Sea of Marmara. Respiration is understudied globally and environmental and biological parameters are not fully representing respiration rates. This thesis work covers the gap of knowledge on CR and NCP rates in the Sea of Marmara. This study aimed to quantify CR and NCP rates in the Sea of Marmara.

This thesis is constructed around these fundamental questions in order to achieve the following objectives:

1. Assessment of the spatial change of net community production and community respiration rates in the Sea of Marmara during the spring and summer 2022 seasons.
2. Determination of community respiration rates through the water column in the photic zone and sub-halocline during the spring and summer 2022 seasons.
3. Characterization of ecosystem metabolism for the Sea of Marmara.

CHAPTER 2

MATERIAL AND METHODS

2.1 Sample Collection

Net community production (NCP), community respiration (CR), and sub-halocline community respiration (CR_{sub}) measurements were performed with water samples from the Sea of Marmara. Samples were collected from two separate expeditions in Spring 2022 (27.03.2022 – 01.04.2022) and Summer 2022 (31.05.2022 – 05.06.2022) using the R/V Bilim-2 of METU-IMS. Physical parameters were measured in situ with a CTD (conductivity, temperature, depth) probe (SEABIRD). Samplings were collected with the 12-Niskin bottle Rosette System coupled with CTD. The Rosette System allows the closure of Niskin bottles at desired depths via remote control. Fluorescence, turbidity and oxygen data were continuously recorded in situ throughout the water column by sensors placed on the CTD probe. Moreover, samples for biochemical analysis (dissolved oxygen, dissolved nutrients, particulate organic matter and chl-*a*) were collected for further analysis at the laboratories of R/V Bilim-2 or METU-IMS laboratories. Secchi disk depth measurements were done for each station during the daytime.

In Spring 2022 cruise, water samples were collected from 11 stations (Figure 2.1, Table 2.1 and Table 2.2). On the Spring 2022 Cruise, water samples were collected from the surface water of 7 stations for the NCP experiments. For the CR experiments, samples were collected from all 11 stations and sub-halocline samples were collected from 10 stations as two replicates.

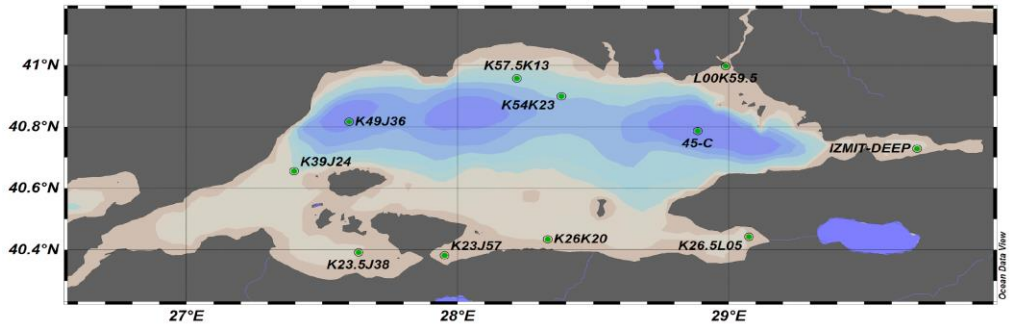

Figure 2.1 Map of Sea of Marmara showing 11 sampling stations on Spring 2022 Cruise

Table 2.1 Geographical locations of sampling station on Spring 2022 Cruise

	Location of Stations on Spring 2022 Cruise		
No	**Station**	**Longitude (E)**	**Latitude (N)**
1	K23.5J38	27.6351204	40.3916016
2	K49J36	27.5994701	40.8161507
3	K39J24	27.3974991	40.65588
4	K26.5L05	29.0743408	40.4425812
5	K26K20	28.3323593	40.4344788
6	K23J57	27.9515095	40.3824997
7	K57.5K13	28.2185898	40.9570503
8	L00K59.5	28.9892292	40.9968987
9	K54K23	28.3828697	40.8989601
10	45−C	28.8857708	40.7860107
11	IZMIT−DEEP	29.6948605	40.7281609

Table 2.2 Sampling Details (Depth, Experiment type) of Stations of Spring,2022 Cruise

Sampling Details of Stations on Spring,2022 Cruise					
No	**Station**	**Sampling Date**	**Depth (m) of samples**		
			NCP	**CR**	**CR_{sub}**
1	K23.5J38	28.03.2022	**0**	**0;15;30**	**39**
2	K49J36	28.03.2022	**0**	**0;15**	**40**
3	K39J24	28.03.2022	**-**	**0;15;32**	**-**
4	K26.5L05	29.03.2022	**-**	**0;13**	**42**
5	K26K20	29.03.2022	**0**	**0;10;30**	**47**
6	K23J57	29.03.2022	**0**	**0;16;29**	**39**
7	K57.5K13	30.03.2022	**0**	**0;9;24**	**48**
8	L00K59.5	30.03.2022	**-**	**0;8;20**	**33**
9	K54K23	30.03.2022	**-**	**0;15**	**42**
10	45−C	31.03.2022	**0**	**0;8;16**	**40**
11	IZMIT−DEEP	1.04.2022	**0**	**0;10;25**	**45**

The map that shows the 7 Stations of the Summer 2022 Expedition is given in Figure 2.2. Geographical locations and sampling details of the Summer 2022 Cruise are listed in Table 2.3 and

Table 2.4, respectively. On the Summer 2022 Cruise, samples were collected from all 7 Stations for NCP experiments. Samples were collected from the all 7 Stations as two replicates for CR experiments. For the sub-halocline experiment samples were collected from 4 Stations as two replicates. Stations were reduced from 11 to 7 from

Spring to Summer cruise. However, in both cruises, stations were selected to represent the entire Sea of Marmara.

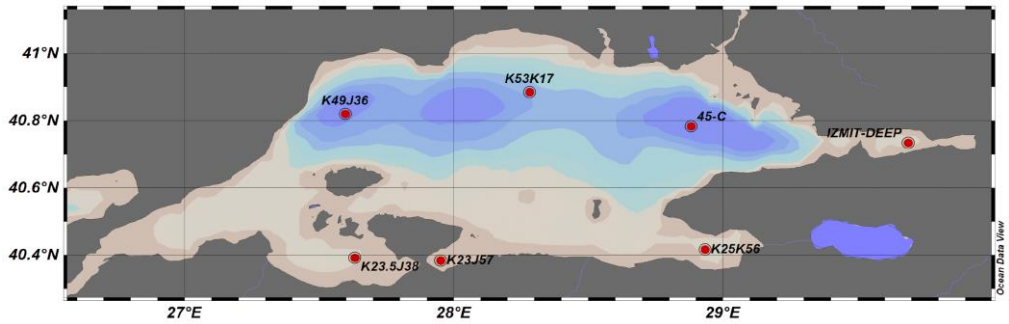

Figure 2.2 Map of the stations that are sampled on Summer,2022 Cruise

Table 2.3 Geographical location of stations sampled at Summer,2022 Cruise

Location of Stations on Summer,2022 Cruise			
No	**Station**	**Latitude (N)**	**Longitude (E)**
1	K23.5J38	27.6323204	40.3920097
2	K49J36	27.5973606	40.8195305
3	K23J57	27.9505997	40.3841095
4	K25K56	28.9326305	40.4170113
5	K53K17	28.2821293	40.8850403
6	45−C	28.8816109	40.78368
7	IZMIT−DEEP	29.6876106	40.7340202

Table 2.4 Sampling Details (Depth, Sampling Date and Experiment type) of Stations of Summer, 2022 Cruise

Sampling Details of Stations on Summer,2022 Cruise					
No	**Station**	**Sampling Date**	**Depth (m) of samples**		
			NCP	**CR**	**CR_{sub}**
1	K23.5J38	1.06.2022	**0;15**	**0;15**	**-**
2	K49J36	1.06.2022	**0**	**0;17**	**40;100**
3	K23J57	2.06.2022	**0;8**	**0;8**	**-**
4	K25K56	2.06.2022	**0**	**0;17**	**40;100**
5	K53K17	3.06.2022	**0**	**0**	**-**
6	45−C	4.06.2022	**0**	**0,19**	**40;100**
7	IZMIT−DEEP	5.06.2022	**0**	**0;15**	**35;100**

2.2 Biochemical Analysis

2.2.1 Dissolved Nutrients

The dissolved inorganic nutrients in the sea water, including NO_3^- + NO_2^-, NO_2^-, NH_4^+, PO_4^{3-}, and Si were analyzed using colorimetric methods (Grasshoff & Ehrhardt, 1983). Nutrient analysis was conducted in the METU-IMS laboratory using a Technicon A II Model four-channel autoanalyzer (SEAL Analytical). Seawater samples were collected into pre-washed with diluted HCL 100 mL plastic (HDPE) bottles. Silicate samples were preserved in the fridge whereas phosphorus and nitrate samples were preserved in the freezer until analysis. The detection limits

for the nutrients were found to be 0.05μM for NO_3^- + NO_2^-, 0.05μM for NO_2^-, 0.04μM for NH_4^+, 0.015 μg/L for PO_4^3-, and 0.05 μM for Si.

2.2.2 Chlorophyll-*a*

The concentration of chlorophyll-*a* (Chl-*a)* was determined using the spectrofluorometric method (Strickland & Parsons, 1972) using a HITACHI model F-2500 Fluorescence Spectrophotometer at the METU-IMS laboratory. Samples were taken into dark plastic containers from Niskin bottles. These 1-5 liter of water samples were filtered onto 45 mm Whatman filters (GF/F). Filters were preserved in the dark and frozen until the analysis. Chl-*a* was extracted in a 3 ml 90% (v/v) acetone solution by ultrasonication for 30 seconds. Samples were measured at 420 nm excitation and 669 nm emission wavelengths. A standard linear equation was generated by at least five known Chl-*a* standards to calculate the Chl-*a* concentrations of the samples.

2.2.3 Dissolved Oxygen

The automated Winkler titration method was used to determine the dissolved oxygen concentrations in seawater onboard. Samples were taken into BOD borosilicate bottles by a rubber hose connected to a Niskin bottle without letting air bubbles form. Manganese precipitates that occur proportional to the oxygen amount in the bottle are degraded with acid addition and undergo a reaction with added iodine solution. This iodine was titrated with a thiosulfate solution. The titration equivalence point is determined automatically.

2.2.4 Particulate Organic Matter

GF/F filter papers should be burned at 450-500 °C for an hour to oxidize the organic matter inside the filter before being used. Samples were taken into dark

plastic containers from Niskin bottles. These 5–10-liter seawater samples were filtered immediately with low suction, later, they were washed with 5-10 ml distilled water and preserved in sterile petri dishes in the freezer. Analysis was conducted at the METU-IMS laboratories using the Elementar Vario El Cube model CHN device. Frozen samples were dried at 50 – 60 °C, then placed in an HCL stream for a short while to remove carbonates. Later, they were vacuumed in adesiccator, dried again and cut into 4-5 pieces each containing 15-20 mg to place into tin capsules and seal. After placement on the device the samples went down to the oxidizing colon and were heated up to 1020 °C with the help of oxygen. The TCD detector quantitively measured the generated carbon and nitrogen. Finally, organic carbon and organic nitrogen were calculated.

2.3 Oxygen Measurements with Fiber Optic Oxygen Sensors (OPTODEs)

Oxygen concentrations for the analysis of plankton metabolism (oxygen production-consumption) were measured using the 4-channel FireSting®-O2 (FSO2-C4) OPTODE (PyroScience) (Figure 2.3, right). FireSting has four fiber optic cables that can be connected to oxygen sensor spots. Temperature compensation of the oxygen measurements was done with the Pt100 temperature sensor TSUB21 (PyroScience), connected to FireSting. The software Pyro Workbench automatically arranges temperature compensation for the oxygen measurements. NCP, CR and CR_{sub} measurements with OPTODEs were performed according to the protocol described in Mantikci et al. (2017).

Oxygen Sensor Spots (PyroScience, OXSP5) were used as optical oxygen sensors. These sensors were carefully placed inside 60 - 150 ml borosilicate glass custom bottles without letting air bubbles form (Figure 2.3, left).

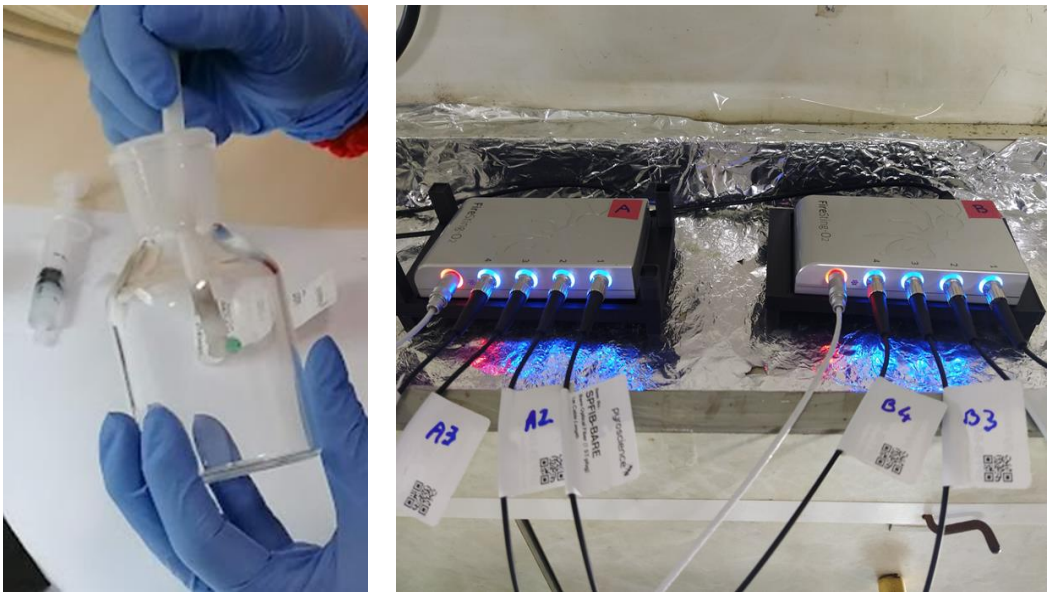

Figure 2.3 (left) Placement of an oxygen sensor spot into a custom bottle, (right) 4-channel FireSting®-O2 (FSO2-C4) optical oxygen–temperature meters connected with fiber optic cables and Pt100 temperature sensor TSUB21.

2.3.1 Calibration and Performance of OPTODEs

Two-point calibration were performed for all sensors. For upper calibration, 100% air saturated water was used. To prepare 100% air saturated samples, an air pump was employed to aerate distilled water for 10 minutes at the desired temperature. Then the aerated bottle was left to equilibrate with air for a couple of minutes. Distilled water was gently poured into the sensor attached bottles and again were remained rested before calibration. For 0% oxygen calibration, OXYCAL (PyroScience) calibration capsules containing sodium sulfite were used to obtain a supersaturated solution for the consumption of oxygen inside the bottles.

OPTODEs have an optimum measuring range of 0-250% air saturation. With 2-point calibration, at 5% air saturation and 95 % air saturation, sensor measurements have an accuracy of ±0.1% a.s. and ±1% a.s. respectively, with a detection limit of 0.1% a.s.. These values were retrieved from the manufacturer's sensor specifications manual.

In order to know the sensitivity of the sensors after calibration, measurements were taken at 100% and 0% air saturation for 30 min. at constant temperatures. Average values of 30 min. measurements and standard deviation values are shown in Table 2.5 and Table 2.6 respectively.

Table 2.5 Mean and standard deviation of % air saturation of 30 min of measurement taken after 0% calibration done.

Sensor No	**Mean Temperature (°C)**	**Mean % Air Saturation**	**SD**
1	11.62	-0.002	0.006
2	11.62	-0.001	0.006
3	11.62	0.002	0.005
4	11.62	0.005	0.005
5	11.90	-0.002	0.008
6	11.90	0.004	0.006

Table 2.6 Mean and standard deviation of % air saturation of half an hour of measurement taken after 100% calibration done.

Sensor No	Mean Temperature (°C)	Mean % Air Saturation	SD
1	10.72	100.12	0.064
2	10.72	99.95	0.048
3	10.72	99.75	0.083
4	10.72	99.59	0.076
5	10.76	99.99	0.060
6	10.76	99.83	0.066

2.3.2 Community Respiration Measurements

CR measurements were conducted in the Biology Lab of R/V Bilim 2 in a dark incubator with temperature-controlled water circulation inside (Figure 2.4). Samples were measured as two replicates, incubation lasted 4 hours; and oxygen measurements were recorded continuously per minute. During the experiment, magnetic beans were placed into the glass bottles, and a magnetic stirrer was placed below the incubator to achieve well mixed samples and improve the accuracy of the oxygen measurement.

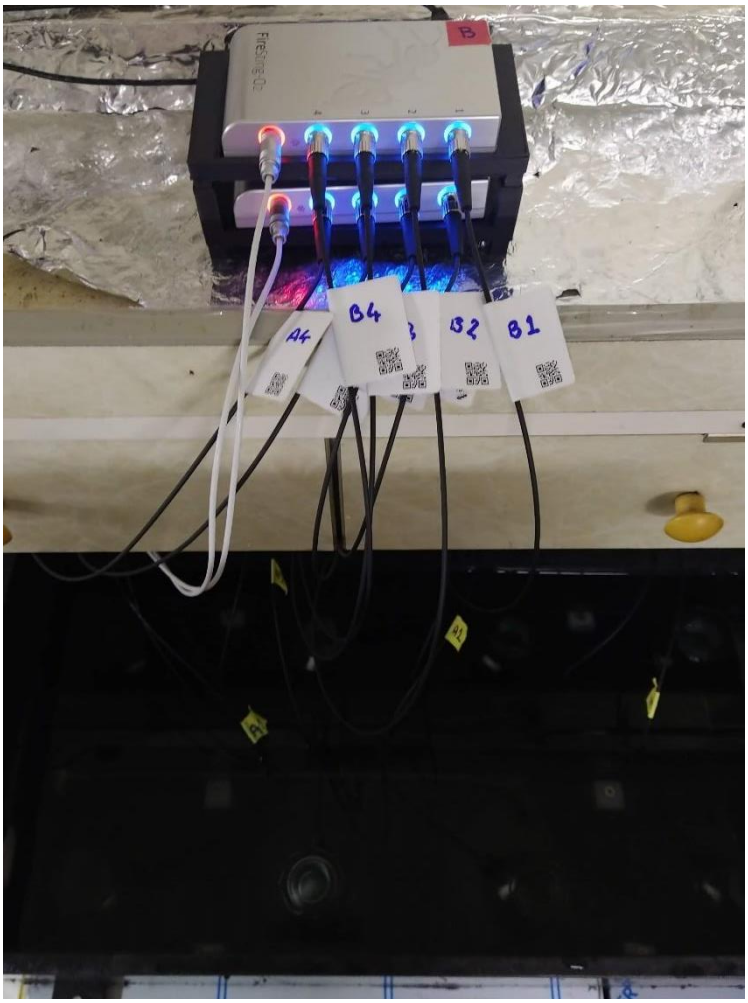

Figure 2.4 OPTODEs and dark incubator system

2.3.3 Sub-Halocline Community Respiration Measurements

Sub-halocline samples were incubated for 3-7 weeks, and oxygen measurements were recorded on a weekly basis, as every second for 5 minutes. The average of 5-minute measurements was logged as the oxygen measurement for the specific day. The incubator temperature was set to 15.4 °C, close to the sub-halocline water temperatures of the Sea of Marmara.

Figure 2.5 Dark Incubator system for Sub halocline samples.

2.3.4 Net Community Production Measurements

NCP measurements were conducted in the Biology Lab of R/V Bilim 2 using a custom-build temperature-controlled light - dark incubator. This custom-designed incubator has eight slots for samples, and each space has a different PAR irradiance due to differences in distance to the light sources and placement of light filters (Figure 2.6). NCP samples were taken as one replicate for each PAR irradiance. Figure 2.7 and

Table 2.7 show the PAR irradiances for each bottle. PAR irradiances in each bottle were measured using a PAR Sensor (Biospherical Instruments Inc.). Temperature-

controlled water circulation inside the incubator provided in-situ temperature conditions. Nitrogen gas was purged into the bottles before the oxygen measurements if oxygen saturation was 100% or above to obtain reliable oxygen production. During the experiment, magnetic beans were placed into the glass bottles, and a magnetic stirrer was placed below the incubator to achieve well-mixed samples and improve the accuracy of oxygen measurements. Incubation lasted for 2 hours, and oxygen measurements were recorded continuously per minute. The initial 30 minutes of measurements were omitted as unstable measurements were observed due to temperature differences.

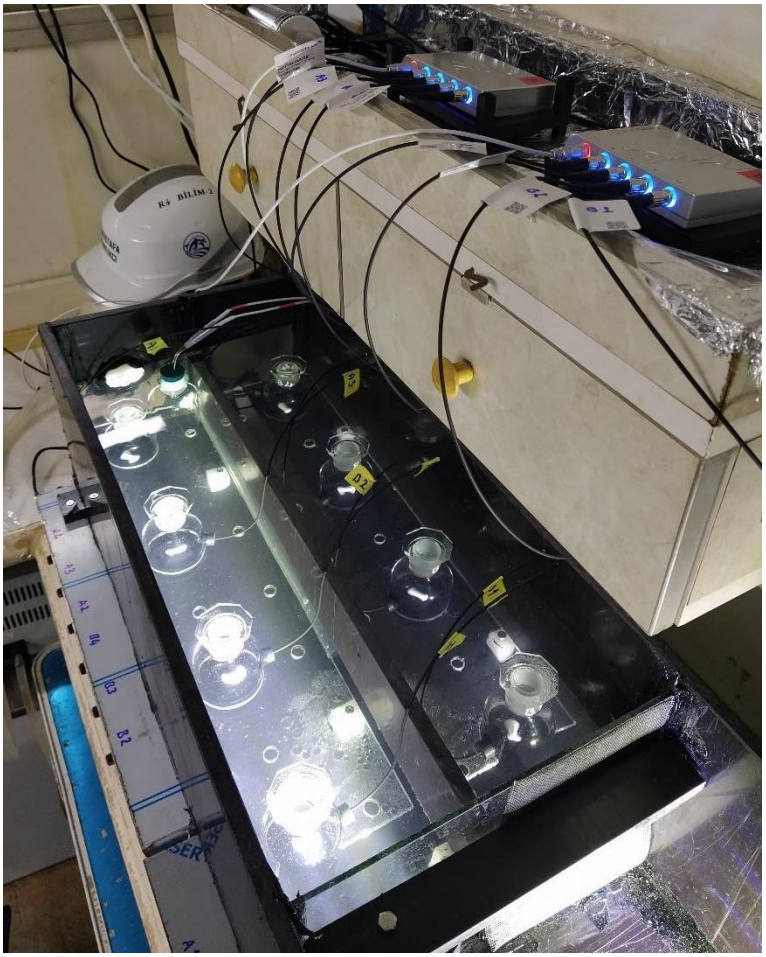

Figure 2.6 OPTODEs and temperature controlled linear light on and dark incubator system

Table 2.7 PAR values of each bottle and percentages.

PAR values		
Slots-Bottle Numbers	**PAR (μ einstein s^{-1} m^{-2})**	**PAR (%)**
1	963	100
2	598	62
3	305	32
4	170	18
5	101	10
6	50	5
7	27	3
8	16	2

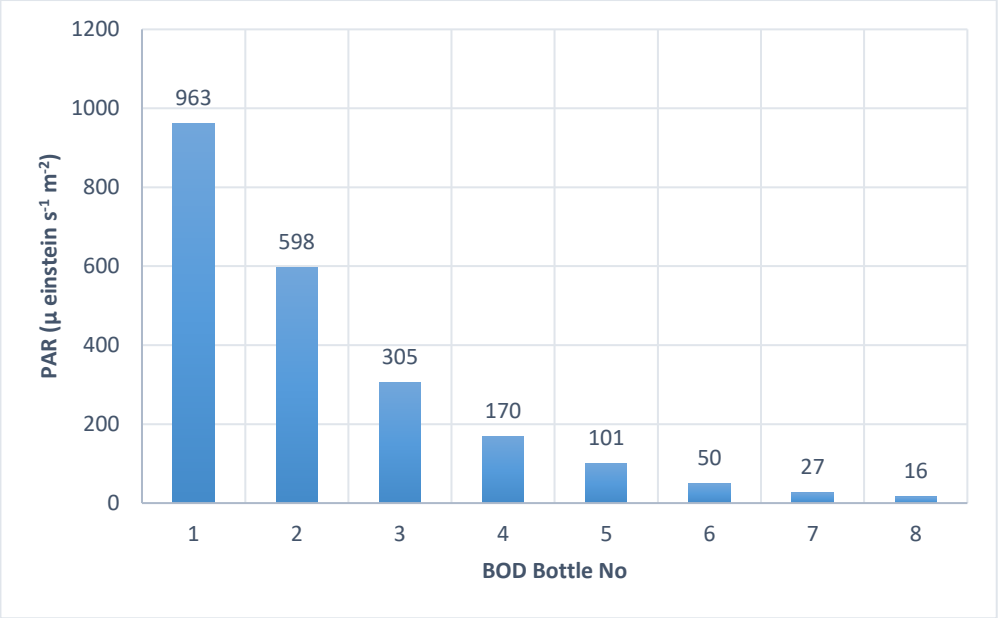

Figure 2.7 PAR values of each BOD bottles

2.4 Calculation of Rates

2.4.1 Calculation of Rates for Community Respiration

Rates of NCP and CR were calculated by a linear regression analysis of O_2 concentration versus incubation time. Raw O_2 data was examined for unstable oxygen measurements, and where necessary, data was corrected or deleted for an accurate rate calculation. Linear regression analysis is performed with the R base package. R^2 and p values were calculated for linear regression. Also, model checking was performed via model checking plots, which are plots of residuals against fitted values; a scale–location plot of √|residuals| against fitted values; a normal quantile-quantile plot; a plot of residuals against leverages. Example of raw oxygen and temperature measurement (Figure 2.8) and corrected and linear regression applied data are shown in (Figure 2.9).

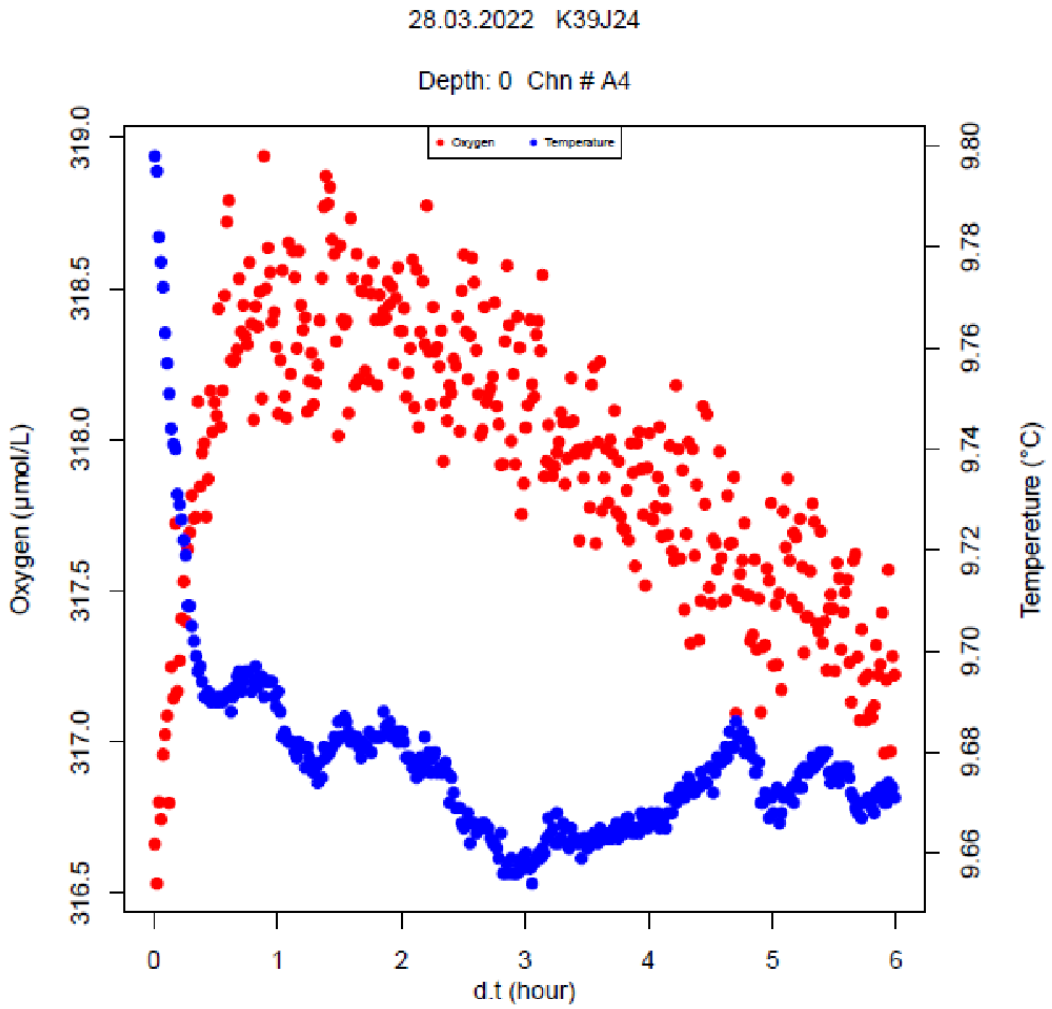

Figure 2.8 Oxygen and temperature measurement example raw data

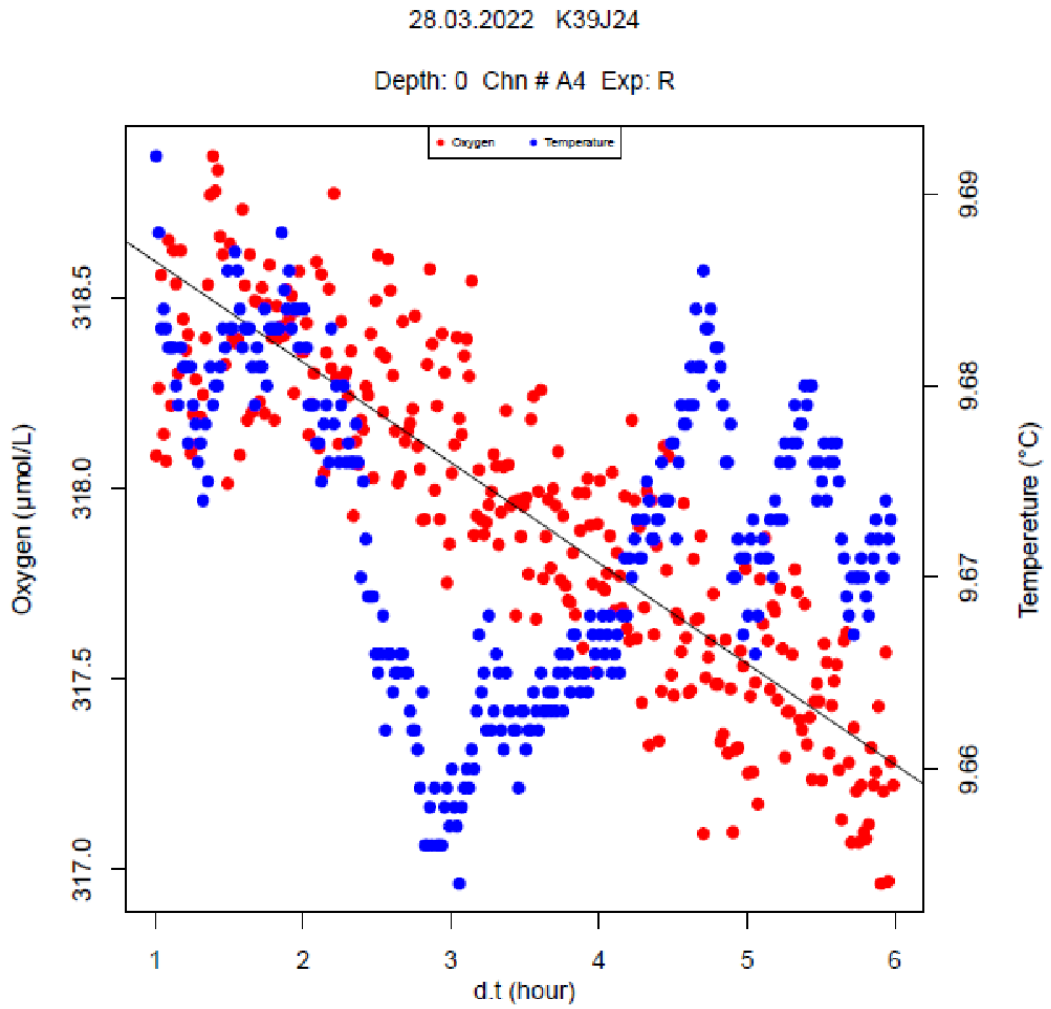

Figure 2.9 Oxygen and temperature measurement example data, first hour of the experiment removed from data due to temperature instability that interrupts quality of measurement to obtain a fine linear section

The linear regression model of corrected data was checked with model checking or diagnostic plots shown in

Figure 2.10. The residual vs. fitted plot is a useful graphical tool for assessing a regression model's goodness of fit and identifying potential outliers. Residuals should be randomly distributed around zero. There should be no apparent pattern. In our example case, there was no solid pattern for disrupting the fit of the regression

model. A normal QQ plot is a valuable tool for assessing a dataset's normality assumption and detecting potential outliers. In a normal QQ plot, if the points in the plot lie close to the diagonal line, it indicates that the data is normally distributed, as in our example plot. If there was an S-shape or banana shape pattern, it would have problems. The scale-location plot helps to evaluate how well the model satisfies the constant variance assumption. The plot shows the square root of the absolute residuals (vertical axis) against the fitted values (horizontal axis). We expect randomly distributed points around a horizontal line at a constant value. In our example case, there is no firm pattern as it is supposed to be. The residuals vs. leverage plot help to evaluate how much impact individual data points have on the regression model or which data points have the leverage to impact more the model coefficients. The plot shows the standardized residuals (vertical axis) against the leverage values. The points on the residuals vs. leverage plot should be randomly distributed, and most points should be close to the horizontal line at zero. Having points beyond Cook's distance is not good, meaning highly impactful data points. With this model checking plots, we are able to say that our example case, the sample from the surface of K39J24 from March Cruise, is well fitted to its linear regression model. (Crawley, 2010; Dalgaard, 2008).

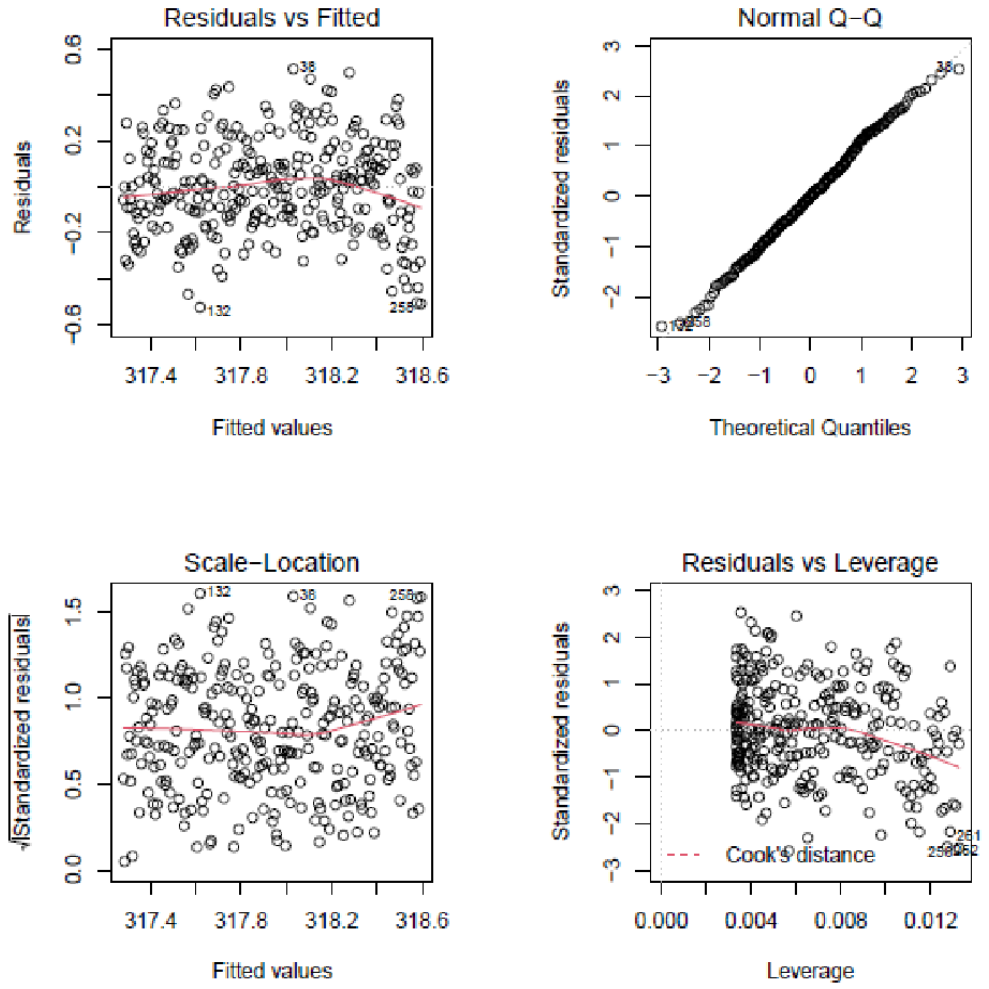

Figure 2.10 Diagnostic plots of linear regression applied to surface of station K39J24 to calculate CR

2.4.2 Calculation of Rates for Sub-halocline measurements

After obtaining average oxygen measurements for certain days for each sample, an exponential model was used to estimate the rate of organic matter decomposition from the oxygen consumption rate (Hansen & Bendtsen, 2014). You may see the model below:

$$O_2(t) = O_2(t_0) - \eta_{O2:C}\, OC(t_0)\, (1 - \exp^{(-\alpha t)})$$

$O_2(t_0)$: initial O_2 concentration, ηO_2:C = 1.2 (remineralization ratio of between O_2 and organic carbon), OC: Initial Organic Carbon Pool, t: time, α: specific turnover rate

Later CR_{sub} rates were calculated as 12* α* OC as in mg C m^{-3} day^{-1} unit by using 1:1 quotient between oxygen and carbon.

2.4.3 Calculation of Rates for Net Community Production

The NCP rate calculation follows the same steps as the rate calculation for CR described in section 2.4.1 above.

Later, CR rates were taken into account as 0 PAR irradiance measurements to conduct the PI curve and calculate maximum the NCP. For Spring 2022 samples, dark and light on experiments were conducted separately. However, in Summer 2022 Cruise for those sampled for NCP, the light was turned off after 2 hours and CR measurements were taken after the NCP measurement. As a result, for summer 2022 measurements, we have 8 replicates of PAR 0 measurements instead of 2 replicates of Spring 2022 cruise samples. For PI curve construction, 2 replicates of the dark measurement from Spring 2022 Cruise both used as separate measurements. However, the mean of 8 replicates of dark measurement from Summer, 2022 Cruise used as PAR level 0 measurement. ANOVA (Analysis of Variance) was performed to check if there was a significant difference in the means of the groups by comparing 8 channels and respiration rates. P value was more than 0.05, fail to reject the null hypothesis. There is no significant difference between the groups. Figure 2.11 below shows a box plot of 8 different slots for measurements and respiration rate.

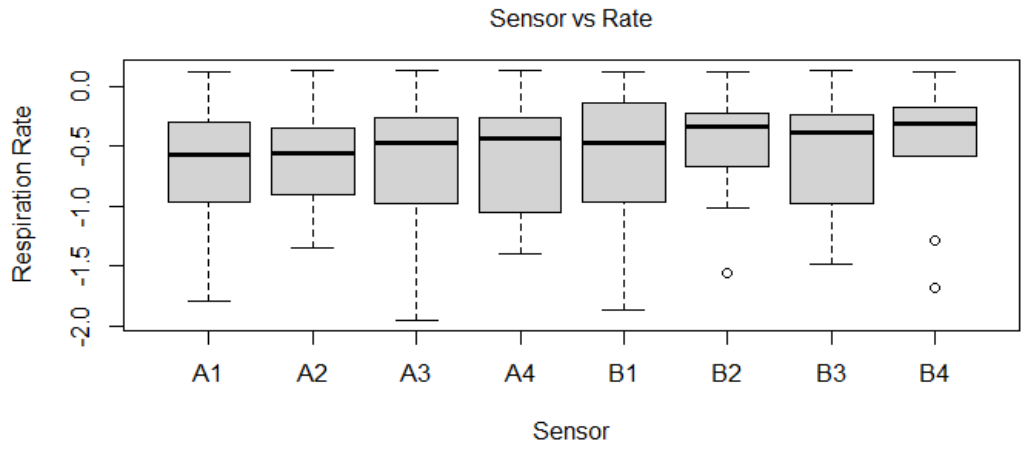

Figure 2.11 Box plot of 8 different channels for measurements and respiration rates taken from that channel.

Saturating exponential model is used to calculate net primary production parameters (Webb et al., 1974). This model was modified by adding an intercept (int) to include respiration below the compensation point (Nielsen & Hansen, 1958).

$$\mathbf{NCP = NCP_{est} * (1 - exp^{(-\alpha * I/NCPest)})+int}$$

NCP: Net Community Production Rate, NCP_{est}: Net Community Production Estimate, I: Irradiance, int: intercept, α: initial slop

Parameters are estimated, and PI curves are constructed via nonlinear curve fitting using the R base package. The NCP_{max} value is calculated as NCP_{est} + int, then chlorophyll normalized values calculated as NCP_{chl} by dividing NCP_{max} to Chl-*a*. NCP_{max} as in μmol O_2 L^{-1} h^{-1} unit converted to mg C m^{-3} day^{-1} unit by using a 1:1 quotient between oxygen and carbon.

CHAPTER 3

RESULTS

3.1 Physical and Biochemical Properties of the Sea of Marmara during the Sample Collection

Temperature, salinity, dissolved oxygen, fluorescence and turbidity were measured continuously by sensors attached to Rosette System coupled with CTD. Spatial changes of these properties in the sea of Marmara are shown below (Figure 3.1, Figure 3.2, Figure 3.3, Figure 3.4) as west – east section and north – south section during spring 2022 Cruise (28.03 – 01.04) and summer 2022 Cruise (31.05 – 05.06) for the first 100 meters of depth. Surface salinity values were about 24 psu and 23 psu in the spring and summer, respectively. Permanent halocline was observed during both sampling seasons between ~20-35m in all areas of the Sea of Marmara. Halocline starting depth was shallower in summer (~20m) than in spring (~25m). Below the halocline up to 100 m, salinity distribution was homogenized in all of the Sea of Marmara and values were around 39 psu. Surface water temperatures varied between 7.05 °C and 11.5 °C in spring. Subsurface temperature minima (7.5 °C) were observed between 20-30 m. In summer, surface mixed layer temperatures were variable and observed between 13.8 and 24.06 °C. Clear temperature minima (9 °C) observed at halocline. In both sampling seasons, below the halocline up to 100m temperature values were almost constant (~15.4 °C). The dissolved oxygen concentrations varied considerably in the water column at both sampling seasons and sections. The oxygen concentration was between 0.1-12.2 mg/L in the entire water column until the offshore of Dardanelles-Biga Peninsula in the spring. Surface dissolved oxygen measured in situ by probes attached to CTD, varies within the 9.7 – 14.8 mg/L range. The deeper parts of the western basin were more oxygenated in

the summer compared to the spring. There was a clear decreasing pattern in dissolved oxygen concentrations from west to east.

Fluorescence values in the euphotic surface mixed zone varied from 0.3 to 12.25 ug/l in Spring 2022 and from 0.01 to 6 ug/l in Summer 2022 (Figure 3.1). Relatively high values (>5 ug/l) observed in İzmit Bay, Çınarcık and Central Basins where Bosporus Jet was effective. In the south-north section, values were higher on the southern than the northern shelf. Generally, maximum values of fluorescence were observed between the surface and 20 m.

In this particular area, above the halocline, dissolved oxygen was high, as indicated by the fluorescence data, as a result of an increase in the biomass of phytoplankton and primary production amount due to nutrient input from Bosporus jet. However, when examining the dissolved oxygen section profile at sub-halocline, it is observed that the western part of the Marmara Basin was more oxygenated than the eastern part.

Turbidity values in the euphotic surface mixed zone varied from 0.13 to 2.4 in Spring 2022 and from 0.0 to 3.2 in Summer 2022 (Figure 3.1). In both of the cruises, İzmit Bay has the highest turbidity.

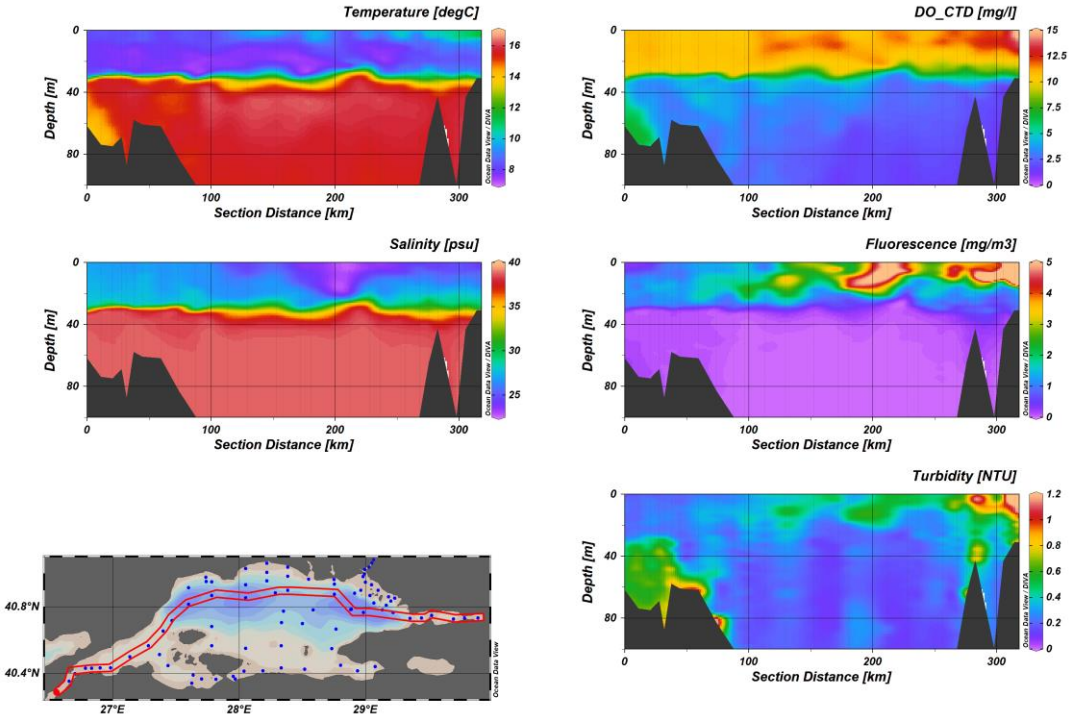

Figure 3.1 Spring 2022 (28.03 – 01.04) from Dardanelles to İzmit Bay west to east section distributions of Temperature (°C), Salinity (psu), Dissolved oxygen measured by probes in situ (mg/L), Fluorescence (mg/m^3) and Turbidity (NTU).

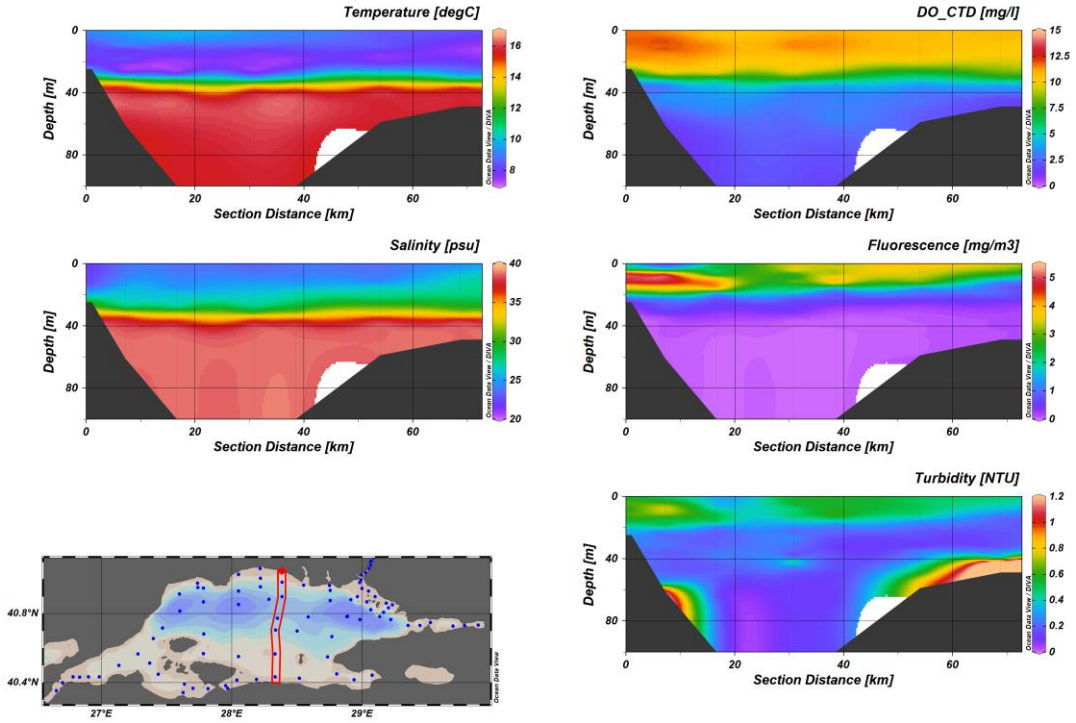

Figure 3.2 Spring 2022 (28.03 – 01.04) north to south section profiles of Temperature (°C), Salinity (psu), Dissolved oxygen measured by probes in situ (mg/L), Fluorescence (mg/m^3) and Turbidity (NTU).

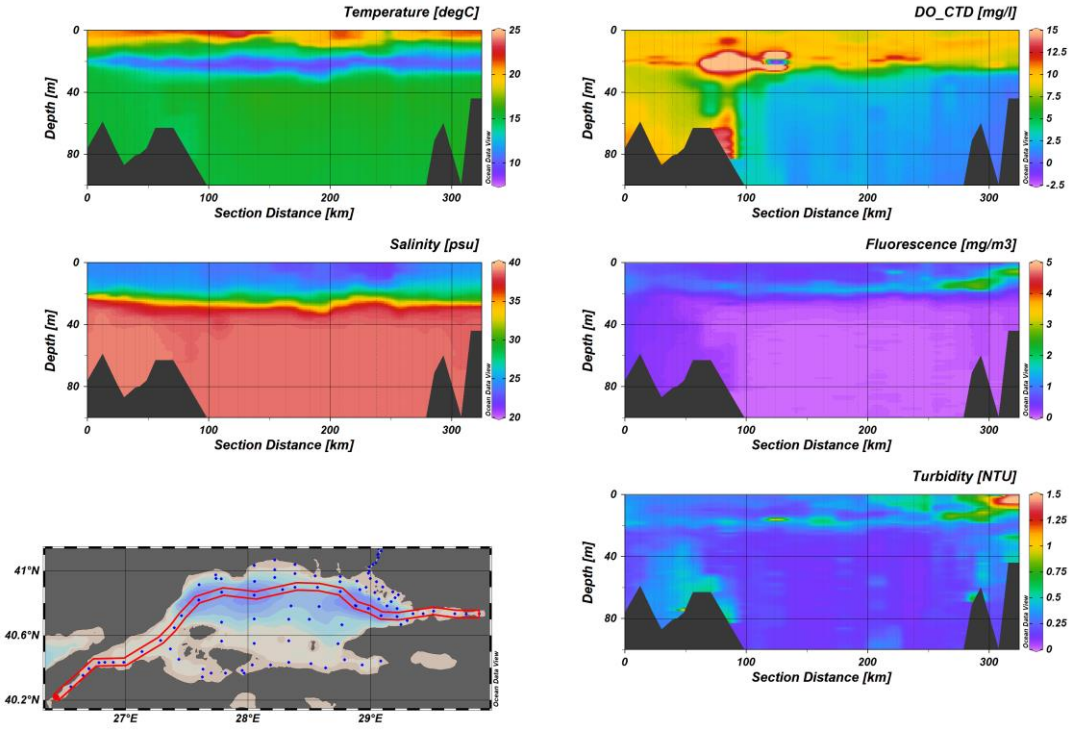

Figure 3.3 Summer 2022 (31.05 – 05.06) from Dardanelles to İzmit Bay west to east section distributions of Temperature (°C), Salinity (psu), Dissolved oxygen measured by probes in situ (mg/L), Fluorescence (mg/m^3) and Turbidity (NTU).

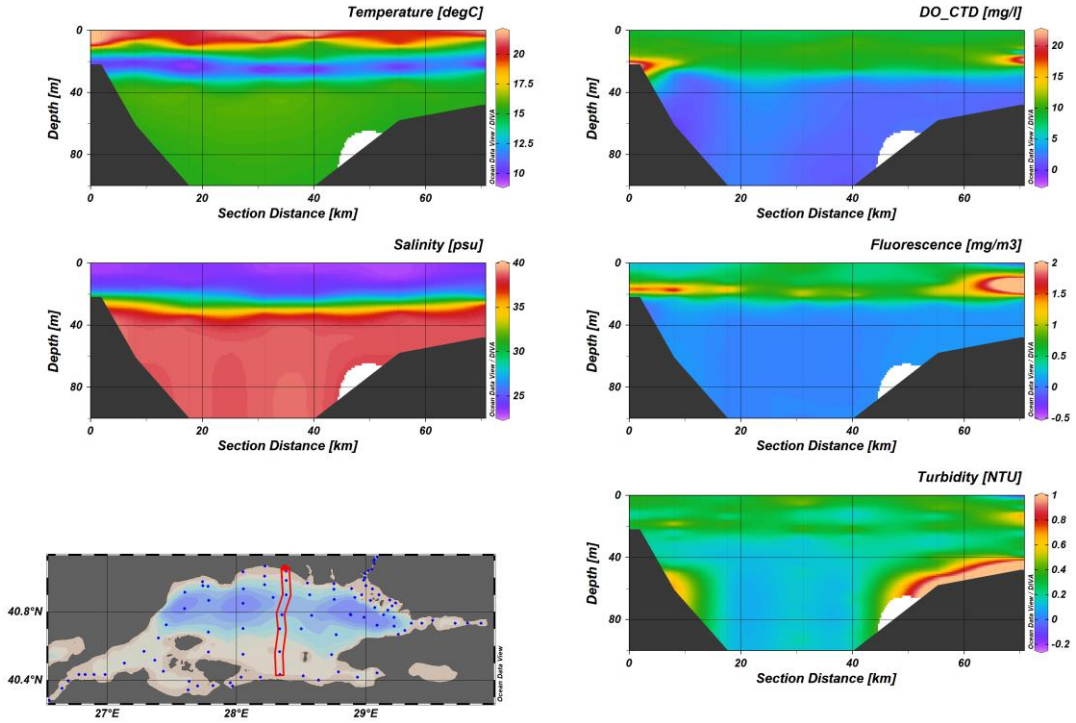

Figure 3.4 Summer 2022 (31.05 – 05.06) north to south section distributions of Temperature (°C), Salinity (psu), Dissolved oxygen measured by probes in situ (mg/L), Fluorescence (mg/m^3) and Turbidity (NTU).

3.1.1 Surface Nutrients and Dissolved Oxygen Distributions

Nutrients (NO_3^- + NO_2^-, NH_4^+, PO_4^{3-}, TP and Si), Dissolved oxygen (Winkler's method), Secchi disk depth (SDD), and fluorescence are shown in the distribution maps generated by surface values for the spring 2022 (Figure 3.5) and summer 2022 (Figure 3.6). Surface dissolved oxygen (DO) concentrations varied within 259 – 412 µM range and were higher in the eastern part than the western part. In the Bosporus area and offshore Gemlik Bay, relatively low DO concentrations were observed. NOx varied from 0.01 to 2.58 µM in surface waters. NOx was generally low and homogenously distributed on the surface, however, at offshore Silivri, Bosporus area and İmralı Island concentrations were relatively high. NH_4^+ concentrations were within the range of 0.07 – 2.11µM for surface waters, and they were observed to be

relatively high in offshore Silivri and İzmit Bay. NH_4^+ concentrations were higher in the eastern basin than in the western one. Phosphate distribution in surface waters varies within the 0.01 – 0.50 µM range. The highest PO_4^{3-} concentrations were observed in offshore Tekirdağ, Bandırma Bay, and outside of Gemlik Bay. TP was within the range of 0.19 – 1.83 µM for surface waters. Bandırma Bay, İzmit Bay, and outside of Gemlik Bay had relatively higher values of total TP. The Si amount in the surface waters varied in the range of 0.219 – 9.35 µM, which was higher in the eastern part. Si concentration reached its highest values, especially outside of the Bosporus and in the region close to where Susurluk flows into the sea. Secchi disk depth measurements varied within 2-13 m, and they were lower in the eastern part of the Marmara Sea. Especially the İzmit Bay had the lowest Secchi Disk depth. Fluorescence was higher in the eastern part, especially in the central basin and Çınarcık Basin, where it was most affected by the Bosporus jet.

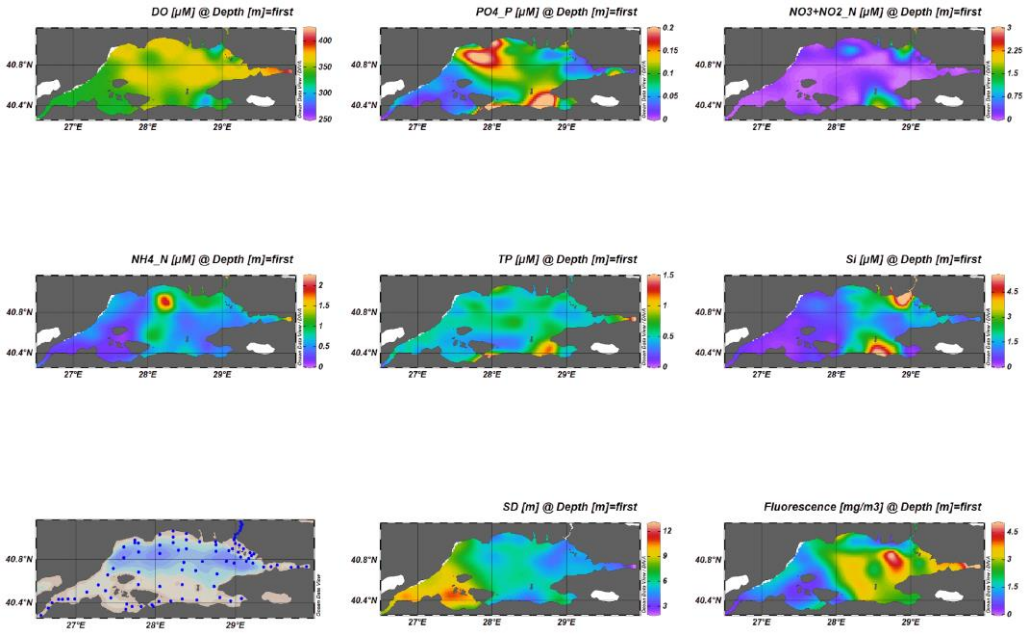

Figure 3.5 Surface distribution maps for Spring,2022 (28.03 – 01.04) for the properties as DO as measure by Winkler's method (µM), PO_4^{3-} (µM), NO_X-N (µM), NH_4^+ (µM), TP (µM), Si, Secchi disk depth (m) and Fluorescence (mg/m^3)

Dissolved oxygen (Winkler's method), nutrients (NO_X-N, TP, Si, PO_4, NH_4), Secchi disk depth taken during the Cruise, and fluorescence are visualized below in the distribution maps generated by using surface measurements for the summer 2022 (Figure 3.6). Surface dissolved oxygen measured by the automated Winkler method varied within the 233 – 405 µM range. Dissolved oxygen concentration was exceptionally high in Bandırma Bay, followed by İzmit Bay. NO_X-N concentrations in nitrate and nitrite varied in the 0.11 – 3.04 µM range. It had a patchy distribution with low concentrations throughout the Marmara Sea. NH_4 concentrations were within the range of 0.11 – 3.52 µM. These concentrations were low in general, except in some coastal regions. PO_4 distribution at surface waters varied within 0.01 – 0.19 µM. PO_4 was reaching its highest value in İzmit Bay. TP was within the range of 0.15 – 1.51 µM, which was generally low. The Si amount in the surface waters varied in the 0.22 – 5.49 µM field. The Si amount was high outside the Bosporus and central region. The Secchi disk depth changed within 2 – 10 m. The western part had a higher Secchi disk depth than the eastern region. İzmit Bay had the lowest Secchi disk depth. Fluorescence was down throughout the Marmara Sea except in Bandırma and İzmit Bays.

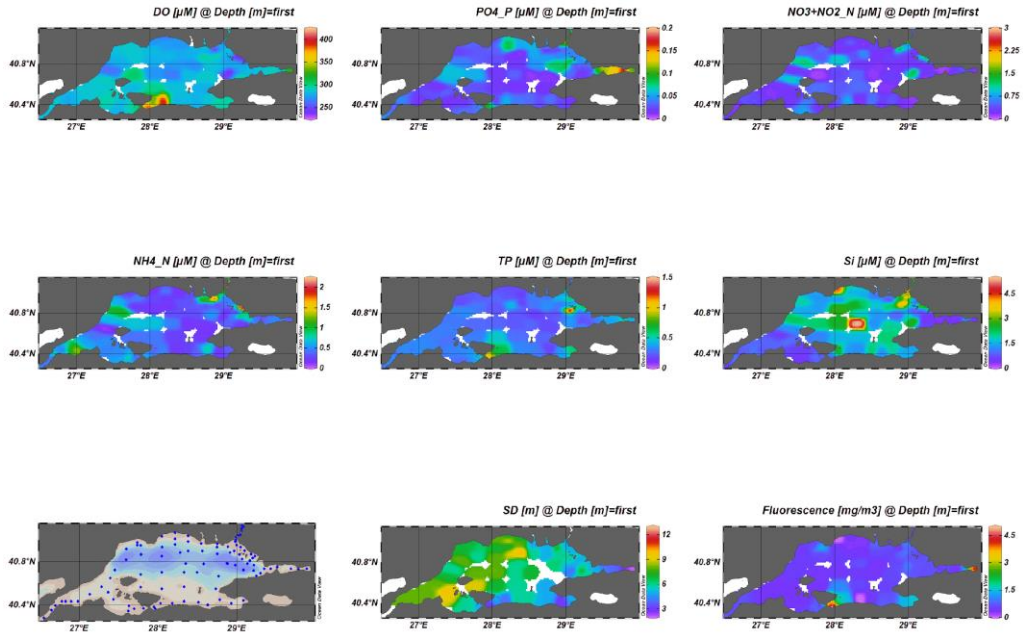

Figure 3.6 Surface distribution maps for Summer,2022 (31.05 – 05.06) for the properties as DO measure by Winkler's method (µM), PO_4^{3-} (µM), NO_X-N (µM), NH_4^+ (µM), TP (µM), Si, Secchi disk depth (m) and Fluorescence (mg/m^3)

Fluorescence was higher in the spring than the summer; correspondingly, dissolved oxygen was higher on the surface in March 2022 than in June 2022. Generally, nutrients were higher in the Spring cruise than in the summer cruise. On the summer, certain coastal regions, such as İzmit Bay or Bandırma Bay, had higher nutrients than other regions of the Sea of Marmara. For both seasons, the differences between the eastern and western basins were apparent.

3.1.2 Nutrients and Chlorophyll-*a* Distributions

West to east (from Dardanelles to İzmit Bay) section Chlorophyll-*a* distribution for Spring,2022 and Summer 2022 given below. In March, chlorophyll-*a* values were in the range of 0.13-5.55 µg/L. In June, chlorophyll-*a* values were in the range of 0.14-4.94 µg/L.

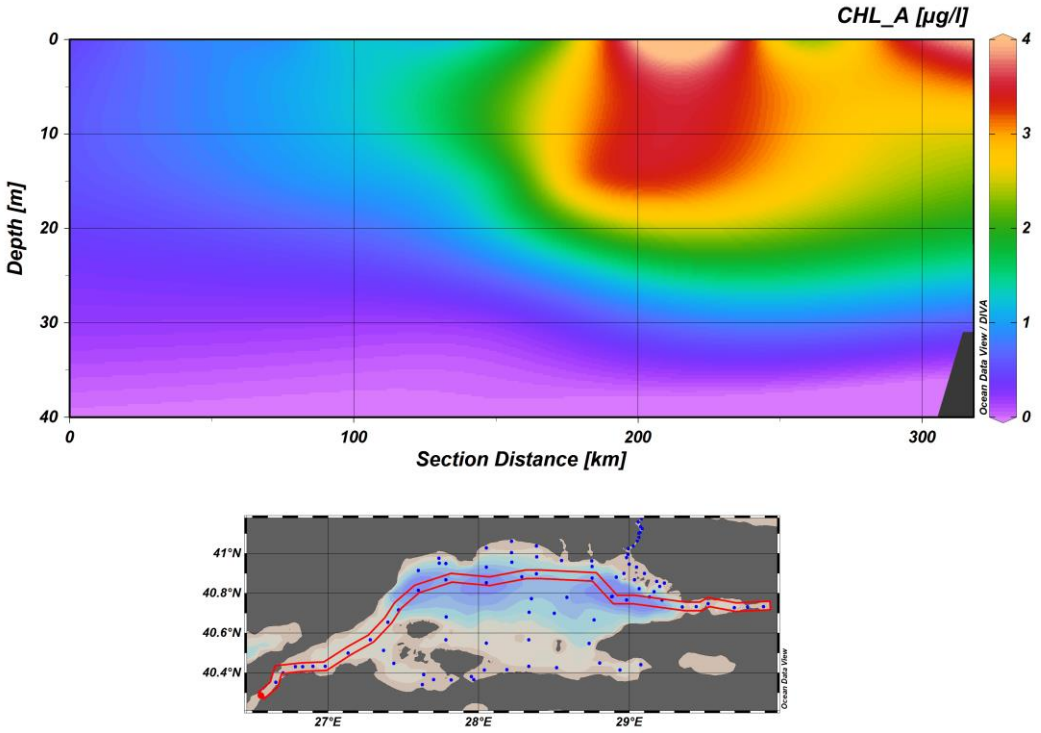

Figure 3.7 Spring 2022 (28.03.2022 – 01.04.2022) from Dardanelles to İzmit Bay west to east section distributions of Chlorophyll-*a*

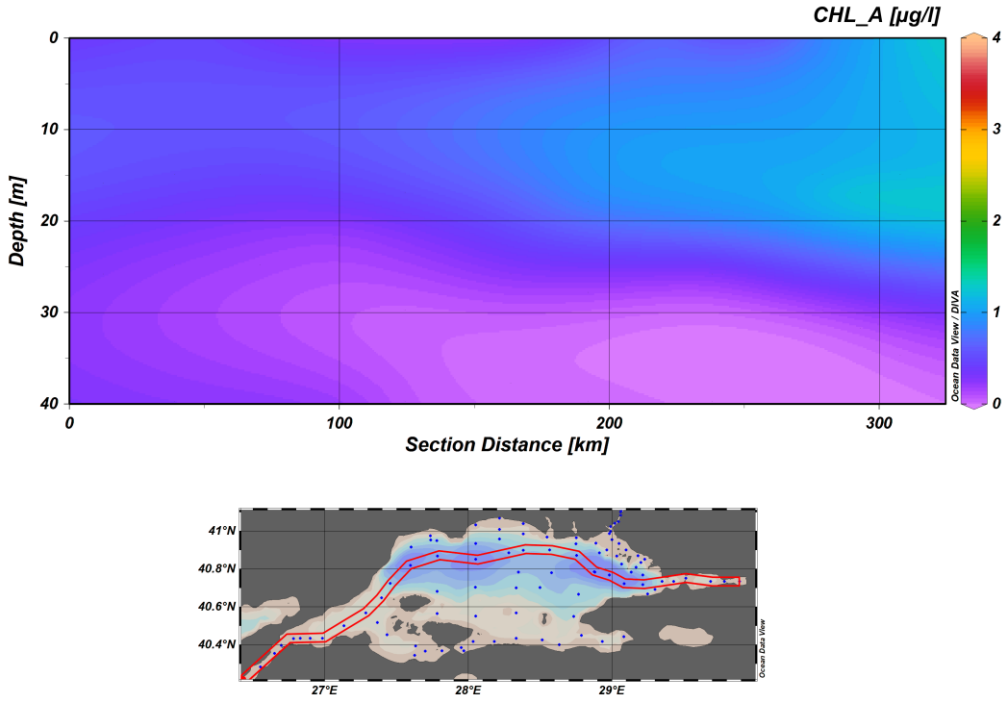

Figure 3.8 Summer 2022 (31.05 – 05.06) from Dardanelles to İzmit Bay west to east section distributions of Chlorophyll-*a*

West to east (from Dardanelles to İzmit Bay) section (Figure 3.9) and north to south section (Figure 3.10) nutrient distributions of the Sea of Marmara at the Spring Cruise are given below. NO_X-N, TP, Si, and PO_4 concentrations were low on the surface, and they tend to increase with depth due to excessive usage of these nutrients by phytoplankton at the surface.

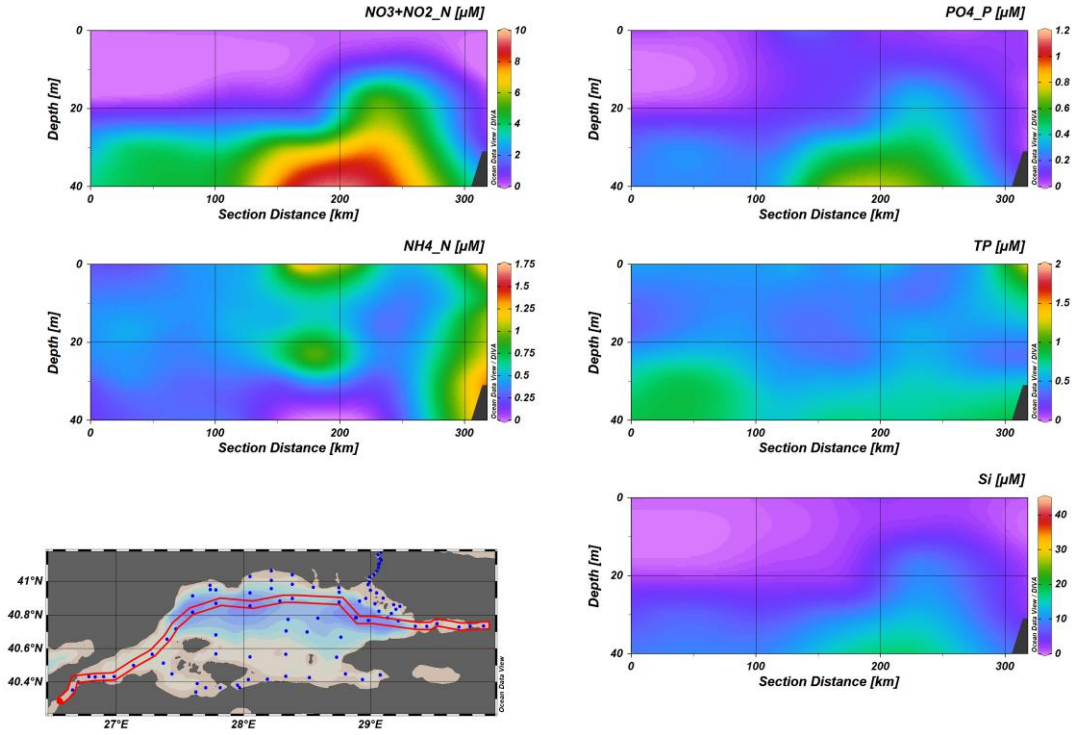

Figure 3.9 Spring 2022 (28.03.2022 – 01.04.2022) from Dardanelles to İzmit Bay west to east section distributions of NO_X-N (µM), PO_4^{3-} (µM), NH_4^+ (µM), TP (µM), and Si (µM).

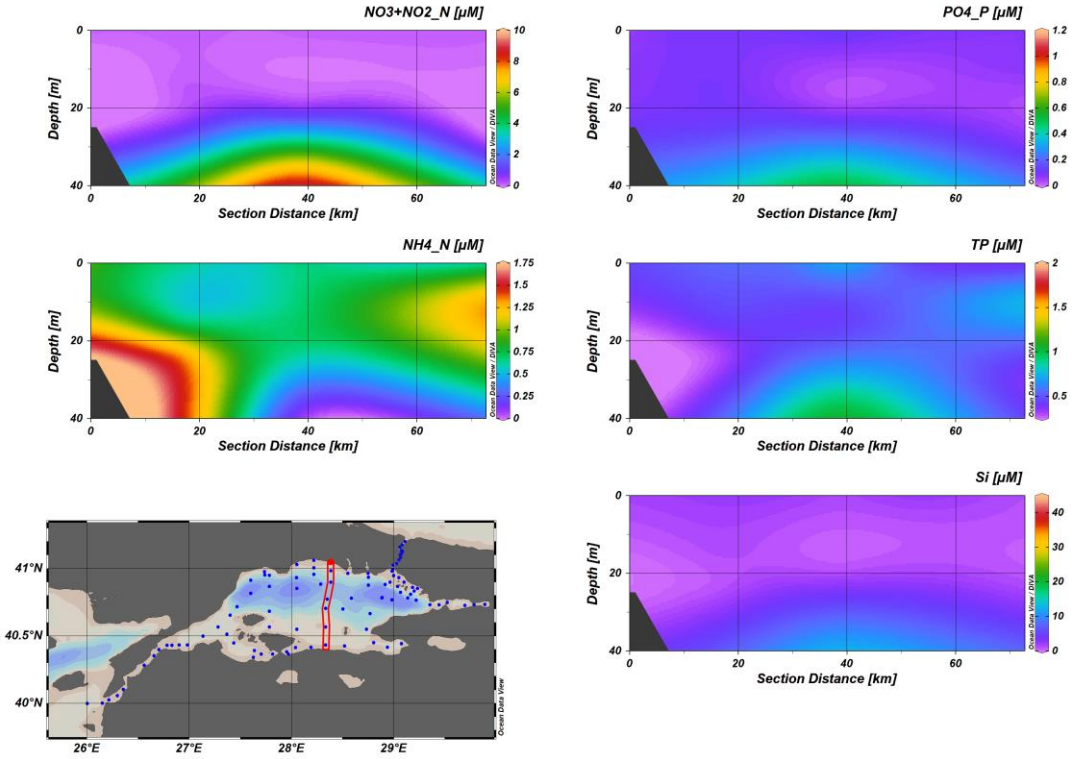

Figure 3.10 Spring 2022 (28.03 – 01.04) north to south section distributions of NO_X-N (µM), PO_4^{3-} (µM), NH_4^+ (µM), TP (µM), and Si (µM).

West to east (from Dardanelles to İzmit Bay) section (Figure 3.11) and north to south section (Figure 3.12) profiles of the Sea of Marmara at the Summer Cruise are given below. Shared properties observed between March and June cruises as nutrients (NO_X-N, TP, Si, PO_4, NH_4) were at low concentrations at the surface.

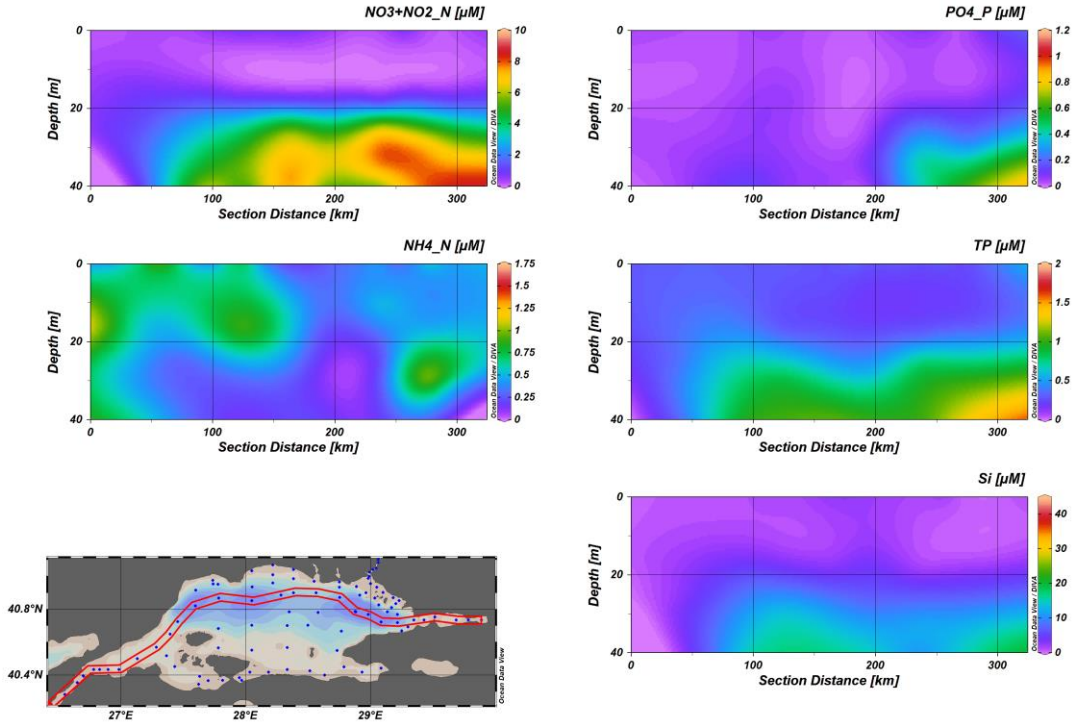

Figure 3.11 Summer 2022 (31.05 – 05.06) from Dardanelles to İzmit Bay west to east section distributions of NO_X-N (µM), PO_4^{3-} (µM), NH_4^+ (µM), TP (µM), and Si (µM).

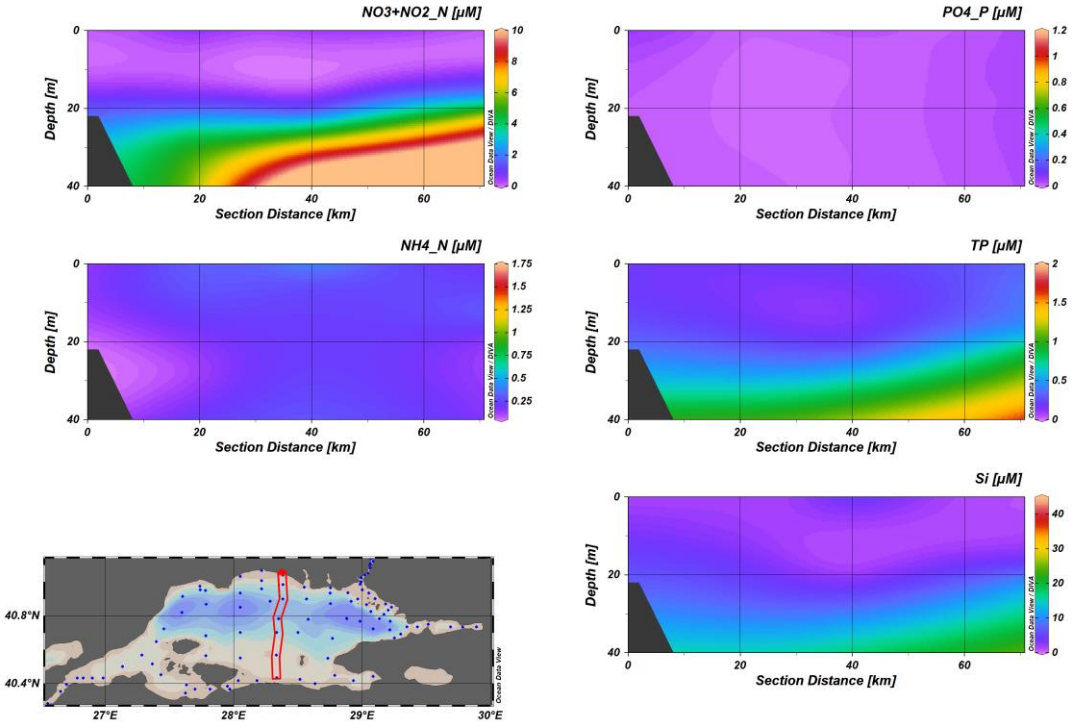

Figure 3.12 Summer 2022 (31.05 – 05.06) north to south section distributions of NO_X-N (µM), PO_4^{3-} (µM), NH_4^+ (µM), TP (µM), and Si (µM).

Southern shelf nutrients section distributions are given from Bandırma Bay to Gemlik Bay in Figure 3.13 and Figure 3.14 for spring,2022 and summer, 2022 respectively. In Spring, regions closer to Bandırma Bay had higher amounts of PO_4, TP and NH_4. Si and NO_X-N were uniformly low at the surface and increased with depth. In Gemlik Bay, TP, Si and PO_4 increased with depth. In June, NO_X-N is uniformly low on the surface, then it reaches beyond 10 µM at 20-40 m depth interval.

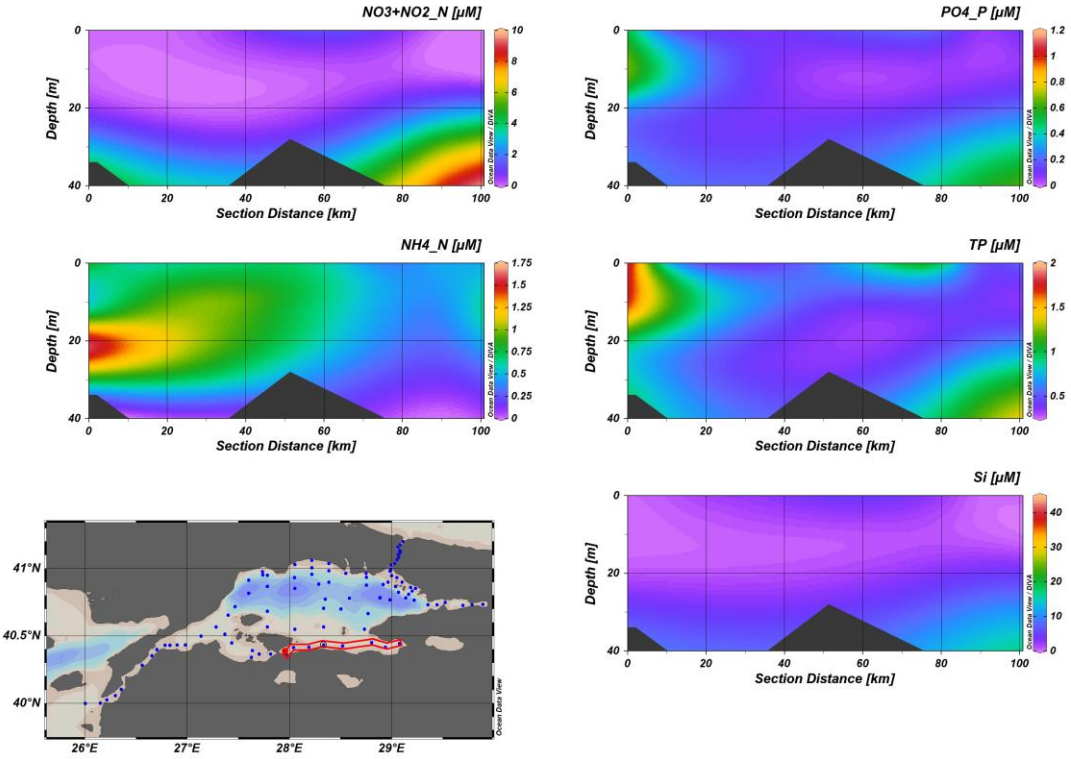

Figure 3.13 Spring 2022 (28.03 – 01.04) Southern Shelf section distributions of NO_X-N (µM), PO_4^{3-} (µM), NH_4^+ (µM), TP (µM), and Si (µM).

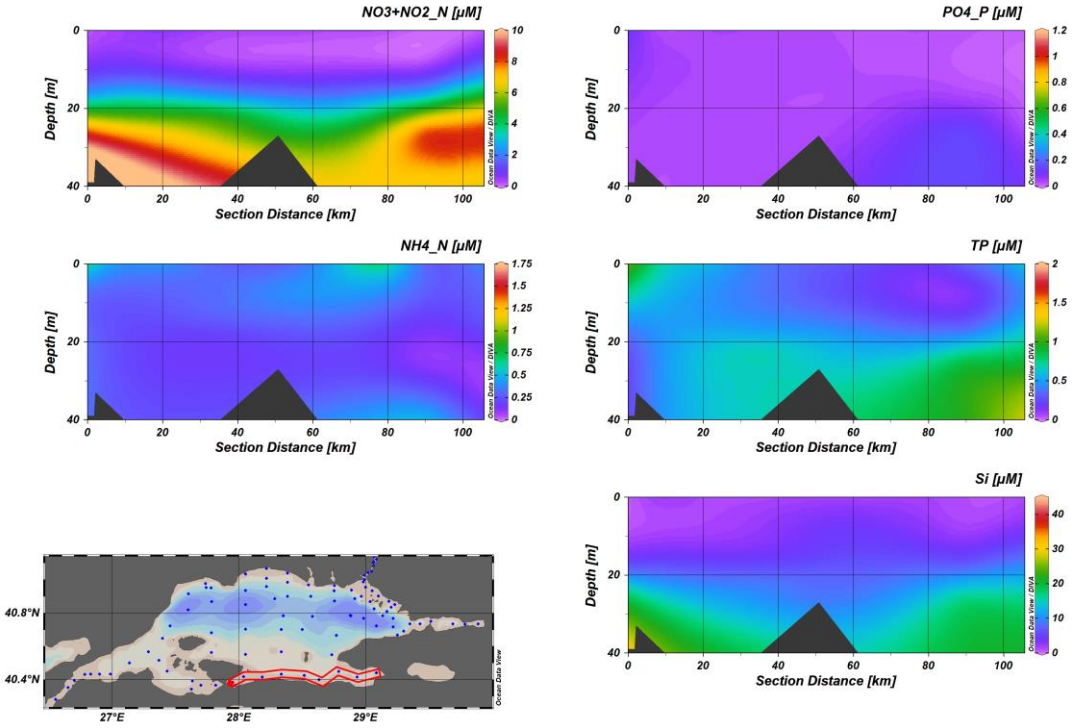

Figure 3.14 Summer 2022 (31.05 – 05.06) Southern Shelf section distributions of NO_X-N (µM), PO_4^{3-} (µM), NH_4^+ (µM), TP (µM), and Si (µM).

İzmit Bay nutrients section distribution from offshore to İzmit coast is given in Figure 3.15 and Figure 3.16 for the spring,2022 and summer, 2022 cruises, respectively. In Spring cruise, NO_X-N levels were low in the surface and increased with depth for both seasons. A higher amount of NO_X-N was observed in the Spring.

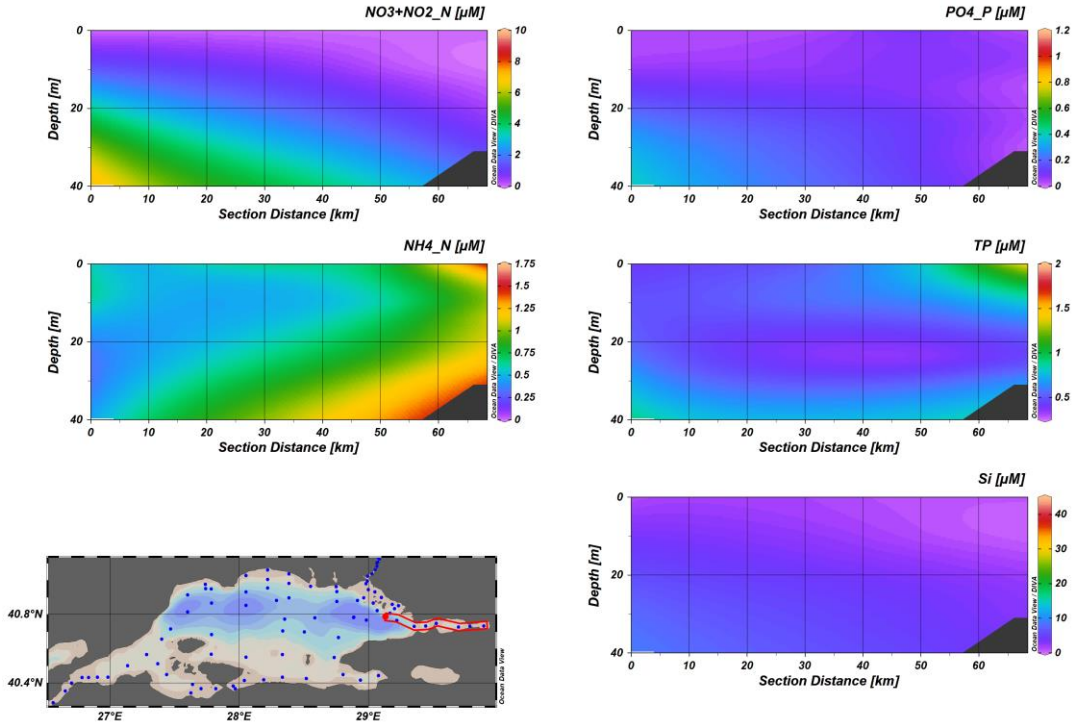

Figure 3.15 Spring 2022 (28.03 – 01.04) İzmit Bay section distributions of NO_X-N (µM), PO_4^{3-} (µM), NH_4^+ (µM), TP (µM), and Si (µM).

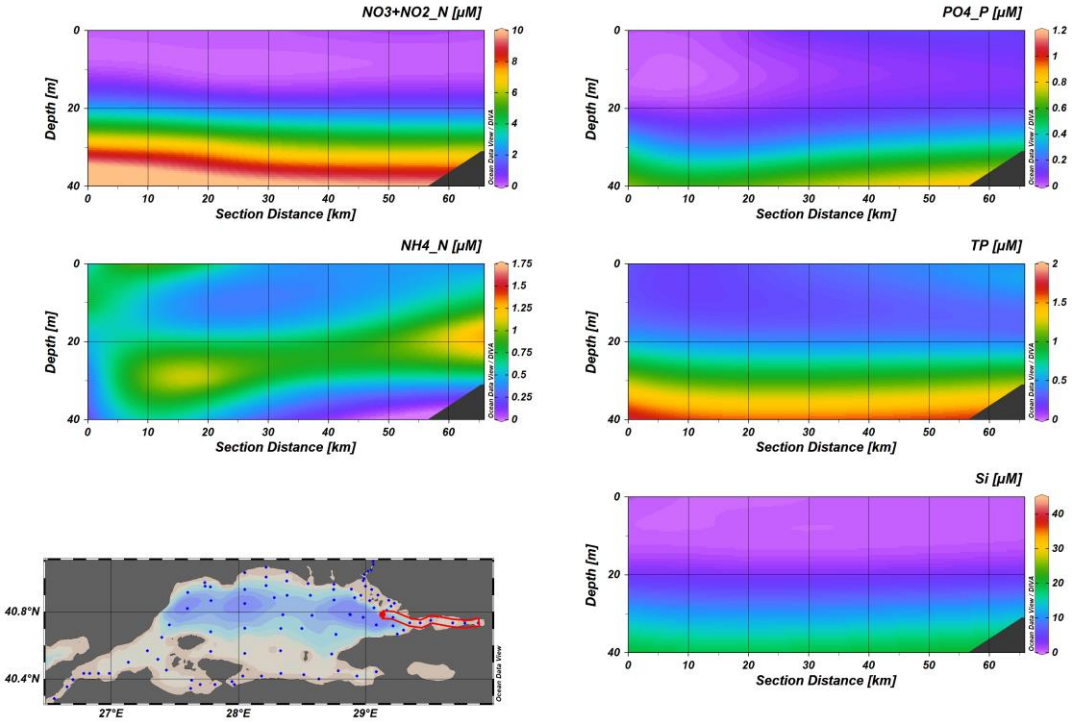

Figure 3.16 Summer 2022 (31.05 – 05.06) İzmit Bay section distributions of NO_X-N (µM), PO_4^{3-} (µM), NH_4^+ (µM), TP (µM), and Si (µM).

3.1.3 Particulate Organic Carbon

POC results of the corresponding stations and depth are shown in Figure 3.17 below. Average surface POC concentrations for March, 2022 were 37.5 ± 18.9 µmol C l^{-1}. Average surface POC concentrations for June, 2022 were 43.1 ± 28.5 µmol C l^{-1}. POC concentrations decreased with depth in both seasons.

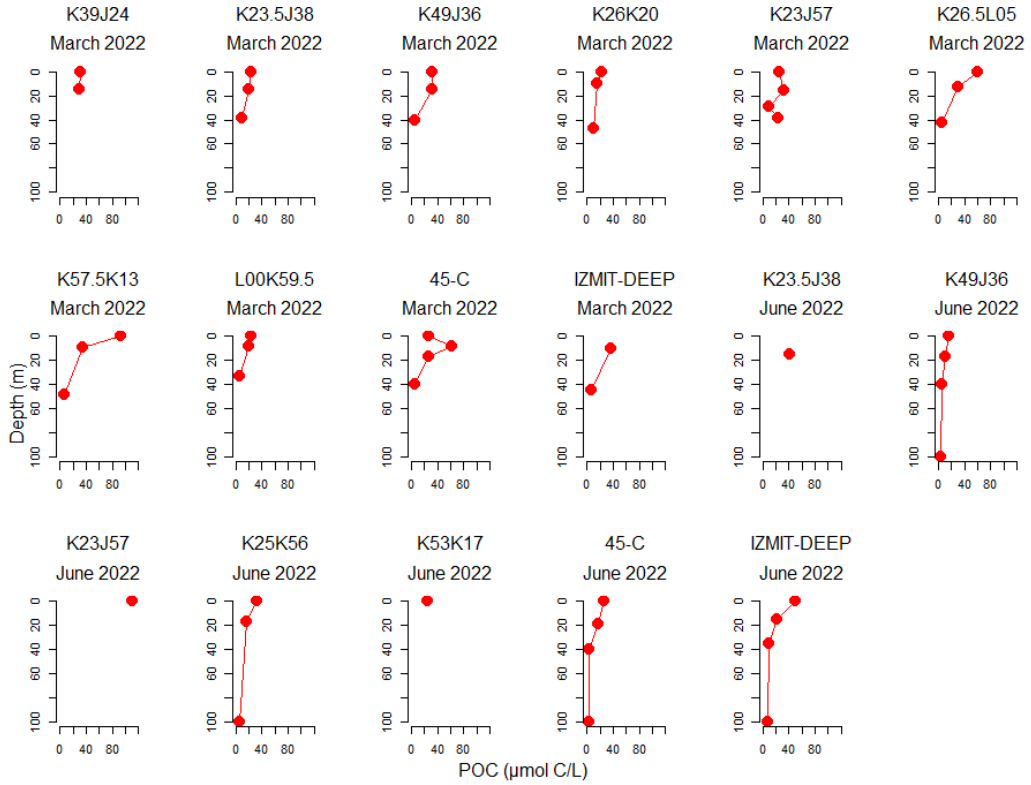

Figure 3.17 POC concentrations of corresponding stations and depths on March,2022 and June, 2022.

3.2 Community Respiration Rates

In spring 2022, community respiration (CR) rates for all sampling at stations and depths of 0-32 m varied from 0.01 to 2.04 µmol O_2 L^{-1} h^{-1}(Figure 3.18). The highest value (2.04 µmol O_2 L^{-1} h^{-1}) was observed in Station K23.5J38 (Erdek Bay). Other relatively high values (>1 µmol O_2 L^{-1} h^{-1}) were measured at 15 m depth of Station K49J36 (1.12 µmol O_2 L^{-1} h^{-1}, offshore of Tekirdağ, Western Basin) and at the surface of Station K57.5K13 (1.04 µmol O_2 L^{-1} h^{-1}, offshore of Silivri). In general, the lowest values were observed below 20 m and a decreasing trend of CR with increasing depth was observed.

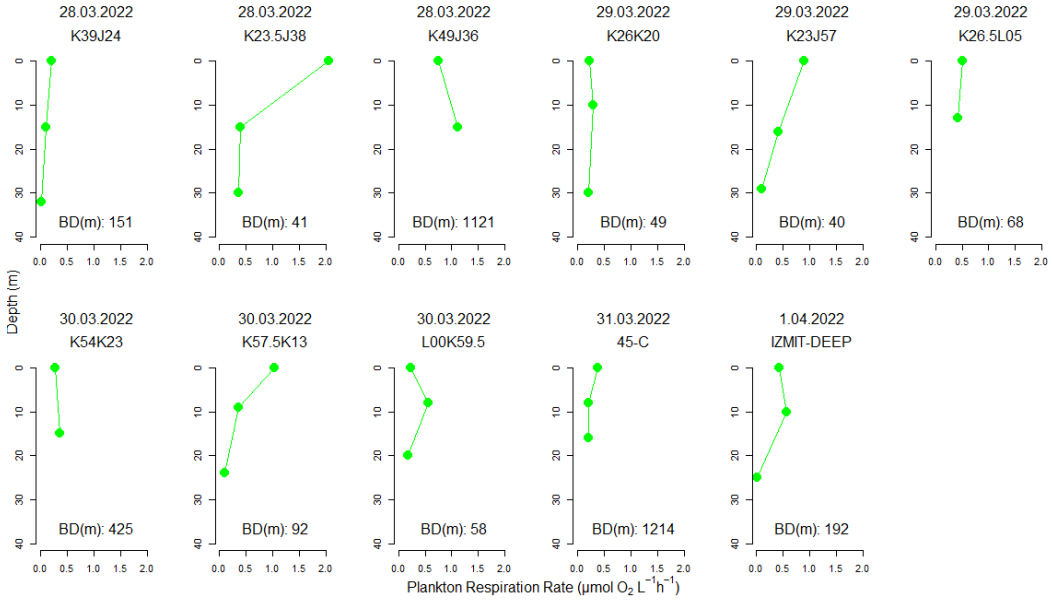

Figure 3.18 Spring, 2022 Cruise CR (µmol O_2 $L^{-1}h^{-1}$) versus Depth (m) plots for all corresponding stations. Bottom depths are given for all stations as BD in short as m.

The distribution maps of CR in Spring 2022 are given as 3 layers by averaging the rates at certain depths: layer 1 (0-10 m), layer 2 (11-20), and layer 3 (21-32 m) (

Figure 3.19). In layer 1, relatively high CR (>0.5 µmol O_2 L^{-1} h^{-1}) had been found in bays (Erdek Bay, Bandırma Bay, Gemlik Bay, İzmit Bay) and Western Basin, and Tekirdağ. In layer 2, CR values were significantly decreased, and only in Western Basin CR value was ~1 µmol O_2 L^{-1} h^{-1}. At layer 3, CR values were the lowest (< 0.5 µmol O2 L-1 h-1) compared upper layers.

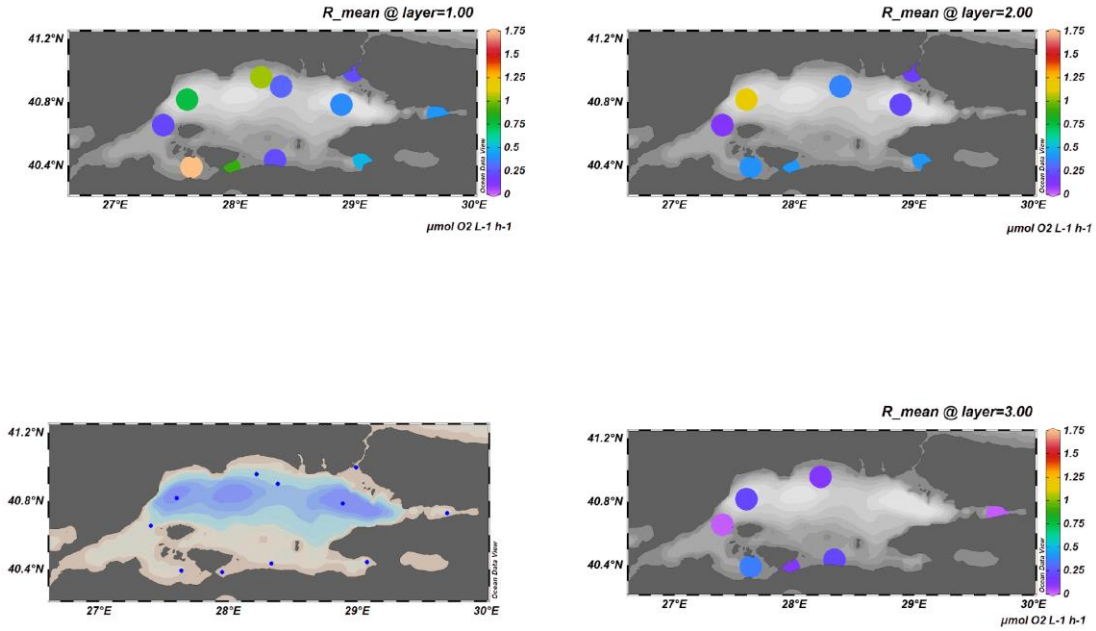

Figure 3.19 Distribution maps for CR rates of corresponding stations shown for 3 separate layers as layer 1 (0-10 m), layer 2 (11-20), and layer 3 (21-32 m) for the spring,2022 cruise.

In summer 2022 samples, CR rates for all stations between 0-20 m were measured between 0.15-1.63 µmol O_2 L^{-1} h^{-1}. The highest value (1.63 µmol O_2 L^{-1} h^{-1}) was observed in the surface water of Station K23J57 (offshore Bandırma). Other relatively high values (>1 µmol O_2 L^{-1} h^{-1}) were observed on the surface of Station K25K56 (offshore Mudanya). Except for K49J36 (western deep), all remaining stations followed a decreasing trend of respiration rate with depth. K49J36 showed a similar pattern with its March 2022 results. Results are shown in the figure below (Figure 3.20).

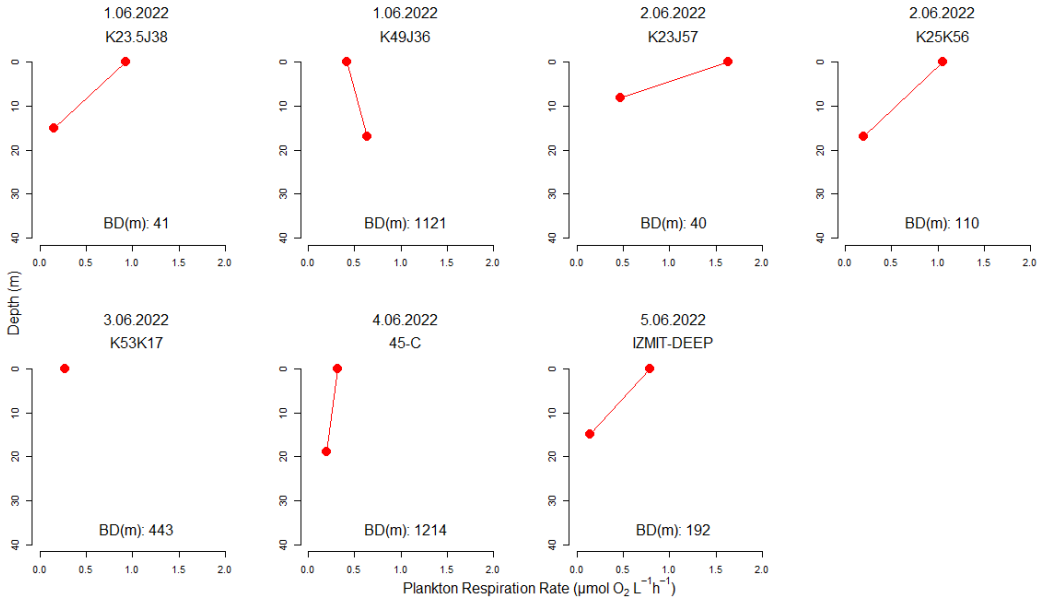

Figure 3.20 Summer, 2022 Cruise CR Rates (µmol O_2 $L^{-1}h^{-1}$) versus Depth (m) plots for all corresponding stations. Bottom depths are given for all stations as BD in short as m.

In June 2022, Cruise, at the distribution maps (Figure 3.21) visualized stations as colored according to CR rates separately for layer 1(0-10 m) and layer 2 (11-20). For the upper 10 m southern shelf, Erdek Bay and İzmit Bay had relatively higher values. The upper 10 m depth had higher rates than the 11-20 m depth interval. The western dip at layer 2 had a somewhat higher value; however, at layer 2, rates are usually lower than at layer 1.

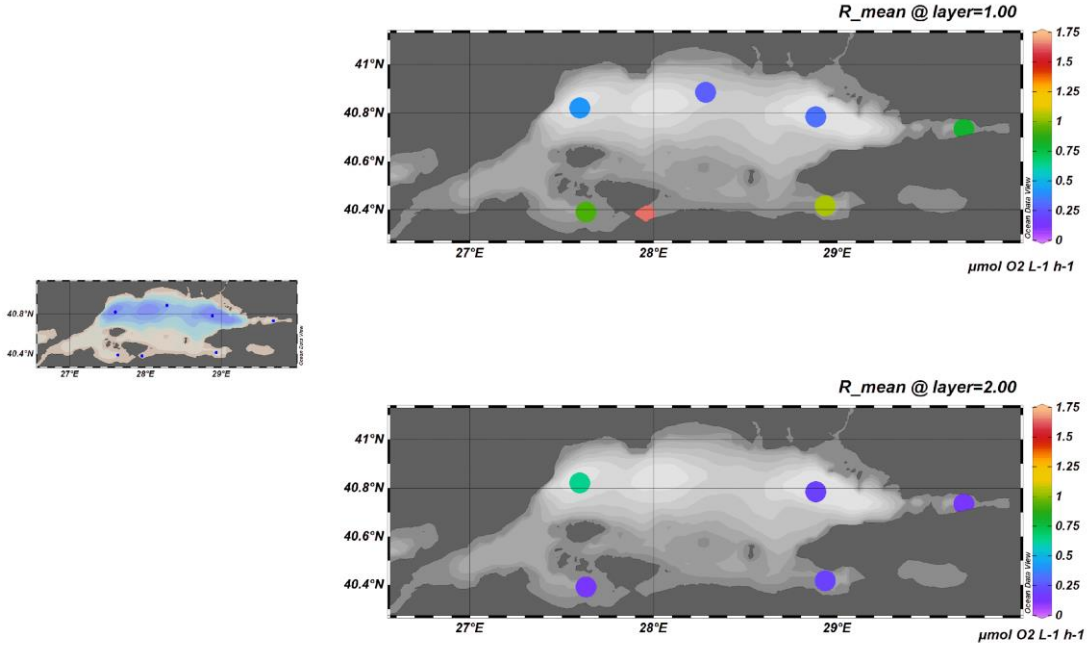

Figure 3.21 Distribution maps for CR rates of corresponding stations shown for 2 separate layers as layer 1 (0-10 m), layer 2 (11-20) for the summer 2022 cruise.

3.3 Sub-Halocline Community Respiration Rates

For the spring and summer of 2022, sub-halocline (> 32 m) oxygen changes over daily intervals are given in Figure 3.22 and Figure 3.23 respectively. Also, the Table 3.1 shows model results on respiration rate and estimated initial organic carbon. Stations K54K43 (42 m, Spring Cruise) and K25K56 (40 and 100 m, Summer Cruise) were omitted in the model. Furthermore, the "α" value or specific turnover rate shown in Table 3.1. In the Spring Cruise, the α value was within the 0.010 – 0.204 Day^{-1} interval for the samples between 33 and 48 m depth. Furthermore, respiration rate changed within the range of 33.20 - 384.92 mg C m^{-3} day^{-1}. The highest “α" and highest respiration rate were calculated in K23.5J38, located in Erdek Bay. On the other hand, the smallest “α" and smallest respiration rate were calculated in K26.5L05, located in Gemlik Bay.

In the summer cruise, results took place at 3 Stations in 2 different depths of 100 m and within 35-40 m intervals. α values were within 0.01-0.81 Day^{-1}, and respiration rates were within 41.53 – 137.25 µM breaks. Station K49J36 at 40 m was calculated to have the highest “α" value and the highest respiration rate. Station İzmit Deep at 35 m has the smallest “α" value and the lowest respiration rate.

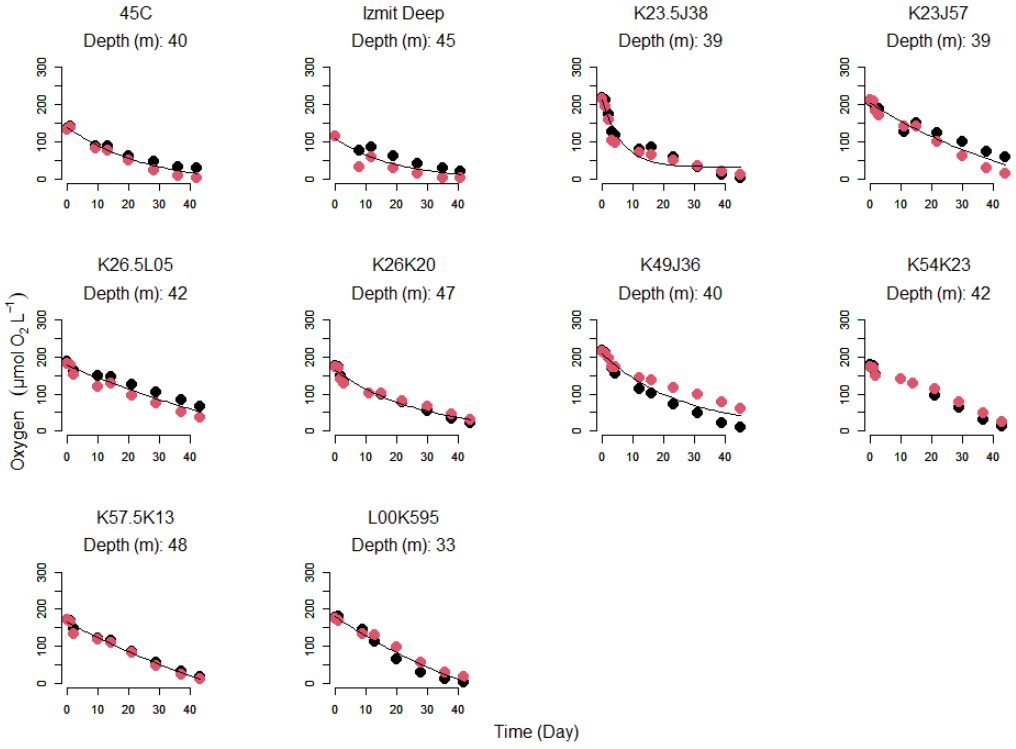

Figure 3.22 Spring, 2022 cruise, model fitted plots to show daily change of oxygen (µM) of sub -halocline samples

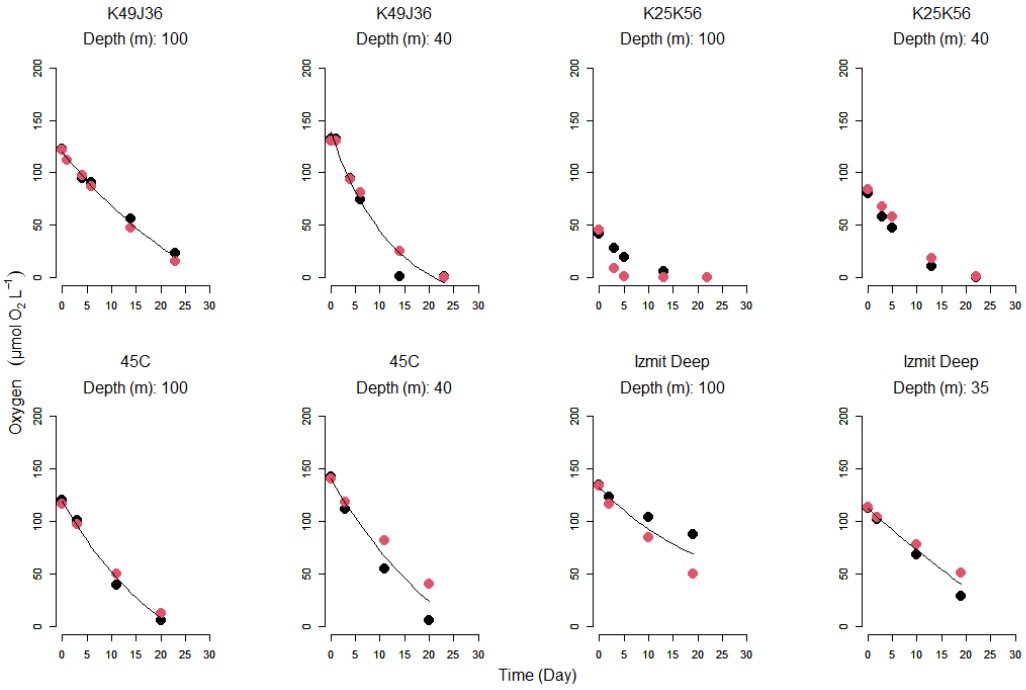

Figure 3.23 Summer, 2022 cruise, model fitted plots to show daily change of oxygen (µM) of sub-halocline samples

Table 3.1 Model results on respiration rate, α (specific turnover rate) value and estimated organic carbon (OC) concentration of corresponding stations and depths for Sub-halocline samples of both of the cruises.

Station	**Depth (m)**	**Cruise**	**OC (μmol L^{-1})**	**α (Day^{-1})**	**Respiration rate (mg C m^{-3} day^{-1})**
45C	40	March	138	0.035	57.44
Izmit Deep	45	March	115	0.036	49.42
K23.5J38	39	March	157	0.204	384.92
K23J57	39	March	434	0.009	47.02
K26.5L05	42	March	505	0.005	33.20
K26K20	47	March	153	0.030	54.90
K49J36	40	March	172	0.036	75.25
K57.5K13	48	March	361	0.010	43.92
L00K595	33	March	294	0.016	57.43
K49J36	100	June	177	0.028	58.70
K49J36	40	June	141	0.081	137.25
45C	100	June	158	0.044	84.25
45C	40	June	201	0.033	79.63
Izmit Deep	100	June	96	0.042	48.46
Izmit Deep	35	June	363	0.010	41.53

Model estimated respiration rates distribution maps are given below Figure 3.24 and Figure 3.25 as Spring, 2022 and Summer, 2022 Cruise respectively. In spring, 2022 cruise all sub-halocline samples belonged to layer 4 (33 – 48 m). On the other hand, in summer,2022 cruise samples were collected from two separate layers: layer 4 (35 – 40 m) and layer 5 (100 m). In March 2022, at layer 4, Erdek Bay had the highest sub-halocline respiration rate. In June 2022 cruise fewer samples, but in two different layers are shown. Western Deep had the highest sub-halocline respiration rate at layer 4 in june,2022. In here, Çınarcık Deep had the highest sub-halocline respiration rate in layer 5.

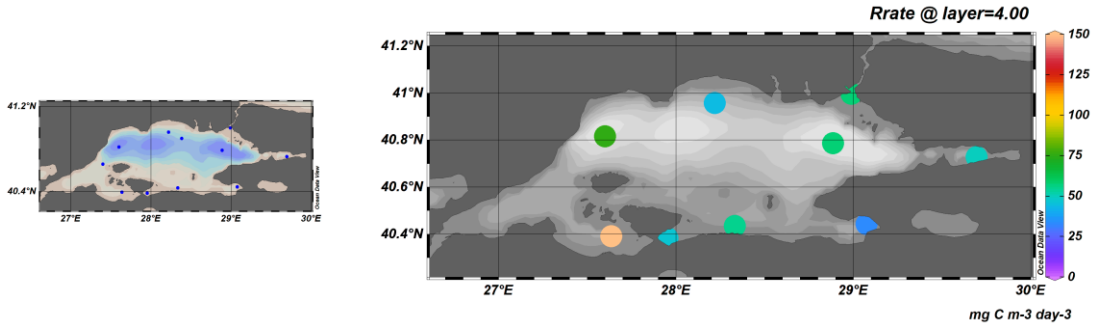

Figure 3.24 Spring, 2022 layer 4 (33 – 48 m) sub-halocline samples respiration rates distribution map.

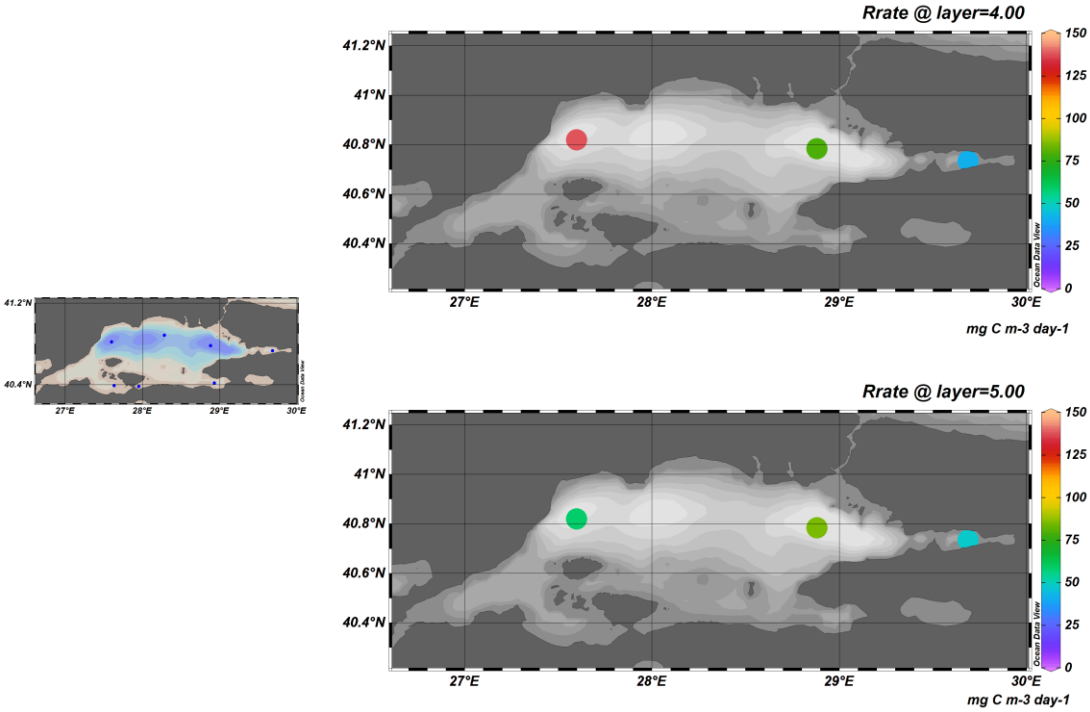

Figure 3.25 Spring, 2022 layer 4 (35-40 m) and layer 5 (100 m) sub-halocline samples respiration rates distribution map.

In the graph (Figure 3.26) below, bars represent mean CR rates, and error bars represent standard deviation. 2 different seasons, spring and summer 2022, are shown with separate colors. Five layers are shown: layer 1 (0-10 m), layer 2 (11-20), layer 3 (21-32), layer 4 (33-50 m) and layer 5 (100 m). The plot indicates a decreasing trend in CR rate with depth. In Table 3.2 the average salinity and temperature values of samples that belong to separate layers are shown.

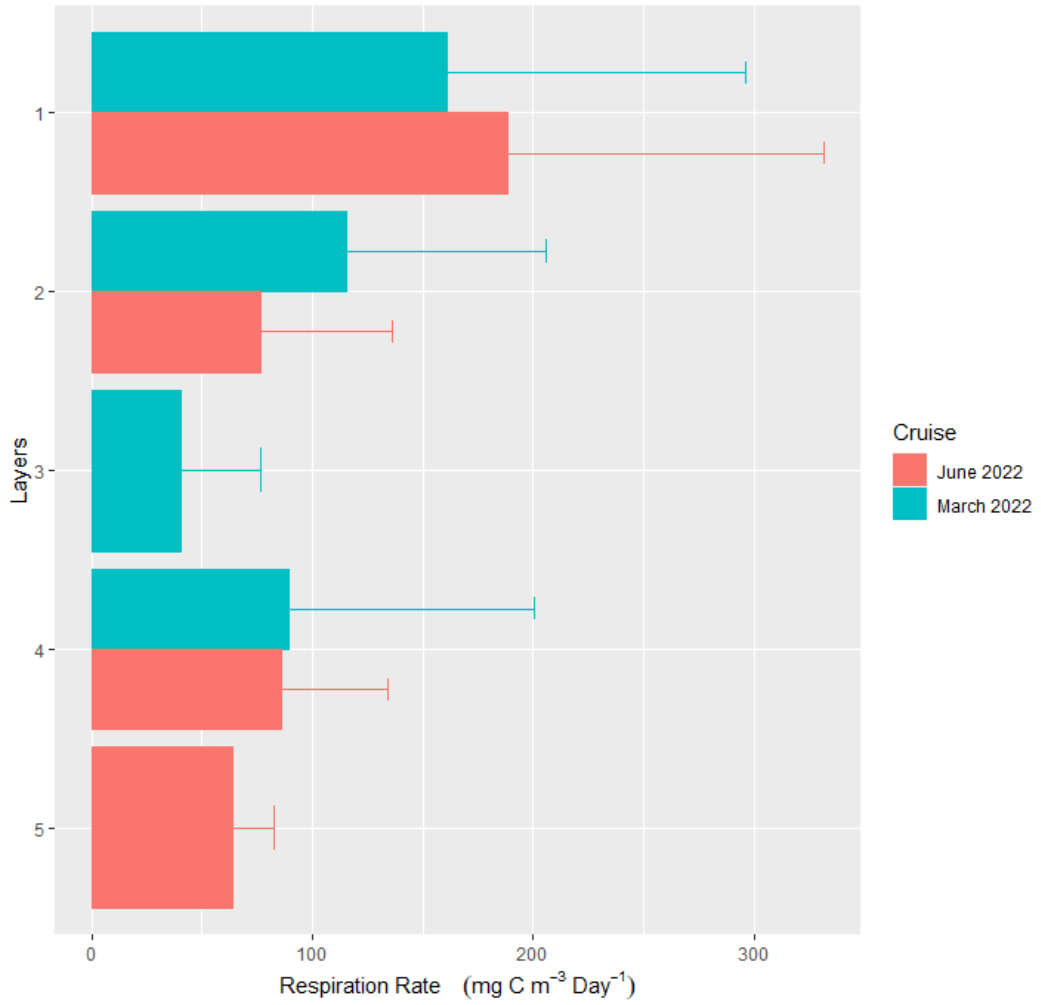

Figure 3.26 Bar plot of average CR and CR_{sub} values at layers in both sampling periods. Error bars represent standard deviation. Corresponding layers are as following: layer 1 (0-10 m), layer 2 (11-20), layer 3 (21-32 m), layer 4 (33-50 m) and layer 5 (100 m). Separate cruises shown in different colors.

Table 3.2 Average temperature and salinity values of samples belongs to different layers as layer 1 (0-10 m), layer 2 (11-20), layer 3 (21-32 m), layer 4 (33-50 m) and layer 5 (100 m).

Cruise	**Layer**	**Mean Temperature (°C)**	**Mean Salinity (psu)**
March 2022	1	8.8±0.9	24.7±2
March 2022	2	8.0±0.4	27.0±1.2
March 2022	3	9.7±1.6	30.4±2.4
March 2022	4	15.4±0.9	38.0±1.2
June 2022	1	21.4±2.0	25.2±4.6
June 2022	2	12.6±1.5	26.2±0.4
June 2022	4	15.8±0.2	38.6±0.2
June 2022	5	15.5±0.2	38.8±0.1

3.4 Net Community Production Rates

In spring 2022 Cruise, maximum NCP values were in the -0.02 – 2.68 μmol O_2 L^{-1} h^{-1} interval range. A negative value was observed in Station K49J36 (western deep). The highest value was observed in Station İzmit Deep (the deepest part of İzmit Bay). NCP_{chl} changed within -0.01 – 1.58 mol O_2 g^{-1} Chl-*a* h^{-1} interval. The highest value was achieved at station K26K20 on the southern shelf.

In the summer 2022 Cruise, four experiments did not complement the PI curve; the mean value for all corresponding experiments at each PAR level was considered NCP_{max}. These stations (K23.5J38, K49J36, K25K56, IZMIT-DEEP) have negative NCP_{max} values at the surface. Maximum NCP value changed in -0.80 – 3.14 μmol O_2 L^{-1} h^{-1} interval. The highest value was observed at the 8 m depth of K23J57 (Bandırma Bay), and the lowest was observed at the surface of K23.5J38 (Erdek

Bay). NCP_{chl} changed in the -0.88 – 1.35 mol O_2 g^{-1} Chl-*a* h^{-1} interval. In general Summer, 2022 samples' NCP_{max} values were lower than Spring 2022 samples. Maximum NCP and NCP_{chl} values are shown in

Table 3.3. PI curve fitted rates vs. PAR level values for each station for spring and summer can be found in Figure 3.27 and Figure 3.28 respectively.

Table 3.3 Maximum NCP, Chl-*a* and NCP_{chl} values for corresponding Stations and Depths for both Spring and Summer Cruises.

Station ID	**Sampling Date**	**Depth (m)**	**Chl-*a* (µg/L)**	**NCP_{max} (µmol O_2 l^{-1} h^{-1})**	**NCP_{max} (mg C m^{-3} day^{-1})**	**NCP_{chl} (mol O_2 g^{-1} Chl *a* h^{-1})**
13 Experiments are complementary with PI curve presented below						
K49J36	28.03.2022	0	2.50	-0.02	-5.76	-0.01
K23.5J38	28.03.2022	0	0.91	0.58	167.04	0.63
K23J57	29.03.2022	0	0.53	0.60	172.8	1.14
K26K20	29.03.2022	0	1.01	1.60	460.8	1.58
K57.5K13	30.03.2022	0	1.14	1.50	432	1.32
45-C	31.03.2022	0	5.10	1.54	443.52	0.30
IZMIT-DEEP	1.04.2022	0	5.88	2.68	771.84	0.46
K23.5J38	1.06.2022	15	0.84	0.11	31.68	0.13
K23J57	2.06.2022	0	3.45	2.31	665.28	0.67
K23J57	2.06.2022	8	2.32	3.14	904.32	1.35
K53K17	3.06.2022	0	0.32	0.02	5.76	0.08
45-C	4.06.2022	0	0.38	0.42	120.96	1.08

Table 3.3 (cont'd)						
4 experiments are not complementary with PI curve, mean rate shown as NCP_{max} presented below						
K23.5J38	1.06.2022	0	0.95	-1.80	-518.4	-1.88
K49J36	1.06.2022	0	0.30	-0.37	-106.56	-1.24
K25K56	2.06.2022	0	0.87	-0.64	-184.32	-0.73
IZMIT-DEEP	5.06.2022	0	1.08	-0.04	-11.52	-0.03

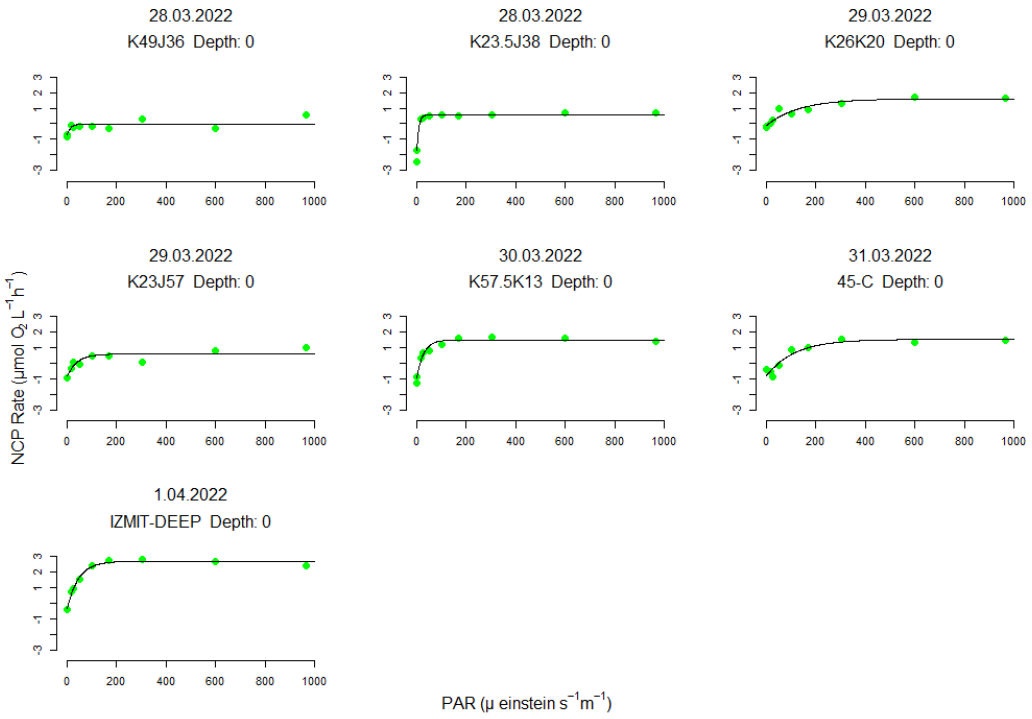

Figure 3.27 Spring, 2022 Cruise PAR (µ einstein $s^{-1}m^{-1}$) versus NCP rate µmol O_2 L^{-1} h^{-1} PI curve fitted plots of corresponding stations and depths.

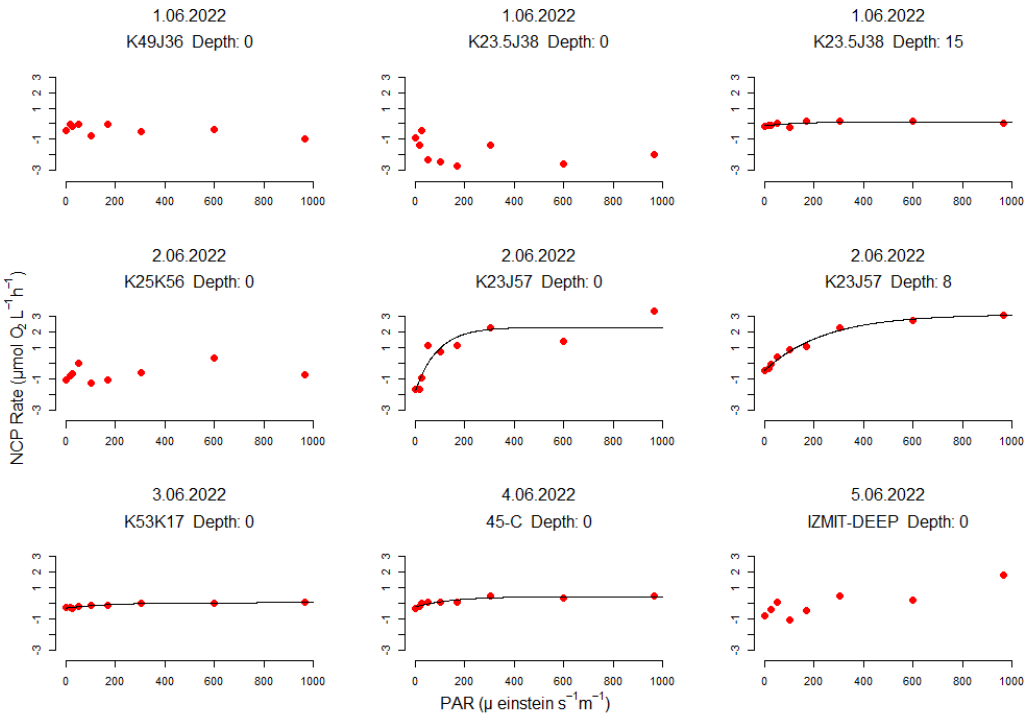

Figure 3.28 Summer, 2022 Cruise PAR (µ einstein $s^{-1}m^{-1}$) versus NCP rate µmol O_2 L^{-1} h^{-1} PI curve fitted plots of corresponding stations and depths.

3.5 Statistics

According to Spearman's correlation results conducted with untransformed data, CR was found to be negatively correlated with depth (R^2 = -0.44; *p*-value = 0.04; n = 25) and positively correlated with DO (R^2 = 0.54; *p*-value = 0.03; n = 25) and POC (R^2 = 0.40; *p*-value = 0.01; n = 25) and slightly positively correlated with Chl-*a* (R^2 = 0.21; *p*-value = 0.03; n = 25).

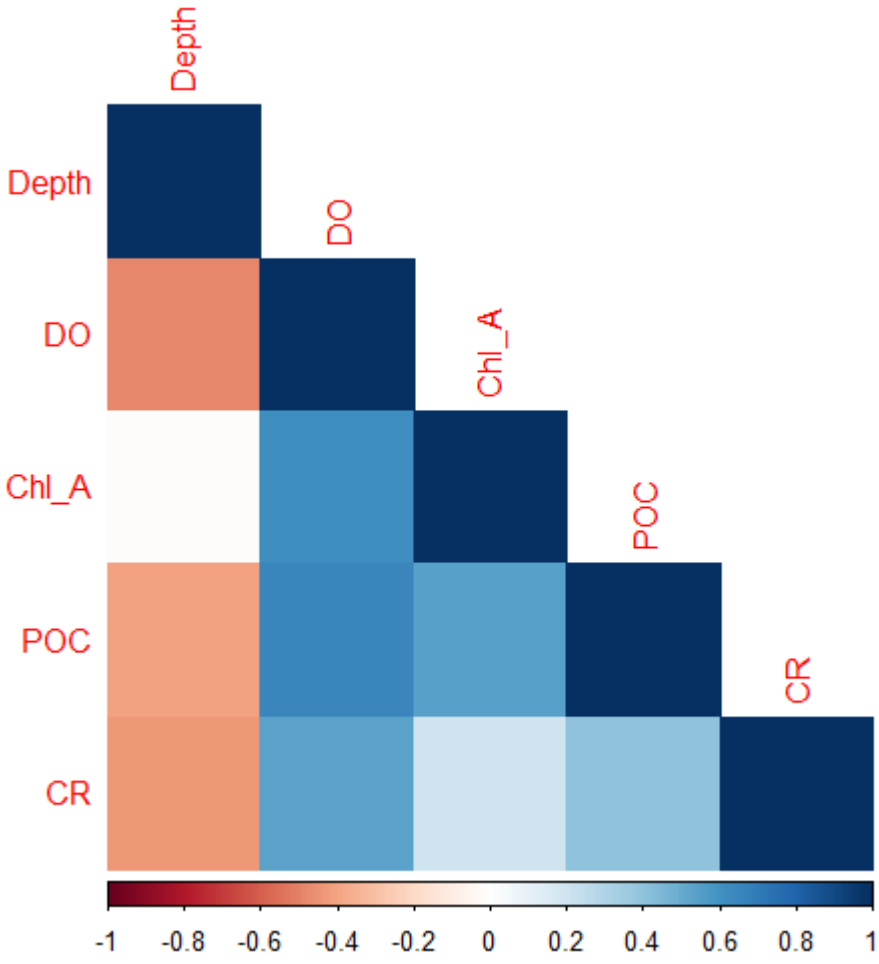

Figure 3.29 CR rates correlation table with depth (m), DO (µM), Chl-*a* (mg/L) and POC (µmol C/L)

According to this study's Spearman's correlation results conducted with untransformed data, NCP rates were found to be negatively correlated with bottom depth (R^2 = -0.63; n = 12). Also, it was negatively correlated with water temperature (R^2 = -0.54; n = 12). However, these correlation results do not have sufficient p-values (p-value > 0.05). This could be caused by an insufficient sample size. On the other hand, NCP was found to be highly and positively correlated with DO (R^2 = 0.72; p-value = 0.005; n = 12) and positively correlated with Chl-*a* (R^2 = 0.57; p-value = 0.004; n = 12).

CHAPTER 4

DISCUSSION

This study allows us to obtain qualitative and quantitative knowledge on net community production and community respiration in the spring and summer of 2022 in the Sea of Marmara. This study supplies comprehensive knowledge on community respiration through the water column and shows that community respiration is not constant throughout the water column, as assumed in many modeling studies.

4.1 Parameters towards Eutrophication

Since the 1980s, an excessive nutrient increase has been observed in the Sea of Marmara (Polat et al., 1998; Yalçın et al., 2017,) which has led to eutrophication in all basins (Yücel et al., 2021). European Union Marine Strategy Directive (MSFD) and many other national and international regulations have created indicators to assess eutrophication. Primary indicators are; i) Nutrient ii) Chlorophyll-a iii) Dissolved Oxygen concentrations, Secondary indicators are; i) Transparency ii) Harmful algal blooms iii) Macroalgae iv) Macrophyte and v) Macrofauna. In this chapter, all primary indicators (nutrients, Chl-*a* and DO) and one secondary indicator (transparency as secchi disk depth) are given.

Seasonal variations of nutrients occur due to the changes in primary production and nutrient inputs caused by Black Sea flow, precipitation, and coastal inputs. Nutrients tend to be low at the surface due to the photosynthetic activity of phytoplankton. However, an apparent increase in silicate, phosphate, and total nitrogen with depth was observed. Especially off the coast of Tekirdağ, İzmit Bay, and the southern shelf, we observed relatively high amounts of nutrients. Nutrient concentrations were higher in the eastern part of the Sea of Marmara than in the western part. Nutrient

concentrations measured in this study were similar to the average measurements conducted in the 1990s (Polat et al., 1998; max NO_X-N: 10.5 μM, max PO4: 1.2 μM).

Halocline and limited ventilation affect the distribution of DO in the water column of the Sea of Marmara. High DO is observed on the surface due to primary production decreasing sharply after 20-25 m, where light cannot penetrate deeper. Oxygen levels decreased throughout the water column, with increasing depth observed in both seasons. In addition, oxygen levels decreased from west to east in both seasons.

Chl-*a* concentrations measured in this study (0.32-5.88 μg/L) are in good agreement with measurements in previous studies (0.2-18 μg/L) which increase from the Dardanelles to İzmit Bay (Ediger et al., 2016 and references therein). We observed similar patterns during our samplings with previous studies.

The Secchi disk depth varied in the range of 3-13 m. The lowest Sechi disk depth values were found in the southern shelf and İzmit Deep. Ediger et al. (2016) showed that the Secchi disk depth varied from 8 to 14 m during the years 1986-1994 and from 4 to10 m during 2009-2014, which indicates a narrowing down of the euphotic zone and thus a thinner layer for primary production.

With the given indicators, during our sampling seasons, the sea of Marmara was still eutrophic. Unfortunately, there has been no improvement in the eutrophication status of the Sea of Marmara since earlier studies (Ediger et al., 2016; Yücel et al., 2021).

4.2 Pelagic Plankton Metabolism

Phytoplankton composition and abundance were studied for the March, 2022 stations and depths. At this period, the most abundant group observed was diatoms. The first four abundant species belong to diatoms and these species are followed by *Emiliania huxleyi* as the fifth abundant species which is a coccolithophore. Furthermore, species count per liter and cell count per liter decreased with increasing depth and

statistical differences between above halocline and sub-halocline phytoplankton communities were observed (Mantıkçı et al., 2022).

In March 2022, the average NCP value for all stations was 1.21± 0.9 μmol O_2 l^{-1} h^{-1} whereas, NCP_{chl} average was 0.77 mol O_2 g^{-1} Chl-*a* h^{-1} for the Sea of Marmara. Station K49J36, located in the western basin, had near zero negative NCP_{chl} (-0.01 mol O_2 g^{-1} Chl-*a* h^{-1}), and thus the station was the least productive one. All remaining stations from the March 2022 cruise had positive NCP rates. By looking at NCP_{chl} to achieve a better comparison between stations, we can say that the most productive ones were K26K20 (Southern Shelf), K57.5K13 (offshore Silivri), and K23J57 (Bandırma Bay), respectively. Although station İzmit-Deep, located at the deepest point of İzmit Bay, had the highest NCP rate (2.68 μmol O_2 l^{-1} h^{-1}), when normalized with chlorophyll, the value was 0.46 mol O_2 g^{-1} Chl-*a* h^{-1}. Its NCP measurement was not coherent with its Chl-*a* amount. The same pattern was observed at Station 45-C in the Çınarcık basin. Additionally, observing that there was not a fully correlated relationship between NCP and chlorophyll-a values showed that biomass or chlorophyll-a values were insufficient to determine the NCP value as the only parameter.

In June 2022, the mean NCP value for all stations was 0.35 ± 1.42 μmol O_2 l^{-1} h^{-1}. The Chl-a average for the Sea of Marmara was -0.06 μmol O_2 l^{-1} h^{-1}. Low nutrient availability in this season may cause lower rates of NCP as well as chlorophyll. In this season, the highest productivity was achieved in Station K23J57 (Bandırma Bay), 8 meters depth (1.35 μmol O_2 l^{-1} h^{-1}), followed by Station 45-C (Çınarcık Basin) surface depth (1.08 μmol O_2 l^{-1} h^{-1}).

In March 2022, the mean value of hourly CR was 0.42 (0.01-2.05 μmol O_2 l^{-1} h^{-1}) for the upper layer. On the other hand, in June 2022, the mean value of the hourly CR was 0.51 (in the range of 0.01-1.63 μmol O_2 l^{-1} h^{-1}). When only surface CR rates are considered, the average rate for March 2022 was 0.63 μmol O_2 l^{-1} h^{-1} and it was 0.68 μmol O_2 l^{-1} h^{-1} for June, 2022. Bacteria are the most significant contributors to CR especially in eutrophic systems (Robinson & Williams, 2005). This study's CR

rates are slightly lower than bacterial respiration rates (0.7 μmol O_2 L^{-1} h^{-1}) taken in September 2008, representing surface waters of the Sea of Marmara (Zeri et al., 2010). This difference could be due to seasonal variation.

In general, respiration tend to decrease with depth in both seasons. Only K49J36 did not follow this trend in both seasons. Southern Shelf, Erdek Bay, and İzmit Bay had relatively high oxygen consumption rates, possibly related to higher production rates coupled with higher heterotrophic activity.

We calculated the daily NCP on the surface for March 2022 by assuming a 12:12 h dark light period. Average oxygen consumption in the 12-hour dark period (0.63 μmol O_2 l^{-1} h^{-1}*12= 7.56) and net production in 12 hours of light (1.21 μmol O_2 l^{-1} h^{-1}*12= 14.52) calculated. By subtracting 12-hour dark community respiration from 12-hour light community production (14.52-7.56), we can get 6.96 μmol O_2 l^{-1} day^{-1} as daily net oxygen production. If we make the same calculation for June 2022, we can get 1.08 μmol O_2 l^{-1} day^{-1}as daily net oxygen production. For both estimates, actual values for NCP should be much lower because, in our calculation, we assumed 12 hours of maximal NCP. This can be due to two reasons; the PAR on the surface of the water varies depending on the time of day and the PAR decreases with depth in the water column. In the Sea of Marmara, PAR values were found to drop to 1% at 25-35 m on January 2021 except for the station highly affected by anthropogenic forces, where the euphotic depth had been calculated as 15 m (Öztürk & Ediger, 2023). Below euphotic depth, no photosynthetic activity can be observed, whereas heterotrophic respiration continues. The variability of PAR that had not been considered for the calculation above converges to the real net metabolism value, which indicates heterotrophic.

Due to daily and water column PAR irradiance variances neglected in these calculations for both of the seasons, we can conclude that the euphotic zone of the Sea of Marmara is net heterotrophic in both of the seasons. This calculation also showed that the system was more productive in March 2022 than in June 2022. Although this study only represents two periods in a year, we can also speculate that

in less productive seasons, the euphotic zone becomes more heterotrophic. This indicates photosynthetically produced fresh labile organic matter is consumed within the euphotic zone and almost none of this dissolved organic matter transfers to the sub-halocline. This finding is coherent with the results of the DOM stoichiometry study conducted in the Sea of Marmara in September 2008, which concluded newly produced surface DOM in the Marmara Sea is consumed in shorter time scales than the surface water residence time (Zeri et al., 2010). Aged material subjected to pelagic degradation for a prolonged time is more refractory. Suspended organic matter in the bottom layer should become more refractory due to low input rates from the surface (Hansen & Bendtsen, 2014). Therefore, the substrate for sub-halocline respiration should be particulate organic matter.

The CR_{sub} rates measured around 40 m depth in March 2022 have a mean of 89 ± 111mg C m^{-3} day^{-1}. In June 2022, we conducted these experiments with samples from 40 m and 100 m. Community respiration at these two different depths had similar values. The mean value of CR_{sub} was 75 ± 35 mg C m^{-3} day^{-1}. α value which indicates specific turnover rate showing the degradability of organic carbon, found to be 0.042 ± 0.06 day^{-1}as the average of March 2022 samples and 0.039 ± 0.02 day^{-1} as the average of June 2022 samples. The low α values indicate the slowest consumable organic carbon. In March 2022, it was slightly higher than in June 2022. The low specific turnover rate obtained for both seasons indicates mostly refractory organic carbon is available, which is compatible with the euphotic zone being heterotrophic.

4.3 Comparison of the Sea of Marmara with other similar systems

In this study, in March 2022, the mean value of hourly CR for the euphotic zone was 0.42 (0.01-2.05 μmol O_2 l^{-1} h^{-1}) and in June 2022, the mean value of hourly CR for the euphotic zone was 0.51 (in the range of 0.01-1.63 μmol O_2 l^{-1} h^{-1}). As only surface CR rates are considered, the average rate for March 2022 was 0.63 μmol O_2 l^{-1} h^{-1} and it was 0.68 μmol O_2 l^{-1} h^{-1} for June, 2022. Mantıkcı (2015) measured CR rates in

the surface waters of two Danish estuaries in a seasonal cycle and found 0.06-0.30 μmol O_2 l^{-1} h^{-1} at the Great Belt and 0.07-0.78 μmol O_2 l^{-1} h^{-1} at Roskilde Fjord. Our measurements are in good agreement with his study conducted in the summertime. Hansen and Bendtsen (2014) measured bottom water respiration at Kattegat and Belt Sea located in the North Sea and Baltic Sea transition zone. They calculated the average α value as 0.035 day^{-1} (winter: 0.0027 d^{-1} to 0.010 d^{-1}; October: 0.053 d^{-1} to 0.094 d^{-1}) which is consistent with this study's measurements. However, their calculation on bottom water respiration rate was 12 C m^{-3} day^{-1} as annual mean. In this study, we calculated the sub halocline respiration rate (CR_{sub}) as 75 ± 35 mg C m^{-3} day^{-1}. This difference indicates that the initial carbon pool of the Sea of Marmara sub-halocline water is much higher than it is for Baltic Sea bottom water. Organic carbon should be enriched in sub-halocline.

Surface water community respiration rates have been measured in the range of 40 – 70 μg O_2 l^{-1} h^{-1} (1.25 – 2.19 μmol O_2 l^{-1} h^{-1}) for Chesapeake Bay. Bottom water respiration has been measured as 28 μg O_2 l^{-1} h^{-1} (0.88 μmol O_2 l^{-1} h^{-1}, 253.44 mg C m^{-3} day^{-1}) in the mesohaline region of Chesapeake Bay (Sampau & Kemp, 1994). Although, in comparison of the two systems, similar measurements have been observed, in Chesapeake Bay, the top layer minimum water column respiration measurements are higher than those in the Sea of Marmara. The same statement can be made for maximum water column respiration measurements. Furthermore, the bottom water respiration rate in Chesapeake Bay is closer to the maximum sub-halocline respiration rate observed in the Sea of Marmara in this study than its average values.

In the study conducted at the Louisiana continental shelf located in the Gulf of Mexico mean respiration rates have been calculated using data from 2003 to 2007 for Spring, Summer and Fall seasons. All data averages of plankton community respiration have been found to be 11.1±1.1 μmol O_2 l^{-1} h^{-1} for surface waters, 7.5±0.8 μmol O_2 l^{-1} h^{-1} for mid-depth and 7.0±0.4 μmol O_2 l^{-1} h^{-1} for bottom water (Murrell et al., 2013). In comparison with this study, lower respiration rates for both the photic

zone and bottom water have been observed in the Sea of Marmara than on the Louisiana continental shelf.

Plankton respiration has been measured as 0.57 μmol O_2 l^{-1} h^{-1} in July 2015 and 0.36 μmol O_2 l^{-1} h^{-1} in July 2016 at the 15 m depth of the Gulf of Trieste located in the Adriatic Sea (Kralj et al., 2019). Our measurements for the June 2022 sampling period are in good agreement with this study for similar depths.

4.4 Regulation of Plankton Metabolism

Significant correlations have been found between respiration and Chl-*a* and also with particulate organic carbon (POC) in previous studies conducted in the Eastern Atlantic Ocean and North Sea (Robinson et al., 2002a; 2002b). These chemical parameters are less time-consuming to measure, and their measurements are taken more frequently. POC, and Chl-*a*, standing stock, could be predictors for respiration; however, the R^2 of the association between respiration and Chl-*a* is more significant than 0.3 in just 50% of the cases (Robinson & Williams, 2005). In this study, there was a slightly positive correlation (R^2<0.3) between Chl-*a* and CR. On the other hand, there was sufficient positive correlation with POC (R^2 = 0.39). The most significant correlation was found with DO (R^2 = 0.51). One of the important findings of the correlation results was negative correlation with depth (R^2 = -0.41) which is coherent with negative relation of CR with depth stated on previous studies (Robinson & Williams, 2005 and references therein).

There have been studies conducted to investigate the relationship between respiration and production. Community respiration scaled as roughly the equivalent of two-thirds of photosynthesis, and the two parameters had a strong correlation (R^2 = 0.42) (del Giorgio et al., 1997; Duarte & Agusti, 1998). Additionally, photosynthesis's standard deviation was higher than respiration's (Robinson et al., 1999). On the other hand, depth-integrated photosynthesis and respiration have a low correlation (R^2 = 0.13) that indicates areal photosynthesis is a poor indicator of areal

respiration (Williams & Bowers, 1999; Serret et al., 2001; 2002). There are primary factors, in addition to photosynthesis, that impact respiration, and the connection between production and respiration is poor (del Giorgio & Williams, 2005). In this study, there was no significant correlation between NCP rates and CR rates of corresponding stations and depths. DOC incoming from riverine discharge was found to be highly correlated with respiration in northern Baltic Sea where strongly affected by rivers and DOC was found to be exceeding primary production by 4-fold (Vikström et al., 2020). Due to DOC is preferable carbon source for respiration, it should be accounted with primary production. Excess DOC coming from the Black Sea or other sources into the Sea of Marmara may have dominated the effect of NCP on CR.

In March 2022, the surface temperature was around 10 °C; in June 2022, it reached 24 °C. Cellular reactions increase with temperature, following the Arrhenius equation. In summer, average CR increased slightly from March to June; however, it wasn't 2.5 times like temperature. This discrepancy can be explained by the temperature sensitivity-dependence (Q^{10}) of CR ($Q^{10} = (\frac{R_2}{R_1})^{10/(T2-T1)}$).

The calculated CR Q^{10} value was ~1 using temperatures and the average CR rate of two seasons. The CR Q^{10} value of this study is lower than previous studies. In the Antarctic Ocean, the Q^{10} value for plankton respiration found to be 2.8 (Robinson and Williams, 1993) and 3.2 (Vosjan & Olanczukeyman, 1991). For the Atlantic NE coast, it is found as 5.1 (Lefevre et al., 1994) and for the Atlantic NW coast, it is found as 2.5 (Pomeroy et al., 1991). In the Mediterranean Sea, it is found as 6.8 (Robinson, 2000). In Danish estuaries, Mantikci (2015) found as 1.8 and 2.7. In the study conducted in the northern Baltic Sea (Vikström et al., 2020), Chl-*a* and temperature were found to have a low effect on respiration; however, carbon input (riverine discharge total organic carbon and depth integrated plankton production) was found to be only parameter necessary to predict respiration based on multiple regression. On the contrary, in many studies, the relationship between temperature,

Chl-*a* and CR was found to be statistically significant (López-Urrutia & Morán, 2007, Mantikci 2015).

Wikner et al. (2023), tested previous modeling equations on plankton respiration for their explanatory powers on a three-year dataset (Vikström et al., 2020) obtained from the northern Baltic Sea. However, none of the models provide adequate accuracy and precision to explain plankton respiration. Despite the fact that having the model of plankton respiration suitable for all marine environments would be ideal, their study shows current models fail to predict their dataset.

The negative correlation of NCP with bottom depth (R^2 = -0.63) indicates coastal zones are more productive. The negative correlation of NCP with water temperature (R^2 = -0.54) can be explained by the hot summer season being less productive. NCP was found to be highly and positively correlated with DO (R^2 = 0.72) and positively correlated with Chl-*a* (R^2 = 0.57). Although they are good predictors for NCP, they are not fully sufficient to explain the NCP rates. It shows the importance of experimental measurement of NCP to determine the heterotrophy or autotrophy of the system.

In conclusion, the factors affecting respiration vary according to space and time, and in our study, the effect of temperature was very low compared to the values given in the literature. Additionally, CR was found to be highly correlated with DO and POC. To understand the controlling factors of respiration in the Sea of Marmara, it is required to conduct multivariate statistics on a larger and more comprehensive dataset.

CHAPTER 5

CONCLUSION

In summary, community respiration rates throughout the water column were quantified with emphasis on spatial differences both in the euphotic zone and sub-halocline during two different seasons, spring and summer 2022, in the Sea of Marmara. This study presents one of the preliminary studies regarding respiration in the Sea of Marmara. In March 2022, the hourly CR rate was in the range of 0.01-2.05 μmol O_2 L^{-1} h^{-1} and in June 2022, it was in the range of 0.01-1.63 μmol O_2 L^{-1} h^{-1} for the euphotic zone. In this study, we observed a significant negative correlation between respiration and depth. As well, respiration was found to be positively correlated with DO and POC. The temperature effect on respiration in the Sea of Marmara was found to be low, almost not affecting. Sub-halocline community respiration rates were calculated as 89 ± 111mg C m^{-3} day^{-1} (α = 0.042 ± 0.06 day^{-1}) for March, 2022 and 75 ± 35 mg C m^{-3} day^{-1} (α = 0.039 ± 0.02 day^{-1}) for June, 2022. Furthermore, net community production was quantified for the Sea of Marmara and found to be positively correlated with dissolved oxygen and Chl-*a*. This study suggests that the Sea of Marmara is a heterotrophic system, meaning total respiration exceeds gross primary production. In addition, this may indicate photosynthetically produced fresh organic carbon was consumed in the euphotic zone and did not transfer to the sub-halocline.

This study contributes to respiration and net community production studies in the Sea of Marmara, which is a vulnerable ecosystem in regards to oxygen dynamics. Clearly, further studies are needed with a more comprehensive dataset to understand the regulation of respiration in the Sea of Marmara and emphasize the oxygen and carbon dynamics of the system.

REFERENCES

Akçay, İ. (2022). Coastal Eutrophication and Hypoxia Under Focus: Redox Dependent Benthic Nutrient Fluxes Across Sea Boundaries in the Northeastern Mediterranean and Marmara Sea (Doctoral dissertation). Middle East Technical University, Türkiye.

Arslan-Alaton, I., Iskender, G., Tanik, A., Gurel, M., Ovez, S., & Orhon, D. (2009, September). Current situation of urban wastewater treatment plants in megacity Istanbul. Desalination, 246(1–3), 409–416. https://doi.org/10.1016/j.desal.2008.04.055

Bender, M., Grande, K., Johnson, K., Marra, J., Williams, P. J. L., Sieburth, J., ... & Heinemann, K. (1987). A comparison of four methods for determining planktonic community production 1. Limnology and Oceanography, 32(5), 1085-1098.

Beşiktepe, Ş. T., Sur, H. I., Özsoy, E., Latif, M. A., Oğuz, T., & Ünlüata, Ü. (1994). The circulation and hydrography of the Marmara Sea. Progress in Oceanography, 34(4), 285-334.

Coban-Yildiz, Y., Tugrul, S., Ediger, D., Yilmaz, A., & Polat, C. (2000). A comparative study on the abundance and elemental composition of POM in three interconnected basins: the Black, the Marmara and the Mediterranean Seas. Mediterranean Marine Science, 1(1), 51-64.

Conley, D. J., Carstensen, J., Ærtebjerg, G., Christensen, P. B., Dalsgaard, T., Hansen, J. L., & Josefson, A. B. (2007). Long-term changes and impacts of hypoxia in Danish coastal waters. Ecological Applications, 17(sp5), S165-S184.

Crawley, M. J. (2010). The R Book. In John Wiley & Sons Ltd. https://doi.org/10.1016/b978-0-12-374507-1.00050-9

Dalgaard, P. (2008). Introductory Statistics with R. In Springer. https://doi.org/10.2307/2286187

Del Giorgio, P. A., Cole, J. J., & Cimbleris, A. (1997). Respiration rates in bacteria exceed phytoplankton production in unproductive aquatic systems. Nature, 385(6612), 148-151.

Del Giorgio, P. A., & Duarte, C. M. (2002). Respiration in the open ocean. Nature, 420(6914), 379-384.

Del Giorgio P. A., Williams P. J., Le B. (2005). “The global significance of respiration in aquatic ecosystems: from single cells to the biosphere,” in Respiration in aquatic ecosystems. Eds. del Giorgio P. A., Williams P. J., Le B. (Oxford: Oxford University Press), 267–303.

Duarte, C. M., & Agustí, S. (1998). The CO2 balance of unproductive aquatic ecosystems. Science, 281(5374), 234-236.

Ducklow, H. W., & Doney, S. C. (2013). What is the metabolic state of the oligotrophic ocean? A debate. Annual review of marine science, 5, 525-533.

Ediger, D., Beken, Ç., Yüksek, A., & Tuğrul, S. (2016). Eutrophication in the Sea of Marmara. The Sea of, 723.

Falkowski, P., Scholes, R. J., Boyle, E. E. A., Canadell, J., Canfield, D., Elser, J., ... & Steffen, W. (2000). The global carbon cycle: a test of our knowledge of earth as a system. science, 290(5490), 291-296.

Gaarder, T. (1927). Investigations of the production of plankton in the Oslo Fjord. Rapports et Proces-verbaux des Reunions. Conseil International pour 1'Exploration de la Mer, 42, 1-48.

Garside, C., & Malone, T. C. (1978). Monthly oxygen and carbon budgets of the New York Bight Apex. Estuarine and Coastal Marine Science, 6(1), 93-104.

Gilly, W. F., Michael Beman, J., Litvin, S. Y., & Robison, B. H. (2013). Oceanographic and biological effects of shoaling of the oxygen minimum zone. Annual Review of Marine Science, 5, 393–420. https://doi.org/10.1146/annurev-marine-120710-100849

Grasshoff, K., Ehrhardt, M., Kremling, K., & Almgren, T. (1983). Methods of Seawater Analysis 2nd rev. and extended edn Verlag Chemie. Weinheim, 28, p419..

Hansen, J. L., & Bendtsen, J. (2014). Seasonal bottom water respiration in the North Sea–Baltic Sea transition zone: rates, temperature sensitivity and sources of organic material. Marine Ecology Progress Series, 499, 19-34.

Heath, M. (1995). An holistic analysis of the coupling between physical and biological processes in the coastal zone. Ophelia, 42(1), 95-125.

Hedges, J. I., & Keil, R. G. (1995). Sedimentary organic matter preservation: an assessment and speculative synthesis. Marine chemistry, 49(2-3), 81-115.

Howarth, R. W., Schneider, R., & Swaney, D. (1996). Metabolism and organic carbon fluxes in the tidal freshwater Hudson River. Estuaries, 19, 848-865.

Jassby, A. D., Cloern, J. E., & Powell, T. M. (1993). Organic carbon sources and sinks in San Francisco Bay: variability induced by river flow. Marine Ecology Progress Series, 39-54.

Johnson, K. M., Davis, P. G., & Sieburth, J. M. (1983). Diel variation of TCO 2 in the upper layer of oceanic waters reflects microbial composition, variation and possibly methane cycling. Marine Biology, 77, 1-10.

Johnson, K. M., Sieburth, J. M., leB Williams, P. J., & Brändström, L. (1987). Coulometric total carbon dioxide analysis for marine studies: automation and calibration. Marine Chemistry, 21(2), 117-133.

Kemp, W. M., Smith, E. M., Marvin-DiPasquale, M., & Boynton, W. R. (1997). Organic carbon balance and net ecosystem metabolism in Chesapeake Bay. Marine Ecology Progress Series, 150, 229-248.

Kenney, B. E., Litaker, W., Duke, C. S., & Ramus, J. (1988). Community oxygen metabolism in a shallow tidal estuary. Estuarine, Coastal and Shelf Science, 27(1), 33-43.

Klimant, I., Meyer, V., & Kühl, M. (1995). Fiber-optic oxygen microsensors, a new tool in aquatic biology. Limnology and Oceanography, 40(6), 1159–1165. https://doi.org/10.4319/lo.1995.40.6.1159

Kolkwitz, R., & Marsson, M. (1908). Ololog ie des pflanzenlichen Saprobien. Berichte der Deutschen Botanischen Gesellschaft, 26, 505–510.

Kralj, M., Lipizer, M., Čermelj, B., Celio, M., Fabbro, C., Brunetti, F., Francé, J., Mozetič, P., & Giani, M. (2019). Hypoxia and dissolved oxygen trends in the northeastern Adriatic Sea (Gulf of Trieste). Deep-Sea Research Part II: Topical Studies in Oceanography, 164(June), 74–88. https://doi.org/10.1016/j.dsr2.2019.06.002

Lalli, C., & Parsons, T. R. (1997). Biological oceanography: an introduction. Elsevier.

Lefevre D., Bentley T. L., Robinson C., Blight S. P., Williams P. J. L. (1994). The temperature response of gross and net community production and respiration in time-varying assemblages of temperate marine micro-plankton. J. Exp. Mar. Biol. Ecol. 184 (2), 201–215. doi: 10.1016/0022-0981(94)90005-1

López-Urrutia, Á., & Morán, X. A. G. (2007). Resource limitation of bacterial production distorts the temperature dependence of oceanic carbon cycling. Ecology, 88(4), 817-822.,

Mantikci, M. (2015). Significance of plankton respiration for productivity in coastal ecosystems (Doctoral dissertation). Aarhus University, Denmark.

Mantikci, M., Hansen, J. L., & Markager, S. (2017). Photosynthesis enhanced dark respiration in three marine phytoplankton species. Journal of Experimental Marine Biology and Ecology, 497, 188-196.

Mantıkcı M., Örek H., Yücel M., Uysal Z., Salihoğlu B., Arkın S., Kazak M., & Demirtaş E. (2022). Plankton Metabolism and Effects of Mucilage on Oxygen Consumption in the Sea of Marmara. Grand Number: 121G001 TÜBİTAK.

Morkoc, E., & Tugrul, S. (1995). Effects of wastewater pollution on the physical and biochemical characteristics of Izmit Bay. Oceanographic Literature Review, 12(42), 1145.

Murrell, M. C., Stanley, R. S., Lehrter, J. C., & Hagy, J. D. (2013). Plankton community respiration, net ecosystem metabolism, and oxygen dynamics on the Louisiana continental shelf: Implications for hypoxia. Continental Shelf Research, 52, 27–38. https://doi.org/10.1016/j.csr.2012.10.010

Nielsen, E. S. (1952). The use of radio-active carbon (c14) for measuring organic production in the sea. ICES Journal of Marine Science, 18(2), 117–140. https://doi.org/10.1093/icesjms/18.2.117

Nielsen, E. S. (1963). Productivity, definition and measurement. The sea, 2, 129-164.

Nielsen, E. S., & Hansen, V. K. (1958). Measurements with the carbon-14 technique of the respiration rates in natural populations of phytoplankton. Deep Sea Research (1953), 5(2-4), 222-233.

Nixon, S. W. (1995). Coastal marine eutrophication: a definition, social causes, and future concerns. Ophelia, 41(1), 199-219.

Nixon, S. W., & Pilson, M. E. (1984). Estuarine total system metabolism and organic exchange calculated from nutrient ratios: an example from Narragansett Bay. In The estuary as a filter (pp. 261-290). Academic Press.

Odum, H. T. (1956). Primary production in flowing waters 1. Limnology and oceanography, 1(2), 102-117.

Odum, E.P. (1971) Fundamentals of Ecology. Third Edition, W.B. Saunders Co., Philadelphia, 1-574.

Öztürk, İ. D., & Ediger, D. (2023). Effects of mucilage on the optical properties of water column in the Sea of Marmara. Journal of the Black Sea/Mediterranean Environment, 29(1).

Polat, S. Ç., & Tugrul, S. (1995). Nutrient and organic carbon exchanges between the Black and Marmara Seas through the Bosphorus Strait. Continental Shelf Research, 15(9), 1115-1132.

Polat, S. C., Tuğrul, S., Çoban-Yıldız, Y., Basturk, O., & Salihoglu, I. (1998). Elemental composition of seston and nutrient dynamics in the Sea of Marmara. Hydrobiologia, 363(1-3), 157-167.

Pomeroy L. R., Wiebe W. J., Deibel D., Thompson R. J., Rowe G. T., Pakulski J. D. (1991). Bacterial responses to temperature and substrate concentration during the new foundland spring bloom. Mar. Ecology-Progress Ser. 75 (2-3), 143–159. doi: 10.3354/meps075143

Quay, P., Emerson, S., & Palevsky, H. (2020). Regional Pattern of the Ocean's Biological Pump Based on Geochemical Observations. Geophysical Research Letters, 47(14), 1–10. https://doi.org/10.1029/2020GL088098

Raven J. A., Beardall J. (2005). "Respiration in aquatic photolithotrophs," in Respiration in aquatic ecosystems. Eds. del Giorgio P. A., Williams P. J., Le B. (Oxford: Oxford University Press), 36–46.

Riley, G. A. (1940). Limnological studies in Connecticut. Part III. The plankton of Linsley pond. Ecological Monographs, 10(2), 279-306.

Robinson, C., & Williams, P. J. L. (1993). Temperature and Antarctic plankton community respiration. Journal of Plankton Research, 15(9), 1035-1051.

Robinson, C., & Williams, P. J. L. B. (1999). Plankton net community production and dark respiration in the Arabian Sea during September 1994. Deep Sea Research Part II: Topical Studies in Oceanography, 46(3-4), 745-765.

Robinson C., Williams P. J., Le B. (2005). "Respiration and it′s measurement in surface marine waters," in Respiration in aquatic ecosystems. Eds. del Giorgio P. A., Williams P. J., Le B. (Oxford: Oxford University Press), 147–180.

Robinson, C., Archer, S. D., & Williams, P. J. L. B. (1999). Microbial dynamics in coastal waters of East Antarctica: plankton production and respiration. Marine Ecology Progress Series, 180, 23-36.

Robinson, C., Serret, P., Tilstone, G., Teira, E., Zubkov, M. V., Rees, A. P., & Woodward, E. M. S. (2002a). Plankton respiration in the eastern Atlantic Ocean. Deep Sea Research Part I: Oceanographic Research Papers, 49(5), 787-813.

Robinson, C., Widdicombe, C. E., Zubkov, M. V., Tarran, G. A., Miller, A. E., & Rees, A. P. (2002b). Plankton community respiration during a coccolithophore bloom. Deep Sea Research Part II: Topical Studies in Oceanography, 49(15), 2929-2950.

ROMANENKO, V. (1964). RELATION BETWEEN QUANTITATIVE REQUIREMENTS OF O2 CO2 OF HETEROTROPHIC BACTERIA. Doklady Akademii nauk SSSR, 157, 178-179.

Sampou, P., & Kemp, W. M. (1994). Factors regulating plankton community respiration in Chesapeake Bay. Marine Ecology Progress Series, 110(2–3), 249–258. https://doi.org/10.3354/meps110249

Serret, P., Fernández, E., & Robinson, C. (2002). Biogeographic differences in the net ecosystem metabolism of the open ocean. Ecology, 83(11), 3225-3234.

Serret, P., Robinson, C., Fernández, E., Teira, E., & Tilstone, G. (2001). Latitudinal variation of the balance between plankton photosynthesis and respiration in the eastern Atlantic Ocean. Limnology and Oceanography, 46(7), 1642-1652.

Sigman, D. M. & Hain, M. P. (2012) The Biological Productivity of the Ocean. Nature Education Knowledge 3(10):21

Sládecek, V. (1973). System of water quality from the biological point of view.

Smith, S. V., & Hollibaugh, J. T. (1993). Coastal metabolism and the oceanic organic carbon balance. Reviews of Geophysics, 31(1), 75-89.

Smith, S. V., Hollibaugh, J. T., Dollar, S. J., & Vink, S. (1991). Tomales bay metabolism: C, N, P stoichiometry and ecosystem heterotrophy at the land-sea interface. Estuarine, Coastal and Shelf Science, 33(3), 223-257.

Strickland, J. D. H., & Parsons, T. R. (1972). A practical handbook of seawater analysis.

Sverdrup, H. U. (1953). On conditions for the vernal blooming of phytoplankton. J. Cons. Int. Explor. Mer, 18(3), 287-295.

Tüfekçi, V., Balkis, N., Beken, C. P., Ediger, D., & Mantikci, M. (2010). Phytoplankton composition and environmental conditions of the mucilage event in the Sea of Marmara. Turkish Journal of Biology, 34(2), 199-210.

Tugrul, S., & Polat, C. (1995). Quantitative comparison of the influxes of nutrients and organic carbon into the Sea of Marmara both from anthropogenic sources and from the Black Sea. Water Science and Technology, 32(2), 115-121.

Tugrul, S., Besiktepe, T., & Salihoglu, I. (2002). Nutrient exchange fluxes between the Aegean and Black Seas through the Marmara Sea. Mediterranean Marine Science, 3(1), 33-42.

Tuğrul, S., Murray, J. W., Friederich, G. E., & Salihoğlu, İ. (2014). Spatial and temporal variability in the chemical properties of the oxic and suboxic layers of the Black Sea. Journal of Marine Systems, 135, 29-43.

Tuğrul, S., Yücel, N., & Akcay, I. (2016). Chemical oceanography of north eastern Mediterranean. The Turkish Part of the Mediterranean Sea, 15-29.

Tugrul, S., Ozhan, K., & Akcay, I. (2019). Assessment of trophic status of the northeastern Mediterranean coastal waters: eutrophication classification tools revisited. Environmental Science and Pollution Research, 26(15), 14742-14754.

Ulloa, O., Canfield, D. E., DeLong, E. F., Letelier, R. M., & Stewart, F. J. (2012). Microbial oceanography of anoxic oxygen minimum zones. Proceedings of the National Academy of Sciences of the United States of America, 109(40), 15996–16003. https://doi.org/10.1073/pnas.1205009109

Ünlülata, Ü., Oğuz, T., Latif, M. A., & Özsoy, E. (1990). On the physical oceanography of the Turkish Straits. The physical oceanography of sea straits, 25-60.

Van Es, F. B. (1977). A preliminary carbon budget for a part of the Ems estuary: the Dollard. Helgoländer wissenschaftliche Meeresuntersuchungen, 30, 283-294.

Vikström K., Bartl I., Karlsson J., Wikner J. (2020). Strong influence of baseline respiration in an oligotrophic coastal ecosystem. Front. Mar. Sci. 7 (839). doi: 10.3389/fmars.2020.572070

Vosjan J. H., Olanczukneyman K. M. (1991). Influence of temperature on respratory ETS-activity of microorganisms from admirality bay, king George island, Antarctica. Netherlands J. Sea Res. 28 (3), 221–225. doi: 10.1016/0077-7579(91)90019-W

Webb, W. L., Newton, M., & Starr, D. (1974). Carbon dioxide exchange of Alnus rubra: a mathematical model. Oecologia, 17, 281-291.

Wikner, J., Vikström, K., & Verma, A. (2023). Regulation of marine plankton respiration: A test of models. Frontiers in Marine Science, 10, 1134699.

Williams, P. J. L. B., & Bowers, D. G. (1999). Regional carbon imbalances in the oceans. Science, 284(5421), 1735-1735.

Williams P. J., Le B., del Giorgio P. A. (2005). "Respiration in aquatic ecosystems: history and background," in Respiration in aquatic ecosystems. Eds. del Giorgio P. A., Williams P. J., Le B. (Oxford: Oxford University Press), 1–17.

Wilson, J., Abboud, S., & Beman, J. M. (2017). Primary production, community respiration, and net community production along oxygen and nutrient gradients: Environmental controls and biogeochemical feedbacks within and across "marine lakes." Frontiers in Marine Science, 4(JAN). https://doi.org/10.3389/fmars.2017.00012

Winkler, L. W. (1888). Die bestimmung des im wasser gelösten sauerstoffes. Berichte der deutschen chemischen Gesellschaft, 21(2), 2843-2854.

Wright, J. J., Konwar, K. M., & Hallam, S. J. (2012). Microbial ecology of expanding oxygen minimum zones. Nature Reviews Microbiology, 10(6), 381–394. https://doi.org/10.1038/nrmicro2778

Yalçın, B., Artüz, M. L., Pavlidou, A., Çubuk, S., & Dassenakis, M. (2017). Nutrient dynamics and eutrophication in the Sea of Marmara: Data from recent oceanographic research. Science of the Total Environment, 601–602, 405–424. https://doi.org/10.1016/j.scitotenv.2017.05.179

Yılmaz, A., & Tuğrul, S. (1998). The effect of cold-and warm-core eddies on the distribution and stoichiometry of dissolved nutrients in the northeastern Mediterranean. Journal of Marine Systems, 16(3-4), 253-268.

Yücel, M., Özkan, K., Fach, B., et al. (2021). "Marmara Denizi'nin Geçirdiği Biyojeokimyasal Değişimler Bağlamında 2021 Musilaj Patlaması, Güncel Baskılar ve Çözüm Önerileri," in Marmara Denizi'nin Ekolojisi: Deniz Salyası Oluşumu, Etkileşimleri ve Çözüm Önerileri. Eds: Öztürk, İ., Şeker, M. (Turkish Academy of Sciences,Ankara),249-268.

Zeri, C., Beşiktepe, Ş., Giannakourou, A., Krasakopoulou, E., Tzortziou, M., Tsoliakos, D., ... & Papathanassiou, E. (2014). Chemical properties and fluorescence of DOM in relation to biodegradation in the interconnected Marmara–North Aegean Seas during August 2008. Journal of Marine Systems, 135, 124-136.